

A FEASIBILITY STUDY FOR EXTERNAL CONTROL ON SELF-ORGANIZED  
PRODUCTION OF PLASMONIC ENHANCEMENT INTERFACES FOR SOLAR CELLS

A THESIS SUBMITTED TO  
THE GRADUATE SCHOOL OF NATURAL AND APPLIED SCIENCES  
OF  
MIDDLE EAST TECHNICAL UNIVERSITY

BY

MONA ZOLFAGHARI BORRA

IN PARTIAL FULFILLMENT OF THE REQUIREMENTS  
FOR  
THE DEGREE OF MASTER OF SCIENCE  
IN  
MICRO AND NANOTECHNOLOGY

SEPTEMBER 2013



Approval of the Thesis:

**A FEASIBILITY STUDY FOR EXTERNAL CONTROL ON SELF-ORGANIZED  
PRODUCTION OF PLASMONIC ENHANCEMENT INTERFACES FOR SOLAR  
CELLS**

Submitted by **MONA ZOLFAGHARI BORRA** in partial fulfillment of the requirements  
for the degree of **Master of Science in Micro and Nanotechnology Department, Middle  
East Technical University** by,

Prof. Dr. Canan Özgen  
Dean, Graduate School of **Natural and Applied Sciences**

\_\_\_\_\_

Prof. Dr. Tayfun Akın  
Head of Department, **Micro and Nanotechnology**

\_\_\_\_\_

Assist. Prof. Dr. Alpan Bek  
Supervisor, **Physics Dept., METU**

\_\_\_\_\_

Assoc. Prof. Dr. H. Emrah Ünalın  
Co-Supervisor, **Metallurgical and Materials Eng., METU**

\_\_\_\_\_

**Examining Committee Members:**

Prof. Dr. Raşit Turan  
Physics Dept., METU

\_\_\_\_\_

Assist. Prof. Dr. Alpan Bek  
Physics Dept., METU

\_\_\_\_\_

Prof. Dr. Mehmet Parlak  
Physics Dept., METU

\_\_\_\_\_

Assist. Prof. Dr. Emren Nalbant Esentürk  
Chemistry Dept., METU

\_\_\_\_\_

Dr. Halil Berberoğlu  
Physics Dept., METU

\_\_\_\_\_

**Date: 03.09.2013**

**I hereby declare that all information in this document has been obtained and presented in accordance with academic rules and ethical conduct. I also declare that, as required by these rules and conduct, I have fully cited and referenced all material and results that are not original to this work.**

Name, Last Name: *Mona Zolfaghari Borra*

Signature :

## ABSTRACT

### **A FEASIBILITY STUDY FOR EXTERNAL CONTROL ON SELF-ORGANIZED PRODUCTION OF PLASMONIC ENHANCEMENT INTERFACES FOR SOLAR CELLS**

Zolfaghari Borra, Mona

M. Sc. Department of Micro and Nanotechnology

Supervisor: Assist. Prof. Dr. Alpan Bek

Co-Supervisor: Assoc. Prof. Dr. H. Emrah Ünalan

September 2013, 84 pages

The present study is about the improvement of the energy conversion efficiency of solar cells in which plasmonic light-trapping approach has been investigated. In this study, metal nanoparticles are allowed to form in a self-organized fashion on both flat and textured full scale monocrystalline silicon solar cell. These metal nanoparticles with strong optical interaction cross-sections at localized plasmonic resonance energies, improve coupling of the incoming light into the active area of solar cells by wavelength tailored scattering. The decoration of metal nanoparticle by the self-organized mechanism of dewetting is utilized as a suitable method for plasmonic interface integration to large area full-scale solar cell devices. In this bottom-up approach, the self-organization process of plasmonically active metal nanoparticles on solar cell surface only requires metal evaporation and a gentle thermal treatment step and is therefore a low cost fabrication technique. Formation of silver nanoparticles was preferred due to strong plasmon resonance of silver in the solar spectrum. Reflection measurements are performed both on flat and textured silicon cells in order to investigate the local plasmonic resonances of the metal nanoparticles. The effect of particle's size, thickness of silicon nitride anti-reflection coating layer, and dewetting time are investigated by reflection measurements and the shift of plasmon resonance peak position. It is found that surface roughness, annealing time, annealing temperature and varying silicon nitride's thickness can be used as mechanisms to control the size distribution, shape of the resultant nano-islands and solar cell efficiency. The findings on the most suitable nanoparticle system production parameters by this method, depends on the applied substrate properties which are expected to guide further applications of plasmonic interfaces and also to the other kinds of device structures in the ultimate quest for attaining affordable high efficiency solar cells.

Keywords: plasmons, solar cells, dewetting, efficiency, reflection, scattering

## ÖZ

# GÜNEŞ GÖZELERİ İÇİN PLAZMONİK ARTTIRIM ARAYÜZÜ ÜRETİMİNDE KENDİNDEN OLUŞMANIN DIŞ ETMENLER İLE KONTROLÜ ÜZERİNE BİR FİZİBİLİTE ÇALIŞMASI

Zolfaghari Borra, Mona

Yüksek Lisans, Mikro ve Nanoteknoloji Bölümü

Tez Yöneticisi: Yard. Doç. Dr. Alpan Bek

Ortak Tez Yöneticisi: Doç. Dr. H. Emrah Ünal

Eylül 2013, 84 sayfa

Bu tez çalışmasında plazmonlarla ışık hapsedilmesi yöntemiyle güneş gözelerinde verimlilik artırma üzerinde çalışılmıştır. Çalışma esnasında plazmonlar topaklanma yöntemiyle düz ve yüzeyi şekillendirilmiş güneş gözesi üzerinde kendiliğinden oluşturulmuştur. Metal nano parçacıklar güneş gözelerindeki aktif bölgede ışıkla güçlü şekilde etkileşerek gelen ışığın yüzeyde verimli bir şekilde yayılmasına sebep olmaktadır. Topaklanma ile kendiliğinden metal nano parçacık oluşumu geniş alanlara kolayca uygulanabilirliği açısından başarılı bir yöntemdir. Bu yöntem, metal kaplama ve ısıtma işlemi uygulanmasıyla metal nano parçacık üretimine dayandığı için ucuz üretim tekniklerindedir. Bu çalışmada, güçlü rezonans özelliği gösterdiği için gümüş tercih edilmiştir. Yerel plazmon salınımlarını incelemek için düz ve yüzeyi şekillendirilmiş güneş gözelerinde yansıma deneyleri yapılmıştır. Yansıma ölçümleriyle parçacık boyutunun, topaklanma süresinin ve yansıma engelleyici katman olarak kullanılan Silikon Nitrat ( $Si_3N_4$ ) kalınlığının plazmon rezonansı üzerindeki etkileri gözlemlenmiştir. Yüzey pürüzlülüğü, tavlama süresi, tavlama sıcaklığı ve Silikon Nitrat kalınlığı değiştirilerek güneş gözesi verimliliği araştırılmış ve metal nano parçacık boyutu kontrol edilmiştir. Kullanılan yöntemle oluşturulan en uygun metal nano parçacık sisteminin üretilmesinin uygulanabilirliğinin özelliklerine bağlı olduğu görülmüştür. Yürütülen çalışmanın diğer araştırmalara ve yüksek verimlilikte güneş gözesi oluşturmada yol gösterici bir rolü olacaktır.

**Anahtar Kelimeler:** Plazmonlar, Güneş Gözeleri, Topaklanma, Verimlilik, Yansıma, Saçılma

*To my family,  
Those who showed me the path of intellectual pursuits*

## ACKNOWLEDGEMENTS

I would like to express my sincere gratitude to my advisor Assist. Prof. Dr. Alpan Bek for the continuous support of my thesis study and research, for his patience, motivation and immense knowledge. Also I would like to thank Assoc. Prof. Dr. Emrah. Ünalın for his cooperation in studies.

I am thankful to Prof. Dr. Raşit TURAN for giving us the opportunity of working in GÜNAM lab and for his continuous support.

Very special thanks to Seda Kayra Güllü , Yusuf Kasap, Hisham Nasser, Firat Es, Mete Günöven my dear colleague, which assist and help me in all parts of this study. I am also thankful to Yeganeh Bagi, Fariba Yousefi and Negin Bagherzadi that helped me and always supported me. I would also like to thank Prof. Dr. Mehmet Parlak, Engin Özkol, Mürat Öztürk, Elif Sarıgül, Emine Hande Çiftımar, Burcu Altuntaş, Olgu Demirciođlu, Zeynep Demirciođlu, Gülsen Baytemir, Hasan Hüseyin Güllü, Amir Onsori, Parisa Sharif, Salar Habibpour, Iman Ashtiani, Touraj Farsadi and all members of the Center for Solar Energy Resaerch and Application (*GÜNAM*) for their support and friendship. Also, for SEM sessions, I would like to thank METU Central Lab. (MerLab).

I am thankful to my colleagues and the staffs in METU, Physics, Lab.118 for their support and understanding.

Finally, I would like to express my endless thanks and motivation, enthusiasm and gratitude to my mom and dad and supporting me throughout all my life. Without their love, patience i would not have been able to complete this thesis.

## TABLE OF CONTENTS

ABSTRACT .....	v
ÖZ .....	vii
ACKNOWLEDGMENTS .....	ix
TABLE OF CONTENTS .....	x
LIST OF LABELS .....	xii
LIST OF FIGURES .....	xiii
LIST OF ABBRIVATION .....	xv
CHAPTERS	
1. INTRODUCTION .....	1
1.1. History .....	2
1.2. State of the art .....	2
1.3. Introduction to Photovoltaics Technology .....	3
1.4. Photovoltaics Market .....	4
1.5. Types of Solar Cell .....	5
1.5.1. Bulk Crystalline Solar Cells .....	5
1.5.2. Thin Film Solar Cells .....	5
1.5.3. Organic Solar Cells .....	6
1.5.4. Dye Sensitized Solar Cells .....	6
1.6. Plasmonics of Photovoltaics Application .....	6
1.7. Organization of the Thesis .....	9
2. SEVERAL THEORIES ON THE OPTICAL PROPERTIES OF METAL NANOPARTICLES .....	11
2.1. Cross section of scattering, absorption and extinction by small particles .....	11
2.2. Absorption and scattering of spherical MNPs .....	13
2.3. Theories of optical response of MNPs .....	15
2.4. Electro Static Theory .....	15
2.5. Mie Theory .....	18
2.6. The Dielectric Function $\epsilon(\omega)$ .....	20
2.7. Drude Model .....	21
2.8. Lorentz Model .....	22
2.9. Lorentz- Drude Model .....	23
2.10. Solar Irradiation .....	24
2.11. Single Crystal Silicon Solar Cell Structure .....	25
2.12. Single Crystal Solar Cell Operation .....	26
2.13. Basic Photovoltaics Cell Parameters .....	27

3. EXPERIMENTAL METHODS.....	35
3.1. Fabrication methods .....	35
3.1.1. Fabrication of Mono Crystalline Silicone Solar Cell .....	35
3.1.2. Saw Damage Etching (Removal) .....	36
3.1.3. Surface Texturing .....	36
3.1.4. Pre Diffusion Cleaning .....	37
3.1.5. P-N Junction Formation .....	37
3.1.6. Silicon Nitride Coating .....	38
3.1.7. Metallization .....	41
3.1.8. Laser Edge Isolation .....	41
3.1.9. Sputtering System .....	43
3.1.10. The Dewetting Techniques .....	45
3.1.11. Image Analysis .....	48
3.2. Optical Characterization .....	49
3.2.1. Reflectance Measurement Set up .....	49
3.3. Electrical Characterization .....	51
3.3.1. I-V Characterization Set up .....	51
3.3.2. Quantum Efficiency Set up .....	52
4. RESULT AND DISCUSSION .....	55
4.1. Optical Reflection Results .....	55
4.2. Formation of AgNPs by Dewetting Techniques .....	59
4.3. Effect of Temperature on Cell Efficiency of Full Scale Device Without Silver Deposition .....	64
4.4. Quantum Efficiency .....	64
4.5. FWHM and Resonance Peak Position for Both Flat and Textured Silicon without Silicon Nitride .....	69
4.6. Results of Cell Performance Measurement by I-V Characterization .....	70
5. CONCLUSION .....	79
REFERENCES .....	81

## LIST OF TABLES

### TABLES

Table 1. Comparison of the Cell efficiency for flat silicon before and after edge isolation	.42
Table 2. Characteristics of flat and textured silicon solar cells having various silicon nitride film thickness with and without AgNPs .....	77

## LIST OF FIGURES

### FIGURES

Figure 1.1 Evolution of global photovoltaic cumulative installed capacity 2000-2012(MW) [25].....	4
Figure 1.2 Light trapping (a) by scattering from MNPs (b) by excitation of LSP in MNPs ...	7
Figure 2.1 The incident electromagnetic field( $E_i, H_i$ ) gives rise to field inside( $E_1, H_1$ ) and scattered ( $E_s, H_s$ ) of the particle .....	12
Figure 2.2 Shift of the free electron relative to the nuclei leads to plasmon oscillation .....	13
Figure 2.3 Surface Plasmon Polariton .....	14
Figure 2.4 LSP is confined by electromagnetic field.....	14
Figure 2.5 Interaction of incoming light with spherical MNP.....	15
Figure 2.6 Sphere particle in uniform electric field.....	16
Figure 2.7 Illustration of the free electron motion under an external electric field in a Drude model .....	21
Figure 2.8 The spectral of power density of sunlight at AM1.5 & AM0 [37] .....	24
Figure 2.9 Basic schematic of a single crystalline solar cell fabricated .....	26
Figure 2.10 (a) Absorption of incident photon by electron with $h\nu > E_g$ (b) Generation of electron-hole pair .....	26
Figure 2.11 The generated charge carriers (a) before separation (b) after separation .....	27
Figure 2.12 I-V characteristics of solar cell in the dark and under illumination .....	28
Figure 2.13 Current versus voltage curve under illuminated condition.....	28
Figure 2.14 An example of I-V characteristics of photovoltaic cell [38] .....	29
Figure 2.15 The real and ideal current versus voltage curves.....	30
Figure 2.16 Current versus voltage (I-V) and power curve of photovoltaic.....	31
Figure 2.17 I-V characteristic of a solar cell. A drop in the series resistance and an excess in shunt resistance give rise to an increase in the total output of the cell [40] .....	32
Figure 2.18 The external and internal quantum efficiencies as a function of wavelength measuring at GÜNAM center for this study .....	33
Figure 3.1 The production process steps of a mono crystalline solar cells.....	35
Figure 3.2 Reflection of incident light: (a) Flat silicon and (b) Textured silicon .....	36
Figure 3.3 Effect of KOH etching on the formation of pyramid structure .....	37
Figure 3.4 The schematic of p-n junction solar cells .....	38
Figure 3.5 Use of ARC leads to be destructive interference with no reflected light .....	39
Figure 3.6 The schematic representation of silicon nitride deposition by PECVD system ...	40
Figure 3.7 The image of metallization device at GÜNAM.....	41
Figure 3.8 Schematic of the solar cell fabrication (a) before and (b) after edge isolation. ....	42
Figure 3.9 Schematic diagram of the sputtering systems.....	44
Figure 3.10 The samples after silver deposition by sputtering .....	45
Figure 3.11 Specially Design Annealing Chamber for Solar Cells devices .....	46
Figure 3.12 Formation of liquid droplet NP into substrate according to Rayleigh capillary instability .....	47
Figure 3.13 Analysis steps for SEM images: (a) In the SEM image, first grains marking by threshold and reject grains with size less than $10 \text{ px}^2$ and the grains at edge are removed	

from the mask (b) The surface coverage of NPs directly are derived from the statistics on grain radius (c) Gaussian fit are applied on statistics.....	48
Figure 3.14 Schematic diagram of the reflectance measurement setup .....	50
Figure 3.15 Diffuse and Specular reflection of light from surface .....	51
Figure 3.16 Schematic diagram of I-V characterization .....	51
Figure 3.17 I-V characteristic with equivalent circuit of photovoltaic cell under dark condition .....	52
Figure 3.18 I-V characteristic with equivalent circuit of photovoltaic cell under illumination .....	52
Figure 3.19 Schematic diagram of the QE measurement setup .....	53
Figure 4.1 Reflection behavior from AgNPs at different time dewetting for flat Silicon with 10 nm silicon nitride thicknesses .....	55
Figure 4.2 Reflection behavior from Ag NPs at different time dewetting for flat Silicon with 75 nm silicon nitride thicknesses .....	56
Figure 4.3 Reflection behavior from Ag NPs at different time dewetting for textured Silicon, with 10 nm silicon nitride thickness .....	57
Figure 4.4 Reflection behavior from Ag NPs at different time dewetting for textured Silicon, with 75 nm silicon nitride thickness .....	58
Figure 4.5 Reflection of incident light from (a) textured substrate, (b) flat substrate.....	58
Figure 4.6 Representation of Ag NPs fabricated on 10 nm silicon nitride, with 30 minute dewetting time at 200 °C.....	59
Figure 4.7 Representation of Ag NPs fabricated on 75 nm silicon nitride, with 30 minute dewetting time at 200 °C.....	60
Figure 4.8 Influence of dewetting time on mean particle size .....	61
Figure 4.9 Influence of dewetting time on resonance peak positions .....	61
Figure 4.10 Scattering cross-sections obtained from size weighted average of Mie scattering theory with three different effective index models and experimental reflection data belonging to silicon surface decorated with Ag NPs of 70 nm mean diameter .....	63
Figure 4.11 Temperature study on solar cell device .....	64
Figure 4.12 EQE curves for flat silicon with different silicon nitride thicknesses before and after dewetting 2 hours @ 200 °C.....	65
Figure 4.13 EQE vs IQE curves for flat silicon with different silicon nitride thicknesses after dewetting 2 hours @ 200 °C .....	66
Figure 4.14 EQE curves for textured silicon with different silicon nitride thicknesses without Ag NPs and with Ag NPs produce by dewetting 2 hours @ 200 °C.....	67
Figure 4.15 EQE and IQE curves for textured silicon with different silicon nitride thicknesses after dewetting 2 hours @ 200 °C.....	68
Figure 4.16 EQE and reflection for flat silicon with 10 nm silicon nitride thickness.....	68
Figure 4.17 FWHM for both flat and textured silicon .....	69
Figure 4.18 Resonance peak position for both flat and textured silicon .....	70
Figure 4.19 I-V curves for flat silicon with different silicon nitride thicknesses with and without Ag NPs.....	71
Figure 4.20 I-V curves for textured silicon with different silicon nitride thicknesses with and without Ag NPs.....	71
Figure 4.21 I-V curves for textured and flat silicon with different silicon nitride thicknesses before and after dewetting .....	72
Figure 4.22 The open circuit voltage for both flat and textured silicon @ AM1.5G.....	73
Figure 4.23 The short circuit current for both flat and textured silicon @ AM1.5G.....	74
Figure 4.24 The fill factor for both flat and textured silicon @ AM1.5G.....	75
Figure 4.25 The cell efficiency for both flat and textured silicon @ AM1.5G.....	76

## LIST OF ABBVERATIONS

AgNP	Silver Nanoparticle
AuNP	Gold Nanoparticle
NP	Nanoparticle
SEM	Scanning Electron Microscopy
KOH	Potassium Hydroxide
FDTD	Finite Difference Time Domain
SERS	Surface Enhanced Raman Spectroscopy
DDA	Discrete Dipole Approximation
DSSC	Dye Sensitized Solar Cell
SPP	Surface Plasmon Polariton
LSPP	Localized Surface Plasmon Polariton
AM	Air Mass
ARC	Anti Reflection Coating
FWHM	Full Width at Half Maximum
EQE	External Quantum Efficiency
IQE	Internal Quantum Efficiency
Si <sub>3</sub> N <sub>4</sub>	Silicon Nitride



## CHAPTER 1

### INTRODUCTION

In this work, our aim is to study the means of feasible external control parameters on self-organized production of plasmonic interfaces for full scale bulk silicon solar cells. The experimental findings that are obtained from well-known bulk solar cells in this study can be used to shed light toward applications of such self-organized production schemes to eventual plasmonic thin-film solar cells. The prime reason for incorporation of plasmonic interface layers in a solar cell device is to maintain a higher efficiency than the industry standard. Plasmonic interfaces are nanostructured two dimensional metal layers, such as a two dimensional array of metal nanoparticles (MNPs), that operate as an interface between the incoming radiation and the active region of a PV device. Such interfaces can be regarded as “impedance matching layers” between the solar radiation and a solar cell, by increasing the coupling, or decreasing the reflection and giving rise to signal amplification (enhancement), therefore act as “optical antenna”. In an equally valid alternate view, they can be regarded as light trapping layers giving rise to better photon management. Trapping of light (helping light stay longer in active solar cell layers) can lead to affordable solar cells with high efficiency by increasing the absorption and generating more photocurrent. The two main ingredients of nano-photon light trapping for solar cells are plasmon polaritons, which are coupled photons with collective oscillations of free electrons in noble metals, and high-refractive-index dielectrics, which have strong scattering and impedance matching capabilities. Plasmonic solar cell is one of the emerging solar cell technologies to enhance the optical absorption. In this thesis, silver was chosen due to the superior optical extinction properties than the other metals in the visible spectrum of light. Silver nanoparticles (AgNPs) lead to increase of the light scattering into the substrate.

In this study, both flat and textured bulk silicon cells are investigated in the full scale. Both kinds of cells are fabricated in multiplicity with varying dielectric anti-reflective coating (ARC) thickness. The plasmonic interfaces that are studied are fabricated by using the self-organized process of surface dewetting due to the ease of application and ease of integration of this technique to the state-of-the-art bulk solar cell production facility. In this technique, initially a several nanometer thick continuous silver film is deposited on a desired surface of choice, and the solar cell is treated thermally at elevated temperatures such that the atoms comprising the continuous silver film starts to diffuse and form holes, and dewet the surface. These holes in the silver layer eventually merge, giving rise to formation of liquid droplet shaped metal islands of a few to several tens of nanometer large sizes. As the process continues, small islands tend to disappear and the larger ones tend to grow in size by acquiring the atoms of the smaller ones, depicting a morphological coarsening process similar to Ostwald ripening [1].

Several optical and morphological parameters are analyzed by varying the dewetting time, the ARC thickness and annealing temperature. The effects of these variations are investigated on the formation of AgNP and their plasmon resonance. Effects of these AgNPs on the cell parameters such as fill factor, short circuit current, open circuit voltage and efficiency of both flat and textured full scale monocrystalline silicon solar cell devices are investigated.

### **1.1. History**

Optical behavior of metals alters when their dimensions are in the range of nanoscale structure than the bulk materials. Nowadays, MNPs are the important material used for guiding electromagnetic radiation. In detail, presence of MNP enhanced the optical path length of incoming light in the active cell areas. One of the most famous examples that demonstrate the subtle optical properties of MNPs in ancient times is the Lycurgus cup of Romans. The presence of the Au and AgNPs incorporated in the cup's body, show unusual optical behavior with different colors. The Au and AgNPs were used to color the glass windows in medieval churches during the middle ages. The work of Michael Faraday came out about 1500 years later, at 1857. He discovered the differences in the optical characteristics of bulk and colloidal MNPs. In particular, he recognized the significant dependence of the color of gold NPs (AuNPs) on their size [2]. In 1904, a theory by Maxwell and Garnett introduced the optical behaviors of MNP embedded in glass [3]. In parallel with experimental work, in 1908 Gustav Mie proposed the theory of interaction of light with MNPs by solving Maxwell's equations, supposing MNPs as spherically symmetric particles [4]. Mie theory is restricted to spherical MNPs. The developments in the controlled formation of MNPs in other geometries such as metallic disks and cylinders, led to advances in numerical methods for providing solutions applicable to these complex geometries. These analytical methods such as Finite Difference Time Domain (FDTD) and Discrete Dipole Approximation (DDA) have been developed rapidly with the advancement of computer technology. There are many applications of MNPs such as surface enhanced Raman scattering (SERS) and absorption of light enhancement that can be used to increase the device efficiencies. The plasmonic behavior of MNPs especially became more popular after invention of these applications [5]. A demand of MNPs for these applications has arisen because of the large electromagnetic field enhancement associated with these metallic nanostructures. The free conduction electron from a MNP oscillates in the presence of the electromagnetic field. In the case of Raman spectroscopy, large improvement factors as high as  $10^{14}$  from the silver and gold nano-aggregate cluster structures could be obtained. These large improvements allow Raman measurements of single molecules even under non-resonant conditions [6].

### **1.2. State of the art**

After the discovery of Raman scattering, plasmonic metal nanostructures became more important issue to generate highly light sensitive devices which increase efficiency. One of the first examples provided by Stuart and Hall, in which, they showed an enhancement in the photocurrent of a factor of 18 for a 165 nm thick silicon-on-insulator photo-detector at a

wavelength of 800 nm using AgNPs on the surface of the device created by dewetting technique [7]. Schaadt et al. deposited AuNPs on highly doped wafer-based solar cells, in which enhancements in the photocurrent up to 80% at plasmonic resonance wavelengths around 500 nm were demonstrated [8]. Derkacs et al. deposited AuNPs on thin film amorphous silicon solar cells, which improved short circuit current density and achieved an 8% overall increase in conversion efficiency [9]. Pillai et al. deposited silver particles on thick silicon-on-insulator with 1.25  $\mu\text{m}$  silicon solar cells and planar wafer with 300  $\mu\text{m}$  based cells, and reached overall photocurrent increases of 33% and 19%, respectively [10]. Applications and improvements by MNPs in other types of semiconductor solar cells than crystalline silicon appear in the literature. Scattering from metallic nanostructures were used to enhance the performance of amorphous silicon solar cells and conversion efficiency [11-13]. Stenzel et al. reported an enhancement in photocurrent by up to a factor of 2.7 for In:TiO<sub>2</sub> (ITO)-copperphthalocyanine-indium structures. West phalen et al. reported an enhancement for silver clusters incorporated in an ITO and zinc phthalocyanine solar cell [14]. Rand et al. have reported that incorporation of very small AgNPs in the range of approximately 5 nm diameter leads to enhancement in the efficiencies of tandem ultra-thin film organic solar cells [15]. Hägglund et al. show on flat TiO<sub>2</sub> films by combination of dye molecules and utilization of Au disks enhanced charge carriers generation for dye sensitized solar cells [16]. Hairen Tan et al. evaporated Ag layer with a thickness of 12 nm on thin film silicon solar cell, which was followed by a 1 hour anneal at 400 °C in a vacuum. The AgNPs were observed to form by self-assembly on both of textured and flat thin film silicon. Hairen Tan et al. achieved improved cell efficiency by using AgNPs as the plasmonic back reflector. AgNPs have excellent light trapping because of their strong light scattering property. AgNPs annealing at 400°C can reduce the surface coverage and eliminate small and irregular nanoparticles (NPs). As a result, by increasing the annealing temperature up to 400 °C, they obtained surface coverage smaller than 20% and particle size bigger than 100 nm. In texturing silicon solar cell, the high roughness surface of substrates increases the multiple reflections. Light trapping is a factor for improving the current density and cell efficiency. However, the addition of plasmonic NPs on textured silicon can be parasitic and result in large optical loss during multiple reflections. The presence of the AgNPs cause both scattering and absorption of incoming light. However, the effect of absorption cannot be denied as compared to the scattering. This absorption blocks the second order reflections from the surface of textured silicon. Therefore, this situation causes the decrease in the efficiency of solar cell, while in flat silicon with low roughness and smooth substrate, plasmonic NPs themselves can introduce excellent light trapping that leads to improvement of the current density and increase the cell efficiency with respect to the devices without NPs [17-23].

### **1.3. Introduction to the photovoltaics technology**

Nowadays a lot of research is being done on the topic of energy. Energy is critical due to the fact that depleting energy such as fossil fuels, will be exhausted in a close future by increasing in the exploiting and over usage of them. Even if we consider the population of the world to be fixed, fossil fuel reserves will be depleted within 320 years. Besides, recently using of fossil fuels caused the mother earth to be faced by serious problems such as global warming which is mostly due to the CO<sub>2</sub> emission. Consequently, we need a suitable alternative renewable energy such as solar energy. Solar cell and solar collectors can be considered as a part of the solar energy research area. In the solar cells direct conversion of

solar radiation into electricity is being done. This process can be described as a PV energy conversion which is due to the PV effect. Photovoltaic technology is based on silicon technology that contains both mono crystalline and multi crystalline forms of silicon. Dominance of these two types of silicon crystals in PV technology in comparison with other elements is due to abundance of the silicon in the earth crust and thorough information and knowledge about the properties of silicon (e. g. semiconductor) those are result of three decades research.

#### 1.4. The Photovoltaics Market

Recently, despite the difficult economic times that world has been faced, photovoltaics (PV) is considered as a dominant source of power generation for the world. As another word, PV technology has grown over the past decade at a remarkable rate.

The world’s cumulative installed PV capacity was approaching 24 GW, by the end of 2009. In 2010, this capacity enhanced to 40.7 GW and at the end of 2011 it was 71.1 GW. One year later, installed PV capacity was 100 GW [24]. Generally, this amount can generate at least 110 TWh of electricity each year which is enough to cover the annual power supply needs of over 30 million European households.

Europe can be consider as the first rank region from cumulative installed capacity point of view, with more than 70 GW as of 2012. This statistics illustrates about 70% of the world’s cumulative PV capacity. In this ranking china can be the second leading region with 8.3 GW, and, the next is USA with 7.8 GW, followed by Japan with 6.9 GW.

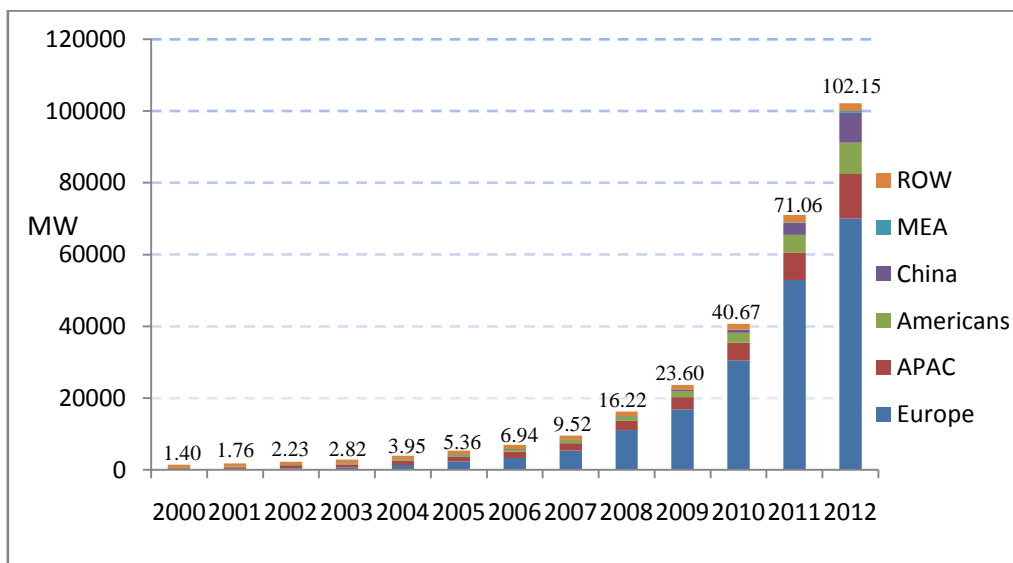


**Figure 1.1** Evolution of global PV cumulative installed capacity 2000-2012(MW) [25].

The forecasting about the PV market evolution over the next five years mostly related on the maintenance of the market conditions at an acceptable level and developments in Europe. From one other point of view though Europe can be considered as the leading region for PV market for years ,the rest of the world, obviously, has the biggest potential for growth which was declared by market developments that showed Europe’s share of the global market being reduced from 74% in 2011 to 55% in 2012.

## **1.5. Types of Solar Cells**

### **1.5.1 Bulk Crystalline Solar Cells**

Development of solar cell technology can be classified by the composition of material in the active layer. Historically, crystalline Si (c-Si) has been the dominant semiconductor for solar cell. This type of PV cells is known as “first generation cells” which are bulk crystalline silicon based technologies. As we all realize, silicon is second most wide element in Earth’s layer. For this reason, silicon was widely used in the earliest PV devices. It is also very popular today. Nevertheless, if silicon is used as semiconductor material, the most important point is that the usage of it should be in 99.999 % purity.

Then, crystalline solar cells can be divided into two kinds with respect to their crystal structure. The first kind is single-crystalline solar cell which is also called as monosilicon. In detail, silicon is in the same crystal form from one side to another. This creates an opportunity to generate very effective solar cell devices, especially, when compared with respect to ratio of power to size. Their efficiencies are about within the range of 135 to 170  $W/m^2$ . Moreover, they have long life span and exhibit magnificent performance in cooler conditions. The second kind of crystalline solar cell is multicrystalline. It is less efficient solar cell compared to the single crystalline. However, it is cheaper than single crystalline because it is produced by easier methods. For this reason, they are preferred in spite of their lower efficiencies which are about within the range of 120 to 150  $W/m^2$ . Furthermore, they show better performance in hot weathers and they have long life span like single crystalline.

To generate solar panels, these kinds of solar cells are connected in series form. Each cell produces 0.5 to 0.6 V. Hence, 20 open-circuit voltage values are acquired by 36 cells. For example, this value is effective to fill 12 V batteries.

### **1.5.2 Thin Film Solar Cells**

This type of PV cells is known as “second generation cells” which are made of several hundreds of nanometers to several microns thickness optically thin-film based technologies. Almost every people use or see calculators or garden lamps which are powered by thin and small cells. It can be easily understood that thin film solar cells get its name by its appearance and size. While crystalline solar cells have about 350  $\mu m$  thickness, thin film solar cells have just a few microns thickness which is enough to absorb light. The basic principle of the production of it depends on light-absorbing materials like amorphous, protocrystalline and nanocrystalline coated onto such substrates like glass, metal or plastic by chemical depositing process. Because of the high absorption performance exhibition of semiconductor materials, thin film solar cells much thinner. As a result, they are cheap and not heavy.

Besides their appearance and cost effectiveness, when describing the efficiency of thin film solar cells, they produce 60 to 80  $W/m^2$ . In other words, they have lower efficiencies than crystalline solar cells. This means that they need large areas compared to crystalline to get same amount of energy. Moreover, slightly lower life span and less effectiveness in cooler conditions are another drawbacks of them.

### 1.5.3 Organic Solar Cells

An organic solar cell is a “third generation solar cell” that contains organic, electronic conductive polymers and small molecules for the absorption of light and electric charge transportation. These high effective thin layers that are used absorb the light and convert it directly to the electric energy. Therefore, organic solar cells cost lower than other types of solar cells. Moreover, being thinner creates an opportunity that it is possible to produce large scale capability with flexibility. In contrast to benefits, organic solar cells have lower efficiency and strength than other types of solar cells.

### 1.5.4 Dye Sensitized Solar Cells

The last one is dye sensitized solar cells (DSSC). It can be described as one of the latest solar cells technologies. In this type of the solar cells, the main important point is focusing on using organic molecules instead of using polymers with nanocrystal conductive structures. One of the most widespread crystal structures in DSSC is  $TiO_2$ .

There is a connection between  $TiO_2$ NPs and dye molecules. When the light interacts with the cell, adsorbed dye molecules pass the excited state. Then, dye molecules which is in the excitation period creates an impact on an electron that moves forward direction to the conduction band of  $TiO_2$ . After this transmission period, they reach the transparent electrode and join the external circuit. This is the basic working principle of DSSC. Describing cell as a one piece, because of easy production methods, they are mostly preferable in spite of less efficiency which is about 10 %. Furthermore, possibility of colorful production of DSSC makes them more esthetic than other types of solar cells [26].

## 1.6. Plasmonics for photovoltaic applications

Up to now we have investigated the interaction of incoming light with spherical MNPs from a general point of view. In this section we describe application of plasmonic for PV.

Plasmonic is a wide area of study which is used for increasing the light absorption that leads to increase the optical path length of photon in surface by using MNPs. Interaction of incoming electromagnetic wave with free conduction electron in MNPs lead to plasmon oscillation around the nanostructure which introduce very strong resonance phenomena at particular frequency that gives rise to very strong scattering.

Absorption and scattering of incident light from MNPs can be used to obtain light trapping effect. Light trapping is important factor for achieving higher energy conversion efficiency as the light settles more time within the active layer. MNPs can be used in two basic mechanisms in PV application, which are called far-field effect and near-field effect. Far-field effect consists of light scattering from the metal particles into the active layer of solar cell which behave as dipole; whereas, near-field effect is the field enhancement in the close surrounding of MNPs.

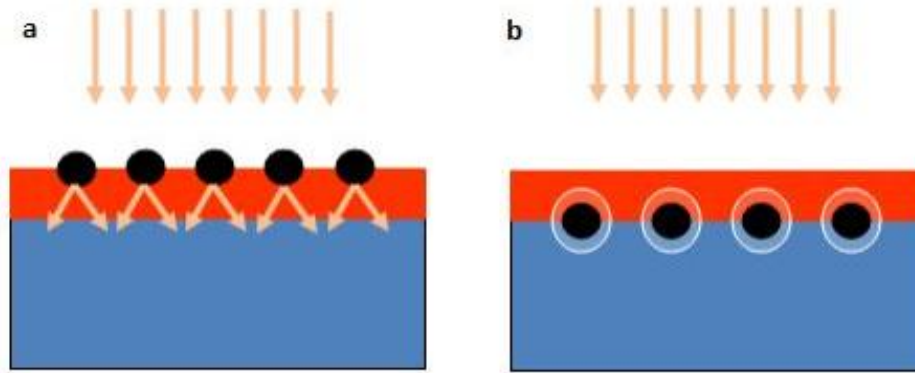


**Figure 1.2** Light trapping (a) by scattering from MNPs (b) by excitation of LSP in MNPs

In previous chapter we discussed the process of scattering of light by a particle in a general case by considering the environment and a uniform nanoparticle. In the following section, the scattering property will be discussed when the particle is located close to the interface. When a particle is located in a uniform medium, the scattering of the incoming light would be both in forward and reverse direction in a symmetrical manner. Due to the fact that the medium around the particle is not uniform, this symmetry is disturbed. Nanoparticles for solar cell applications are embedded on a surface which is among two interfaces of dielectrics, or in a dielectric with interfaces to active region of the cell. The fact that dielectric with higher permittivity makes the light to scatter in it, is considered as an advantage in most solar cell applications [27]. The tendency of the scattering of light into the medium with high index is due to the high density of optical modes in those mediums.

Light scattering from MNPs, scatter incident light into multiple reflections can enhance the travel optical path length of photon in absorber layer which lead to improved light trapping into solar cells devices. On the other hand if we consider the surface without plasmonic NPs, incident light will be partially reflected back and path length will be the thickness of the substrate. However, the existence of plasmonic NPs that are used to scatter the incoming light can lead to increase the optical path length of photon in the solar cell device. The scattering efficiency of NPs depends on the particle size, refractive index of underlying and surrounding environment. There are different MNPs with various scattering efficiency. In this study, silver is used as MNPs because of the lowest absorption coefficient than the other metals [28-31].

The second mechanism, when MNPs are excited with incoming light, the free conduction electrons in the MNPs oscillate collectively. The resonance condition occurs when the frequency of incoming light matches with that frequency of the oscillation. These electrons give rise to the electric field in the vicinity of the MNPs which is placed inside the active layer known as near field effect. It causes improvement of the photocurrent and absorption of light.

For effects of plasmonic process, far- field effect and near-field effect mechanisms would be discussed. In far- field effect scattering of the light to far zones. On the other hand in the near-field effect mechanism, the incident electromagnetic wave can be coupled into plane waveguide modes in the photoactive material. Therefore, an electron-hole pairs in the underlying semiconductor would be excited by the enhanced localized near field that was made around the nanoparticle. This excitement can be even generated without phonon

assistance in the indirect band structure. In this mechanism, nanoparticles can be considered as an effective optical antenna for the incident irradiation. Though this is an advantage, this mechanism is beneficial for nanoparticles below 20 nm in diameter, due to the lower fraction of light emitted as radiation in them [27].

The far-field application relies on the diffusion length of the carriers those are generated. Carrier diffusion length should be larger than the distance of the p-n junction to the electron-hole pairs collecting around nanoparticles; if this condition is not satisfied, generated carriers would get lost before being collected by the p-n junction. This quite should be recited that it is almost impossible to locate the nanoparticles in the close vicinity of a p-n junction to make use of the far-field effects.

Besides, the Plasmon decay time reciprocal should be smaller than the absorption rate in the underlying layers. Otherwise the absorbed energy is dissipated in the metal nanoparticle as ohmic damping.

In this study due to the reasons discussed above, the far field effect of metal nanoparticles was investigated.

## 1.7. Organization of the thesis

This thesis consists of 5 chapters as follows:

In chapter 1, we briefly give review about an introduction of the fundamentals of plasmonics of MNPs, the aim of this thesis study and the outline of the thesis.

In chapter 2, we describe the interaction of incoming light with MNPs. The dielectric function was expressed by using two models which are Drude and Lorentz models. The dielectric function of metals at the particular frequency yields resonance phenomenon. This condition gives rise to very strong light scattering. Moreover, absorption and scattering of incoming light from MNPs are calculated by using two approaches, namely electrostatic and Mie theories. These theories are discussed for spherical MNPs. A short introduction about the solar cell working principles and cell parameters of the plasmonic solar cell application are provided in this chapter.

In chapter 3, we present the main fabrication and optical and electrical characterization methods used throughout this study. As the fabrication methods, solar cell production steps are explained and dewetting approach for the formation of MNP based plasmonic interfaces is introduced as a suitable method for production of plasmonic full scale solar cell devices. The SEM image analysis of NPs was done to characterize the shape, size and surface coverage. The experimental set up for the optical and electrical measurements are described in detail in this chapter.

In chapter 4, the experimental results are provided and discussed. For the optical characterization, the reflection measurements were used to investigate the resonance peak position of MNP plasmons and general reflectance properties of plasmonic interfaces. The SEM image analysis of AgNPs enables us to study the effect of the particle dimensions after dewetting the samples at different times. Therefore image analysis gives an idea and information about the particle surface coverage, size distribution and dimensions of the particles. The electrical characterizations include current-voltage (I-V) characteristics under illumination, cell parameters that are extracted by I-V curves and quantum efficiency (QE) which is discussed for full scale large area solar cells.

In chapter 5, the results and discussions of this thesis work are summarized and we present the main conclusions.



## CHAPTER 2

### SEVERAL THEORIES ON THE OPTICAL PROPERTIES OF METAL NANOPARTICLES

In this chapter the optical properties of MNPs which are widely used in plasmonic application as light-trapping leading to an improvement of the optical path length of incident photon in the solar cell device are theoretically introduced. The absorption and scattering of incident light by particles are most important process for solar cell operation to achieve enhancement of the cell efficiency. Hence some basic physical theories are defined to explain the plasmonic concepts and their applications. In the last part of this chapter the basic solar cell working principle and the solar cell parameters are defined.

#### 2.1. Cross sections of scattering, absorption and extinction by small particles

In order to understand the optical properties of particles with interaction of light, two mechanisms namely scattering and absorption must be considered. From a general point of view, scattering from particles in any system is investigated from heterogeneity of that system. The obstacle in that system is considered as a single electron, an atom, a liquid or solid particle which is subjected to electromagnetic wave. Regardless of the type of the obstacle, they can be considered as a matter containing of electrons and protons. When the obstacle is illuminated by electromagnetic field, the electric charge in it causes oscillation motion with electric field of the incident light. Acceleration of electric charge in the obstacle by radiating electromagnetic energy leads to the scatter of incident lights as a secondary radiation in all direction and that can be defined as:

$$\textit{Scattering} = \textit{Excitation} + \textit{Reradiation}$$

In addition of scattering, one other mechanism takes place in the obstacle. Some part of the excited charges when is subjected to incident light transform into other types of energy named as thermal energy. This mechanism called as absorption. Both of two scattering and absorption mechanisms considered as dependent together. Scattering and absorption depend on structure of particle when it encounters illumination. Both of these processes behave differently from each other. Scattering and absorption depends on shape, size, structural composition and optical properties of material.

When electromagnetic wave passes through the particle, scattering and absorption by particle remove energy from incident radiation of light leads to attenuation of incident light. This attenuation is called as extinction [32].

It means that the energy change when the light passes through the particle due to the extinction, so the relation across the energy transfer is represented:

$$\textit{Extinction} = \textit{Scattering} + \textit{Absorption}$$

The incoming electromagnetic field when interacts with the particles, affects the field inside the particle which is defined as  $(E_1, H_1)$  and the field in the surrounding medium  $(E_2, H_2)$ . The incident and the scattered field respectively are represented by  $(E_i, H_i)$  and  $(E_s, H_s)$ . The figure 2.1 illustrates the interaction of incident light with the particle.

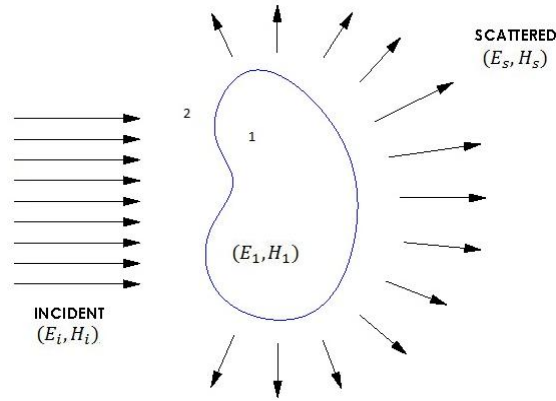


**Figure 2.1** The incident electromagnetic field  $(E_i, H_i)$  gives rise to field inside  $(E_1, H_1)$  and scattered  $(E_s, H_s)$  of the particle

Maxwell equations must be satisfied by considering electromagnetic field where  $\epsilon$  and  $\mu$  belong to continuous medium. However, generally there is a boundary between the particles and medium in which the particles properties such as  $\epsilon$  and  $\mu$  suddenly change due to the discontinuity formed at the boundary between the particle surface and medium. For this condition the field satisfies the following equation:

$$[\vec{E}_2(x) - \vec{E}_1(x)] \times \hat{n} = 0 \quad 2.1.1$$

$$[\vec{H}_2(x) - \vec{H}_1(x)] \times \hat{n} = 0 \quad 2.1.2$$

Boundary conditions between interface of the particle surface and the medium according to equation above explain that the tangential components of E and H are continuous. In addition, the rate at which electromagnetic energy is transferred through a closed surface near region 1 and region 2 are defined as the following equation:

$$\int \vec{S}_1 \cdot \hat{n} dA = \int \hat{n} \cdot (\vec{E}_1 \times \vec{H}_1) dA \quad 2.1.3$$

$$\int \vec{S}_2 \cdot \hat{n} dA = \int \hat{n} \cdot (\vec{E}_2 \times \vec{H}_2) dA \quad 2.1.4$$

Where 1 and 2 are represented the inner and outer surface. If the conservation of energy across the boundary is equivalent to this condition, therefore:

$$\int \vec{S}_1 \cdot \hat{n} dA = \int \vec{S}_2 \cdot \hat{n} dA \quad 2.1.5$$

For a particle that is subjected in a medium to illumination, the power energy is given by the change after passing from the particle due to scattering and absorption by particle. The relation between these processes under energy transfer rate is given by this equation:

$$W_{ext} = W_a + W_s \quad 2.1.6$$

Optical cross section is defined as ratio of the energy rate to the incident illumination. Extinction, absorption and scattering cross sections are important parameters in plasmonic concept. The relations between these parameters are given by following equations [33]:

$$C_{ext} = \frac{W_{ext}}{I_i}, C_{abs} = \frac{W_{abs}}{I_i}, C_{sca} = \frac{W_{sca}}{I_i} \quad 2.1.7$$

$$C_{ext} = C_{abs} + C_{sca} \quad 2.1.8$$

In this section the absorption and scattering processes by particles are investigated. For the next section the interaction of spherical MNPs with electromagnetic wave is discussed.

## 2.2. Absorption and scattering of spherical MNPs

The interaction of MNPs with electromagnetic wave is determined by the free conduction electrons in the metal. When MNPs interact with incoming light charge polarization takes place in MNPs due to the presence of free conduction electrons. The electrons move in the opposite direction of the electric field and leaving behind the positive ion cores on the other side of MNPs. When the direction of the electric field alters, direction of charge polarization gets reverses. They act as opposite direction from each other. Figure 2.2 is illustrates the MNPs when interact with incident electromagnetic wave.

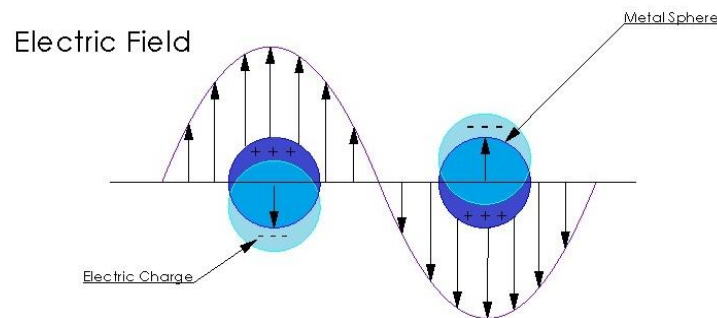


**Figure 2.2** Shift of the free electron relative to the nuclei leads to plasmon oscillation

The presence of the free conduction electrons in the MNPs leading to the collective oscillation due to the interaction of incoming light is called plasmon. There are two types of plasmons named as surface plasmon polariton (SPP) or localized surface plasmon (LSP). These plasmons when coupled with incoming photon are called polaritons.

SPP occurs when the free conduction electron in metal surface couples with incoming light between the metal-dielectric interfaces. With respect to the surface charges, the electromagnetic wave propagates along interface of metal and dielectric material. Oscillation of electromagnetic wave will induce collective oscillation of surface charges at the metal-dielectric interfaces.

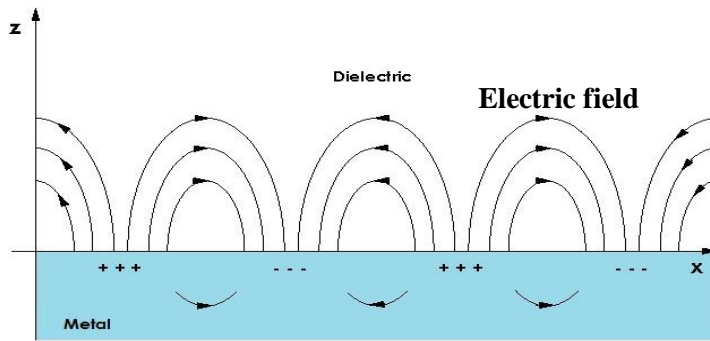


**Figure 2.3** Surface Plasmon Polariton

In this work, we investigate the effect of LSP on substrate. Interaction of MNP with the electromagnetic field occurs at the interface between the MNP and the dielectric. The electromagnetic wave is confined in all 3 dimensions, hence gives rise to LSP.

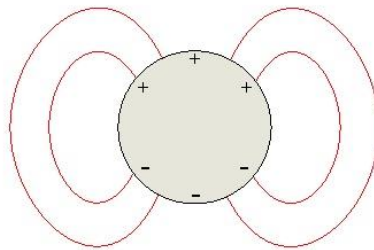


**Figure 2.4** LSP is confined by electromagnetic field

Excitation of free conduction electron in metallic NP with the incident light at particular frequency introduces very strong resonance and gives rise very strong scattering. The resonance phenomenon occurs when the frequency of incident light matches with the natural frequency of the electrons in the particle. Electrons oscillate opposite direction with respect to the positively charged nuclei.

The frequency of oscillation depends on the density of electrons, the shape and the size of the charge distribution. The collective oscillation depends on the size of the MNPs. This oscillation is either coherent or incoherent. If the particle size much smaller than the wavelength of incoming light, the oscillation is coherent. With the increasing ratio of particle size over wavelength, the incoherent oscillation will occur. Furthermore, dipole modes are mostly seen in coherent oscillation while the higher other modes can exist in incoherent oscillation.

The plasmon resonance also leads to enhance the charge separation because of the dipole effect, which in result into giving rise the two important factors:

1. Increase the total extinction of light, can be quantified by sum of scattering and absorption
2. Increase the electric near field vicinity of particle

Both of these factors depend on shape, size distribution and dielectric medium surrounding the particle.

In the following sections, the optical responses of the spherical particles are evaluated with two basic theories, which are electrostatic and Mie theory according to size of the spherical metal particles.

### 2.3. Theories of optical response of MNPs

First of all we give a brief introduction about the MNP when encounter with incident light. Afterward we investigate the quasistatic approximation for the optical response of MNP which dimensions are much smaller than the electromagnetic wave. With this theory we can determine the condition to get LSP. Then we investigate Mie theory that can be used for spherical NPs that can have dimension in any size. In the last section we define the dielectric function of MNPs.

The optimum quantities of scattering theory for MNPs are possible for restricted scales and light which is confined in spherical shapes. As we discussed already, there are two important theories in electromagnetism related to scattering of MNP for restricted scales and light confined in spherical shapes when interact with incident light, respectively electrostatic theory and Mie theory. The theories and approximation are investigated in the following section. The figure below demonstrates when the electromagnetic field encounters with spherical metal interaction of free conduction electron with the incident light induces oscillation at the particular frequency with respect to the positive ions in the lattice creating an oscillating charge at the surface of particle. If the frequency of collective oscillation is in resonance with the frequency of the electromagnetic wave, due to the exciting field create strong oscillation. When the dimension of NPs is much smaller than the excitation wavelength, surface charges carriers because of interaction with incident wavelength behave as dipole and leads to oscillating due to the strong electric field in the close vicinity and inside of the particle.

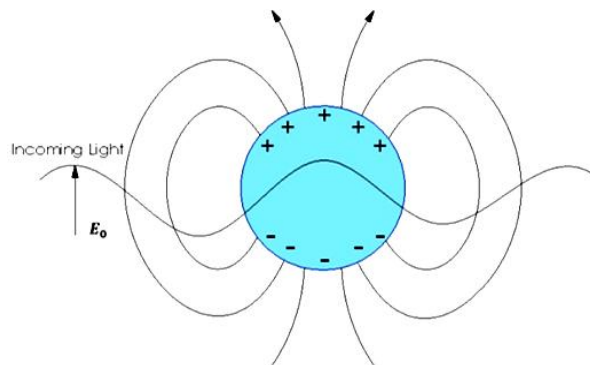


**Figure 2.5** Interaction of incoming light with spherical MNP

### 2.4. Electrostatic theory:

The optical response of MNPs in which the radius of the sphere is much smaller than the incident wavelength ( $R \ll \lambda$ ) can be calculated by electrostatic approximation. In this approach, the electric field of incoming light is considered as constant; therefore, the electric field of incident light as given in 2.6 is represented as  $E_0$  in the z-direction.

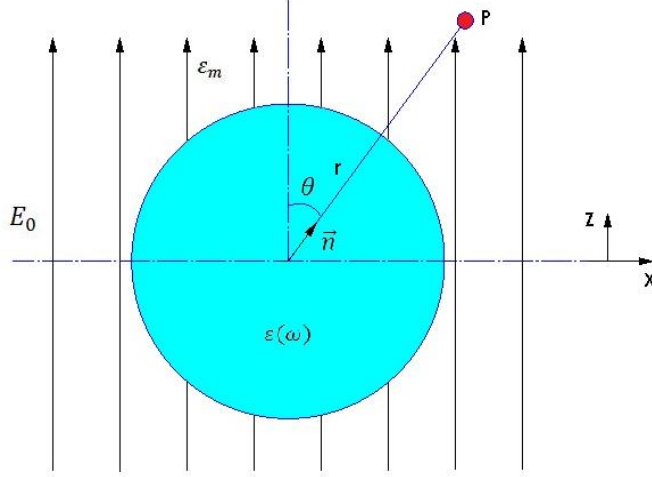


**Figure 2.6** Sphere particle in uniform electric field

As we discussed, this approximation occurs when the structures of NPs have spatial dimensions much smaller than wavelength. It implies that electromagnetic field is static, has no retardation effects. For calculation of electromagnetic field outside and inside of particle, the Laplace's equation, which is the fundamental equation in electrostatics, should be solved in spherical system [34]:

$$\frac{1}{r^2} \frac{\partial}{\partial r} \left( r^2 \frac{\partial \phi}{\partial r} \right) + \frac{1}{r^2 \sin \theta} \frac{\partial}{\partial \theta} \left( \sin \theta \frac{\partial \phi}{\partial \theta} \right) + \frac{1}{r^2 \sin^2 \theta} \frac{\partial^2 \phi}{\partial \varphi^2} = 0 \quad 2.4.1$$

In this approximation, the potential  $\phi$  in the surrounding of environment is the sum of the potential related to electric field by  $E = -\nabla\phi$  that should satisfies Laplace's equation

$$\nabla^2 \phi = 0 \quad 2.4.2$$

The general solution for electrical potential is written by following equation:

$$\phi(r, \theta) = \sum_{l=0}^{\infty} [A_l r^l + B_l r^{-(l+1)}] P_l(\cos \theta) \quad 2.4.3$$

Where  $P(\cos \theta)$  is associated with the  $L^{th}$  order Legendre polynomial, and  $\theta$  is the angle between the z-axis and position vector  $r$  at point P with respect to the figure 2.4.1. The boundary condition implies a finite potential energy value at the origin. By taking the potential  $\Phi_{in}$  inside and  $\Phi_{out}$  outside of the sphere, equation can be written as:

$$\Phi_{in}(r, \theta) = \sum_{l=0}^{\infty} A_l r^l P_l(\cos \theta) \quad 2.4.4$$

$$\Phi_{out}(r, \theta) = \sum_{l=0}^{\infty} [B_l r^l + C_l r^{-(l+1)}] P_l(\cos \theta) \quad 2.4.5$$

The potential outside of the sphere is  $\Phi_{out} = \Phi_s + \Phi_0$  in which  $\Phi_s$  is the scattering potential,  $\Phi_0 = -E_0 z = -E_0 r \cos \theta$  is the external potential and the potential inside the sphere is  $\Phi_{in}$  must satisfy boundary condition at the surface of the sphere.

Two boundary conditions for the inside and outside of the sphere are essential for the exact solution. Hence, both of conditions should be applied at both regions with respect to the potential constraints.

$$\left[ \frac{\partial \Phi_{in}}{\partial \theta} \right]_{R=r} = \left[ \frac{\partial \Phi_{out}}{\partial \theta} \right]_{R=r} \quad 2.4.6$$

$$\varepsilon_{in} \left[ \frac{\partial \Phi_{in}}{\partial r} \right]_{R=r} = \varepsilon_{out} \left[ \frac{\partial \Phi_{out}}{\partial r} \right]_{R=r} \quad 2.4.7$$

Where  $r$  is the sphere radius,  $\varepsilon_{in}$  and  $\varepsilon_{out}$  are the dielectric constants of the spherical particles and the environment, respectively.

By utilizing these equations and orthogonality of the associated Legendre polynomials, the potential inside and outside of the sphere are evaluated as [35]:

$$\Phi_{in} = -\frac{3\varepsilon_{out}}{\varepsilon_{in} + 2\varepsilon_{out}} E_0 r \cos \theta \quad 2.4.8$$

$$\Phi_{out} = -E_0 r \cos \theta + \frac{\varepsilon_{in} - \varepsilon_{out}}{\varepsilon_{in} + 2\varepsilon_{out}} E_0 r^3 \frac{\cos \theta}{r^2} \quad 2.4.9$$

The electric field distribution  $E = -\nabla \Phi$  can be found by derivation of potential is given by:

$$E_{in} = E_0 \frac{3\varepsilon_{out}}{\varepsilon_{in} + 2\varepsilon_{out}} (\cos \theta \hat{r} - \sin \theta \hat{\theta}) = E_0 \frac{3\varepsilon_{out}}{\varepsilon_{in} + 2\varepsilon_{out}} \hat{x} \quad 2.4.10$$

$$E_{out} = E_0 (\cos \theta \hat{r} - \sin \theta \hat{\theta}) + \frac{\varepsilon_{in} - \varepsilon_{out}}{\varepsilon_{in} + 2\varepsilon_{out}} \frac{a^3}{r^3} E_0 (2\cos \theta \hat{r} + \sin \theta \hat{\theta}) \quad 2.4.11$$

$\Phi_{out}$  explain the superposition of the applied electric field in the first term and that of a dipole placed at the center of the particle. So  $\Phi_{out}$  can be formed as [35]:

$$\Phi_{out} = -E_0 r \cos \theta + \frac{\vec{p} \cdot \vec{r}}{4\pi \varepsilon_0 \varepsilon_{out} r^3} \quad 2.4.12$$

$$\vec{p} = 4\pi \varepsilon_0 \varepsilon_{out} \frac{\varepsilon_{in} - \varepsilon_{out}}{\varepsilon_{in} + 2\varepsilon_{out}} r^3 \vec{E}_0 \quad 2.4.13$$

Where  $p$  defined as dipole moment. According to equation above, the relation between the electric field and dipole moment is defined as  $p = \varepsilon_{out} \alpha(\omega) E_0$ , so the polarizability of the sphere represent as  $\alpha$ , that can be written as:

$$\alpha(\omega) = 4\pi \varepsilon_0 a^3 \frac{\varepsilon_{in}(\omega) - \varepsilon_{out}}{\varepsilon_{in}(\omega) + 2\varepsilon_{out}} \quad 2.4.14$$

The polarizability is the most important parameter and plays a significant role in resonance condition. To obtain a maximum polarizability under specific condition, the denominator of polarizability must be tend to zero. According to above equation, resonance condition directly depends on dielectric constant of both particle itself and surrounding medium.

In the quasistatic approach as we discussed, where the MNPs are much smaller than the wavelength of incoming light and electric field on the particle is constant. Independently of the particle size, both of the cross sections which are absorption  $C_{abs}$  and scattering  $C_{sca}$  are important and strongly affect at the surface plasmon resonance. The scattering and absorption cross sections are given by:

$$C_{scat} = \frac{k^4}{6\pi\epsilon_0^2} |\alpha(\omega)|^2 \quad 2.4.15$$

$$C_{abs} = \frac{k}{\epsilon_0} \text{Im} [\alpha(\omega)] \quad 2.4.16$$

For solar cell application, the important parameter for improvement of cell efficiency is that scattering from MNP is much more than absorption of light by particle  $C_{sca} \gg C_{abs}$ . Hence, in this case due to the particles are much smaller than the incoming wavelength ( $R \ll \lambda$ ), the absorption and the scattering cross sections are ( $R^3$ ) and ( $R^6$ ) parameter dependent. Therefore, for  $R \ll \lambda$  absorption cross section is higher than that of scattering cross section.

In the following section, this size particle limitation is ignored. We investigate the Mie theory which is more useful for any size of the particles.

## 2.5. Mie theory

The limitation of the electrostatic theory is that it can be used for small particles. When the particle size becomes large relative to wavelength of incoming light, the retardation effect cannot be ignored. This problem is solved by Mie theory. In Mie scattering theory, we don't have any size limitation. The scattering light of an arbitrary material's problem has been solved by Gustav Mie theory. It contains particles that can be much larger than wave length of incident light. The reason why Mie theory leads to remain important today is that it gives the solution of Maxwell equation for spherical coordinate of particles. It also defines the spherical particles which their sizes are unlimited [35].

Mie Theory can be explained by solving Maxwell's Equations for electromagnetic wave concept of light demonstrated as a plane wave scattered from a spherical particle.

As a result, the electromagnetic field should satisfy the wave equation in a linear, isotropic or homogenous medium with zero divergence [33]:

$$\nabla^2 E + k^2 E = 0 \quad 2.5.1$$

$$\nabla^2 H + k^2 H = 0 \quad 2.5.2$$

We construct divergence free vector function  $M$  as a result of the electromagnetic field demonstrated above, is generated by

$$M = \nabla \times (c\psi) \quad 2.5.3$$

Where,  $\psi$  and  $c$  represent scalar function and an arbitrary constant vector or pilot vector respectively.

With the help of vector identities  $\nabla \times (A \times B)$  and  $\nabla(A \cdot B)$ , the vector function  $M$  is obtained as:

$$\nabla^2 M + k^2 M = \nabla \times [c(\nabla^2 \psi + k^2 \psi)] \quad 2.5.4$$

If  $\psi$  is expressed as scalar wave function solution,  $M$  must satisfy the vector wave equation

$$\nabla^2 \psi + k^2 \psi = 0 \quad 2.5.5$$

Let us define another vector wave function  $N$  from construction of  $M$ :

$$N = \frac{\nabla \times M}{k} \quad 2.5.6$$

Therefore,  $N$  also satisfies the vector wave equation and it has the required properties of an electromagnetic field too. So, the problem reduces partly to solve the scalar wave equation.

From a consideration of the boundary conditions, we have to construct  $\psi_{emn}$  and  $\psi_{omn}$  functions that fulfill the scalar wave equation in spherical coordinates. The solutions are given below:

$$\psi_{emn} = \cos m\theta P_n^m(\cos \theta) z_n(kr) \quad 2.5.7$$

$$\psi_{omn} = \sin m\theta P_n^m(\cos \theta) z_n(kr) \quad 2.5.8$$

Where,  $z_n$  defines a spherical Bessel function,  $m = \pm 1, \pm 2, \pm 3, \dots, \pm n$  and  $n=0, 1, 2, \dots$

By using such relations,  $M_{emn} = \nabla \times r\psi_{emn}$  and  $N_{emn} = k^{-1}\{\nabla \times M_{emn}\}$ . It is possible to define incident electric and magnetic fields as:

$$E_i = E_0 \sum_{n=1}^{\infty} i^n \frac{2n+1}{n(n+1)} (M_{o1n}^{(1)} - iN_{e1n}^{(1)}) \quad 2.5.9$$

$$H_i = \frac{-k}{\omega\mu} E_0 \sum_{n=1}^{\infty} i^n \frac{2n+1}{n(n+1)} (M_{e1n}^{(1)} - iN_{o1n}^{(1)}) \quad 2.5.10$$

The boundary conditions at the surface of the sphere should match the expansion of the electric field inside the sphere:

$$E_1 = \sum_{n=1}^{\infty} \frac{i^n E_0 (2n+1)}{n(n+1)} (c_n M_{o1n}^{(1)} - i d_n N_{e1n}^{(1)}) \quad 2.5.11$$

$$H_1 = \frac{-k}{\omega\mu_0} \sum_{n=1}^{\infty} \frac{i^n E_0 (2n+1)}{n(n+1)} (d_n M_{e1n}^{(1)} + i c_n N_{o1n}^{(1)}) \quad 2.5.12$$

Again the boundary conditions, the scattered field given by equation 2.5.13 and 2.5.14:

$$E_s = \sum_{n=1}^{\infty} \frac{i^n E_0 (2n+1)}{n(n+1)} (i a_n N_{e1n}^{(3)} - b_n M_{o1n}^{(3)}) \quad 2.5.13$$

$$H_s = \frac{k}{\omega m} \sum_{n=1}^{\infty} \frac{i^n E_0 (2n+1)}{n(n+1)} (i b_n N_{o1n}^{(3)} + a_n M_{e1n}^{(3)}) \quad 2.5.14$$

At this point, it should be considered that the included spherical Bessel functions are recited through the superscripts (1) and (2) which are assigned to the vector spherical harmonics. According to linear equation, the coefficients of the field inside the particle and the scattered coefficient, derived from boundary conditions, are:

$$c_n = \frac{\mu_1 j_n(x) [x h_n^{(1)}(x)]' - \mu_1 h_n^{(1)} [x j_n(x)]'}{\mu_1 j_n(mx) [x h_n^{(1)}(x)]' - \mu_1 h_n^{(1)} [mx j_n(mx)]'} \quad 2.5.15$$

$$d_n = \frac{\mu_1 m j_n(x) [x h_n^{(1)}(x)]' - \mu_1 m h_n^{(1)} [x j_n(x)]'}{\mu m^2 j_n(mx) [x h_n^{(1)}(x)]' - \mu_1 h_n^{(1)}(x) [mx j_n(mx)]'} \quad 2.5.16$$

$$a_n = \frac{\mu m^2 j_n(mx) [x j_n(x)]' - \mu_1 j_n(x) [mx j_n(mx)]'}{\mu m^2 j_n(mx) [x h_n^{(1)}(x)]' - \mu_1 h_n^{(1)}(x) [mx j_n(mx)]'} \quad 2.5.17$$

$$b_n = \frac{\mu_1 j_n(mx) [x j_n(x)]' - \mu j_n(x) [mx j_n(mx)]'}{\mu_1 j_n(mx) [x h_n^{(1)}(x)]' - \mu h_n^{(1)}(x) [mx j_n(mx)]'} \quad 2.5.18$$

The size parameter  $x$  and the relative refractive index of sphere  $m$  are defined as:

$$x = ka = \frac{2\pi na}{\lambda} \quad 2.5.19$$

$$m = \frac{n_1}{n} \quad 2.5.20$$

Where  $a$ , is the radius of the sphere.  $n$  and  $n_1$  represent refractive index of the surrounding medium and particle respectively.

Considering the determination of cross section, there are three parameters of it such as scattering, absorption and extinction. These parameters are so important for expressing the optical behavior of the spherical particle and they can be expressed as [33, 35]:

$$C_{sca} = \frac{2\pi}{k^2} \sum_{n=1}^{\infty} (2n+1) (|a_n|^2 + |b_n|^2) \quad 2.5.20$$

$$C_{ext} = \frac{2\pi}{k^2} \sum_{n=1}^{\infty} (2n+1) Re\{a_n + b_n\} \quad 2.5.21$$

The absorption cross section is also calculated by means of the relation with the other cross sections

$$C_{abs} = C_{ext} - C_{sca}$$

## 2.6. The Dielectric Function $\epsilon(\omega)$

As mentioned in previous sections, the dielectric function  $\epsilon(\omega)$  plays an essential role for definitions of electromagnetic waves. Optical response of the MNPs is determined by resonance condition that arises from collective motion and oscillation of free conduction electron of MNPs. This condition is noted as localized surface plasmons. As known,

dielectric constant of the MNPs and surrounding medium plays an important role in resonance condition. In detail, it depends on dielectric function of material, size, shape and surrounding medium of the NPs. Dielectric function of MNPs is related to sum of the two contributions. First contribution includes free electrons of the metal particles can be defined by Drude Model. The second contribution arises from interband transitions includes metal's core electron depends on the excitation of free electron between two different electronic band [35]

In the following section two models to explain the optical properties base on classical theory to obtain the dielectric constant of MNPs.

## 2.7. Drude Model

Optical properties of the material directly depend on the band structure of materials. Especially, metals are known as free conduction electron. According to the band structure of metal conductor, there is smaller energy needs to transition electron to upper level by exciting photon due to the filled valence band overlap empty conduction band. Unlike in the non-conductor material the band structure due to forbidden energy gap, the electrons need energy larger than band gap for an interband transition. That's a response of why metals relative to the non-conducting material are highly absorbing and reflecting the incoming light than the transparent and weakly reflecting materials. In the figure 2.7 the excitation of the electron when is subjected under illumination by very small energy, is represented.

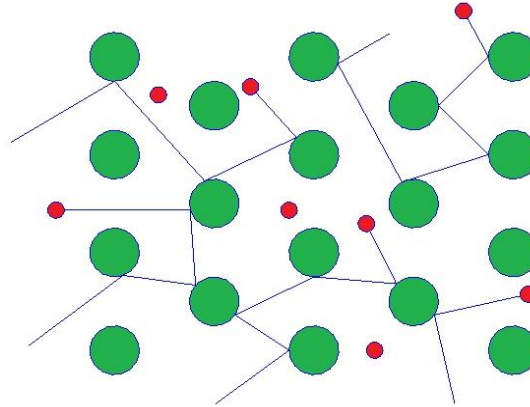


**Figure 2.7** Illustration of the free electron motion under an external electric field in a Drude model

Drude model is similar to Lorentz model except that the spring constant is zero. The equation of motion for the free electron when subjected to an external electric field is represented by following equation [35]:

$$m_e \frac{\partial^2 x}{\partial t^2} + m_e \Gamma \frac{\partial x}{\partial t} = e E_0 e^{-i\omega t} \quad 2.7.1$$

Where,  $m_e$  the effective mass of the free electron and  $e$  is the charge of the electron. The definition of external electric field is given by this equation  $E = E_0 e^{-i\omega t}$ .  $\Gamma$  is damping constant because of the motion of electrons collisions with immobile positive ions can be defined as  $\Gamma = \frac{1}{\tau} = \frac{v_f}{l}$ . Damping constant is proportional inversely relative to average time

between collisions  $\tau$ . It is also directly proportional to Fermi velocity divided by the mean free path for free electron in the metal.

We can consider time harmonic solution for the displacement of electrons according to the time harmonic field applied to the material as:

$$x(t) = x_0 e^{i\omega t} \quad 2.7.2$$

From equation 2.7.1 the amplitude of the oscillation,  $x_0$ , can be found easily. This equation is given as;

$$x_0 = \frac{-e}{m_e} \frac{1}{\omega^2 + i\Gamma\omega} E_0 \quad 2.7.3$$

It is possible to define the polarization ( $P = Np = Nex$ ) based on displacement given in equation 2.7.3:

$$P = \frac{\omega_p^2}{\omega^2 + i\Gamma\omega} \epsilon_0 E_0 \quad 2.7.4$$

Where,  $\omega_p$  is defined as volume plasma frequency of the metal. It can be written as:

$$\omega_p = \sqrt{Ne^2/m\epsilon_0} \quad 2.7.5$$

According to the well known definition for polarization is found as;

$$P = \epsilon_0 \chi_e E \quad 2.7.6$$

The dielectric function as a collection of free electron for metal can be expressed by the Drude model. These electrons under external electromagnetic field of angular frequency ( $\omega$ ) from equation 2.7.4 as;

$$\epsilon_{Drude}(\omega) = 1 - \frac{\omega_p^2}{\omega^2 + i\Gamma\omega} \quad 2.7.7$$

We can separate dielectric function to real and imaginary part; these two parts are important effect on the optical behavior of metal particles. Derivation from Drude Model we can get real and imaginary part of the dielectric function is then,

$$\epsilon' = 1 - \frac{\omega_p^2}{\omega^2 + \Gamma^2} \quad 2.7.8$$

$$\epsilon'' = \frac{\Gamma\omega_p^2}{\omega(\omega^2 + \Gamma^2)} \quad 2.7.9$$

Under this condition we can convert Lorentz model into Drude mode [35].

## 2.8. Lorentz Model

In the preceding section, optical behavior in the Drude model at the high frequency fails because of the interband transition is not account in the calculation. Under this condition the Lorentz Model based on bound electrons can solve the deviation problem. It can be calculate at high frequency dielectric constant. In the Lorentz model the electrons are bound to the atomic nuclei by quasi-elastic forces when they interact with electromagnetic field oscillate and the movement of the bound electron is described by:

$$m \frac{\partial^2 x}{\partial t^2} + m\gamma \frac{\partial x}{\partial t} + kx = eE_0 e^{-i\omega t} \quad 2.8.1$$

There is the same motion of free electron equation like In Drude model by addition spring constant  $k$  into the equation, the Lorentz equation is obtained. Where  $m$  is effective mass of bound electron,  $\gamma$  is the damping constant defines the losses leads to the collisions between the atoms.  $k$  is the spring constant and  $kx$  introduce restoring forces due to electrostatic attraction and keeping electron bounded. The dielectric function of the bounded electron in Lorentz model is defined as;

$$\varepsilon(\omega) = 1 + \frac{\omega_p^2}{\omega_0^2 - \omega^2 - i\gamma\omega} \quad 2.8.2$$

We can separate the real and imaginary part each other, which are shown as:

$$\varepsilon' = 1 + \frac{\omega_p^2(\omega_0^2 - \omega^2)}{(\omega_0^2 - \omega^2)^2 + \gamma^2\omega^2} \quad 2.8.3$$

$$\varepsilon'' = \frac{\omega_p^2\gamma\omega}{(\omega_0^2 - \omega^2)^2 + \gamma^2\omega^2} \quad 2.8.4$$

Where  $\omega_0 = \sqrt{\frac{k}{m}}$  is defined as the frequency of electron oscillation.

Damping constant in both equations of dielectric constant for free electron and bounded electron contain the mean free path of electron through the material. As known for the metals the mean free path is in the order of tens of nanometers. As a result, for NP there is a limitation related to motion of electron when the size of the NPs is comparable with the mean free path. Therefore damping constant is converted to:

$$\gamma_{modified} = \gamma_{bulk} + \frac{v_f}{l} \quad 2.8.5$$

Where,  $\gamma_{bulk}$  is the damping constant  $v_f$  is the Fermi velocity and  $l$  is the effective mean free path because of the particle boundaries.

## 2.9. Lorentz-Drude Model

Because of the high frequency regime, Drude model fails to describe the optical behavior under this condition. The photons with higher energy acts to promote bound electrons, so they create an impact on the optical behaviors on the other side, only bound electrons are considered in the Lorentz Model. Nevertheless, in the real metal, they are not possible to describe the optical properties exactly by considering separately. Therefore, contribution from both theories includes free electron and bounded electron as expected [36].

By adding dielectric constant belonging both Drude and Lorentz model give accurate result. Thus the dielectric constant can be written as:

$$\varepsilon(\omega) = \varepsilon_f(\omega) + \varepsilon_b(\omega) \quad 2.9.1$$

$\epsilon_f$  is defined as free electron from Drude model and  $\epsilon_b$  represent bound electron from Lorentz Model contributions.

$$\epsilon = 1 - \frac{\omega_{pe}^2}{\omega^2 + i\gamma_e\omega} + \sum_j \frac{\omega_{pj}^2}{\omega_j^2 - \omega^2 - i\gamma_j\omega} \quad 2.9.2$$

Where, e is for free electron.

Up to now, we investigated resonance condition for the particle by Mie and electrostatic approach. For determining the resonance condition one of the important parameter is dielectric function that describe by Lorentz and Drude model. If we select the true model to solve the particle dielectric function, this way leads to the interaction of the light and particles give a result with high accuracy.

## 2.10. Solar Irradiation

The surface temperature of the sun is determined about 6000K and can be approximated as blackbody which has surface temperature of this amount. Therefore, the spectrum of the radiation from the sun is similar to blackbody. Solar irradiation when reaching earth's atmosphere is about 1350 W/m<sup>2</sup>. However, the solar energy is attenuated due to the absorption and scattering by molecules and dust particles in the atmosphere in specific spectral region. Some part of incident energy is removed by ozone and oxygen where the wavelength is less than 300 nm. Therefore absorption in the ultraviolet solar irradiance spectrum is affected by ozone and oxygen. In the infrared range absorption is caused by carbon dioxide and water at the wavelength above 1000 nm.

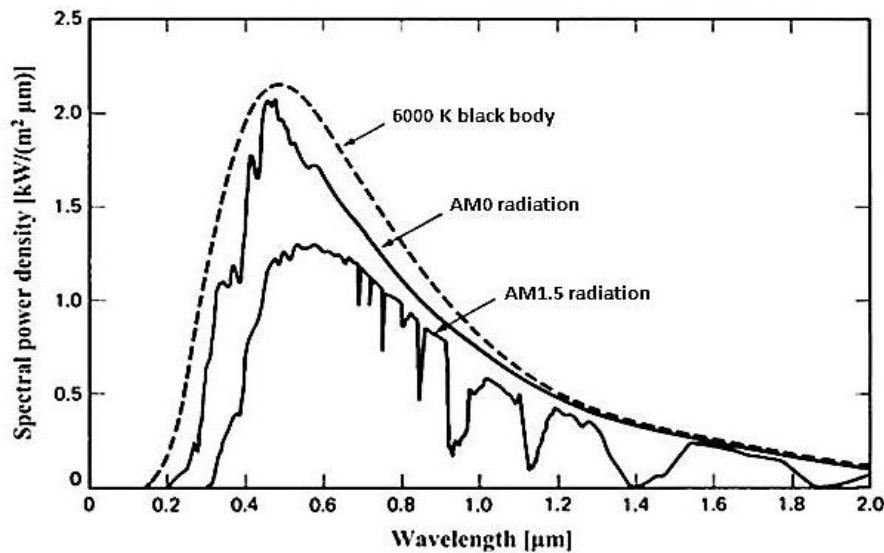


**Figure 2.8** The spectral of power density of sunlight at AM1.5 & AM0 [37]

Distance of the sunlight traveling through the earth's atmosphere is important parameter to determine solar irradiance. The shortest distance occurs when sun is directly overhead. In other words, sun is at the zenith. The terms AM0, AM1 and AM1.5 is defined as Air Mass for particular radiation condition. The relation between lengths of the path from sun to the shortest length is expressed as optical Air Mass. Air Mass zero is defined as sun radiation

outside of the atmosphere. Air Mass one radiation is determined when the sun is at the zenith and refer to the sun at the vertical direction. The Air Mass is calculated as follows:

$$AM = \frac{1}{\cos \theta} \quad 2.10.1$$

Where  $\theta$  is represented the angle of incident between the sun with the vertical. This angle for AM1.5 is 48.

For terrestrial PV standard according to comparison between different position, the performance of solar cell is referred AM1.5. The power generated under this standard AM1.5 (1000 W/m<sup>2</sup>) radiation is considered as PV peak power. The irradiance at this value is the maximum value that is received on earth's surface.

### **2.11. Single crystal silicon solar cell structure**

Crystal silicon is semiconductor material from group IV element that enables to changing the transport of electrical properties by adding impurity. The production of the solar cell is based on doping. In the crystal structure of silicon, each silicon atom shares four electrons in the valance band by covalent bonding to other neighboring silicon atoms. In the silicon crystal lattice, because of an equal number of positive and negative charges, the silicon atom has no net electric charge. Therefore by adding impurity to the intrinsic silicon the electrical property changes in the semiconductor silicon. In the doping process, the n-type materials are formed by the impurity atoms which have five electrons in the valence band. When these atoms are subjected with silicon atoms, the four electrons will be shared with the neighbor's atom. The exceed electrons are free carriers and can move freely in the lattice. Therefore, concentrations of electrons are formed as a majority charges. In the p-type materials similar arguments holds true. The impurity atoms which have three electrons in the valence band, when are subjected with silicon atoms, the three electrons will be shared with the neighbors atom with one electron missing in the covalent bond of the silicon atoms. The exceed holes can be treated as free carriers. Therefore, concentrations of holes are formed as a majority charges.

p-n junction is created by diffusion of phosphorous into the p-type silicon which is demonstrated in figure 2.9. In practice, the front contacts consist of a silver grid; it makes absorption of light in the p-n junction. The back contact which consists of aluminum thin layer can better collect the separated charge. At the front side of the silicon substrate, anti reflection coating (ARC) is used to decrease the reflection of incident light result in increase of the absorption of light into the cell. The figure 2.9 is illustrated the four basic level of single crystalline solar cells production.

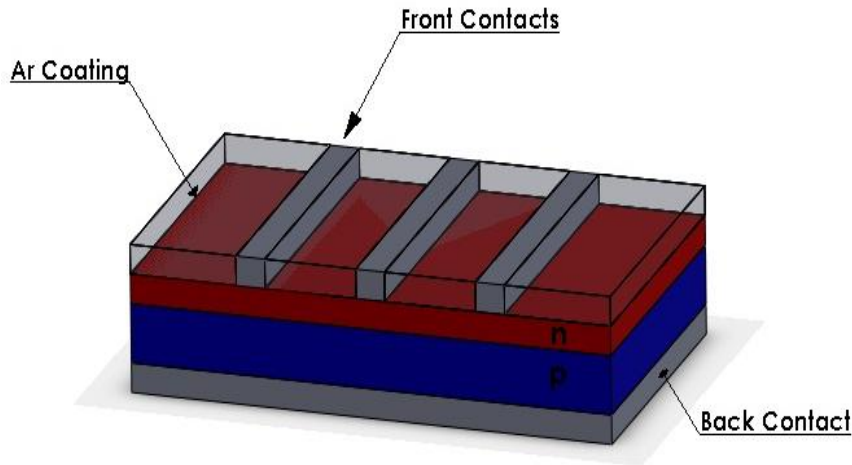


**Figure 2.9** Basic schematic of a single crystalline solar cell fabricated

### 2.12. Single crystal solar cell operation

Direct conversion of incident sunlight into electricity is performed in PV devices for generating power. Important parameters in working principle of solar cell include: generation of electron-hole pairs, separation of photo-generated electron-hole pairs and collection of the photo-generated charge carriers at the terminals of the junction.

When the energy of incident photon is greater than band gap of the semiconductor ( $h\nu > E_g$ ), due to the absorption of incident photon, the electron is excited from valence band to the conduction band. This transition of electron creates a hole in valence band. Both the creation of electron and holes pairs move through the crystal silicon. This movement generates photocurrent which results from incident light absorption. Creation of more electron-hole pair leads to the higher number of incident photon that absorbed by electrons. This absorption of incident photon will increase the current output of the solar cell. Hence, leads to increase the cell efficiency of solar cell.

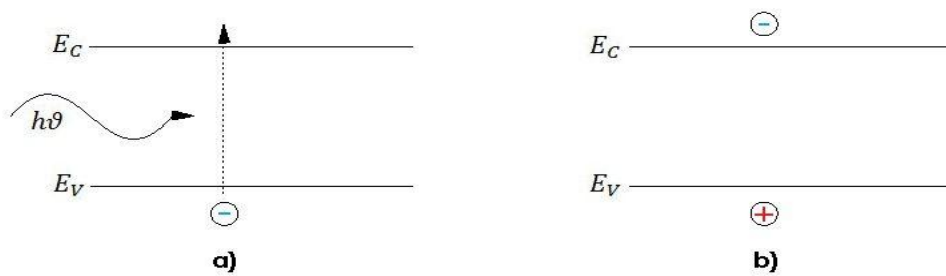


**Figure 2.10** (a) Absorption of incident photon by electron with  $h\nu > E_g$  (b) Generation of electron-hole pair

After an electron-hole pair is generated, the electron and hole should be separated. Because of relatively short time, the charge carriers tend to recombine and return to their original position. This process called as recombination. The formation of p-n junction enables charge carriers separated from each other to prevent this recombination process. Electron must be sent to one side and the holes to the other side of solar cell. The generated charge carriers at the junction due to the presence of the internal electric field are separated from each other.

Existence of the electric field, result in the electron and hole which are separated, move in opposite direction.

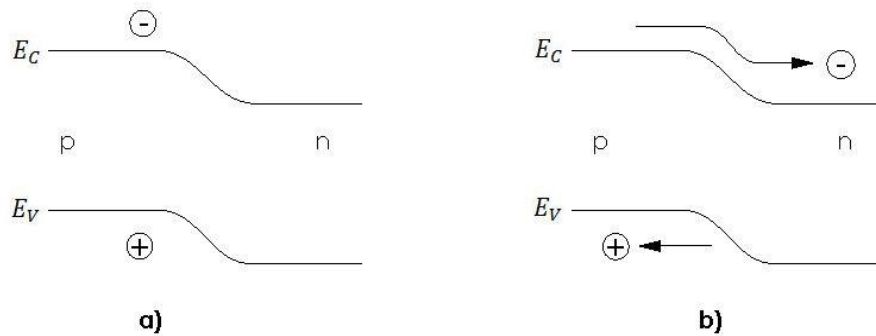


**Figure 2.11** The generated charge carriers (a) Before separation (b) After separation

After the separation, the electrons by the contacts from n side and the holes by the contacts from p side are collected to produce the PV power generation.

### 2.13. Basic Photovoltaic cell parameters

P-N junction of solar cell basically behaves as a diode. In the dark condition when no light is applied, the relation between the current density (I) and voltage (V) is written by following equation:

$$I = I_0 \left[ \exp\left(\frac{qV}{kT}\right) - 1 \right] \quad 2.13.1$$

Where, I is represented as current that flow inside the cell,  $I_0$  is the dark saturation current density of the cell, V is voltage between two doped p and n types regions,  $q$  is the charge of electron,  $k$  is the Boltzmann constant and T is the absolute temperature. The current-voltage characteristics of the solar cells are done in the dark and under illumination. When the cell is illuminated by incident photon, it leads to generate power. Under this condition the I-V curve shifts in the vertical direction. Therefore the equation 2.13.1 changes by addition the current that is generated from light which is calculated as follows:

$$I = I_0 \left( e^{\frac{qV}{kT}} - 1 \right) - I_L \quad 2.13.2$$

Where,  $I_L$  represent current generated by incident light. The current-voltage (I-V) characteristics of p-n junction under dark and illumination conditions are illustrated in figure 2.12. Different parameters can be extracted from (I-V) curve. As we can see, under illumination condition the curve is shifted toward negative direction of current axis.

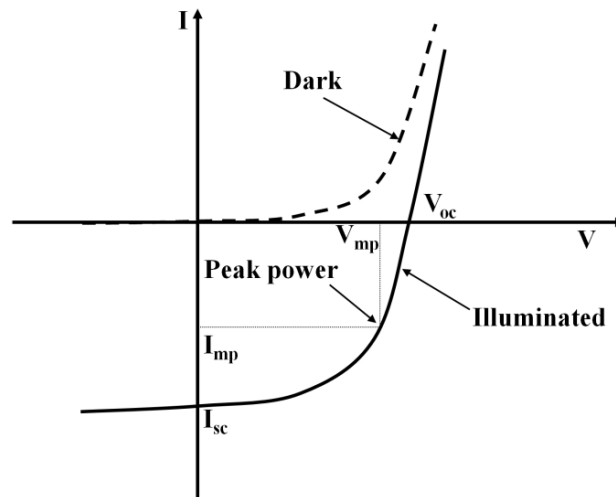


**Figure 2.12** I-V characteristics of solar cell in the dark and under illumination

Generally, in the I-V characteristic of solar cell fourth quadrant of illuminated device is used. Therefore, the I-V characteristic curve of the solar cell device is represented as mirrored version which is shown in figure 2.13.

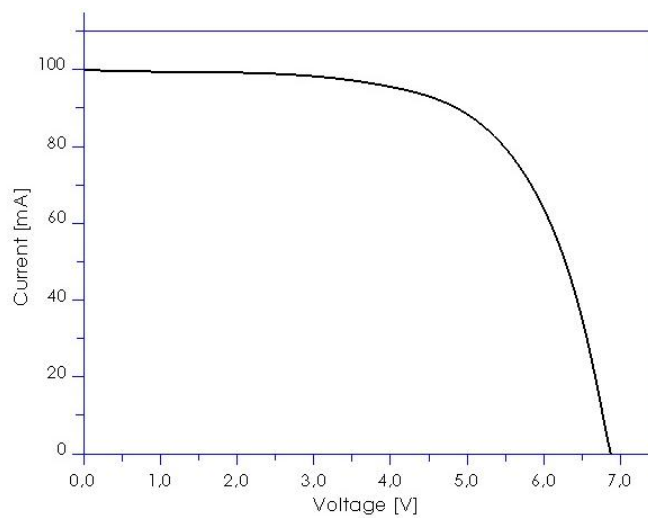


**Figure 2.13** Current versus voltage curve under illuminated condition

In the following section, the main parameters from the I-V current under illumination are commonly utilized in the determination of cell efficiency. These parameters include: the short-circuit current density ( $I_{sc}$ ), the open-circuit voltage ( $V_{oc}$ ), fill factor ( $FF$ ) and energy conversion efficiency ( $\eta$ ). According to these parameters we can characterize the performance of the solar cell device.

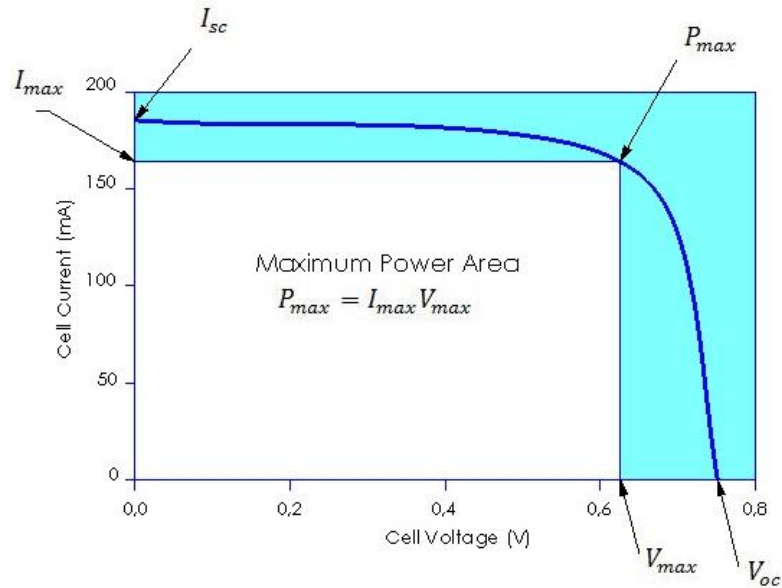


**Figure 2.14** An example of I-V characteristics of photovoltaic cell [38]

**Short circuit current:**

Short circuit current occurs when the current is passing through the cell and there is no voltage difference between terminals of solar cell. The voltage is (V=0).

Short circuit current is important parameter of solar cell. It depends on the number of charge carrier generation and collection across the PV performance. Short circuit current is affected by some parameters. These parameters include reflectance and transmittance amount, cell area and intensity of the light.

**Open circuit voltage:**

Open circuit voltage is the voltage in which flowing current through the external circuit is zero (I=0). It occurs when there is voltage difference between terminals of the solar cell. The open-circuit voltage depends on the photo-generated current density. It can be calculated by following equation:

$$V_{oc} = \left(\frac{nKT}{q}\right) \ln \left(\frac{I_{sc}}{I_o} + 1\right) \tag{2.13.3}$$

**Fill factor:**

$I_{max}$  is maximum current and  $V_{max}$  is maximum voltage in ideal solar cell. Multiplications of them determine the maximum power of solar cell which can be written as:

$$P_{max} = V_{max} \times I_{max}$$

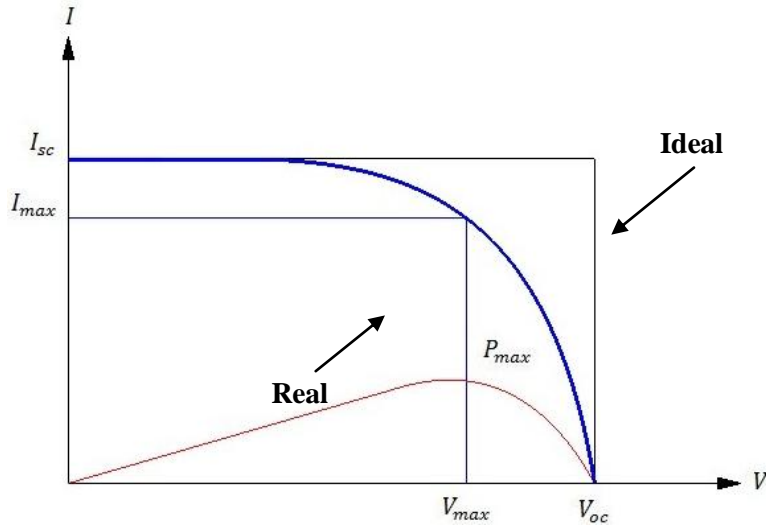


**Figure 2.15** The real and ideal current versus voltage curves

Fill factor is defined as the ratio of the maximum power to the product of short circuit current ( $I_{sc}$ ) and the open circuit voltage ( $V_{oc}$ ). It can be represented by following equation:

$$FF = \frac{V_{max} \times I_{max}}{V_{oc} \times I_{sc}} \quad 2.13.4$$

Where,  $V_{max}$  is defined as output power at the maximum voltage,  $I_{max}$  is output power at the maximum current,  $V_{oc}$  and  $I_{sc}$  is represented open-circuit voltage and short-circuit current respectively. The amount of the series and shunt resistance at cell's performance is directly depends on the fill factor. Minimizing series resistance ( $R_s$ ) and maximizing shunt resistance ( $R_{sh}$ ) in the cell leads to the higher fill factor.

Fill factor is a calculation of the difference between the I-V characteristic of real PV cell from an ideal cell. Thereby is always less than one. The fill factor of ideal solar cell is one but effect of losses from series and shunt resistance leads to minimizing cell efficiency.

### Cell Efficiency:

Cell efficiency determines the ratio of the generated maximum power to the incident power from sunlight. It is represented as following equation:

$$\eta = \frac{P_{max}}{P_{in}} \quad 2.13.5$$

Cell efficiency is the most important parameter for calculating the performance of the solar cell. Measurement of voltage and current depends on illumination condition which affects the value of cell efficiency. Therefore it must be standardized. The convention for utilizing cell efficiency consists of AM 1.5 solar spectrum and about  $1 \text{ kW.m}^{-2}$  light intensity.

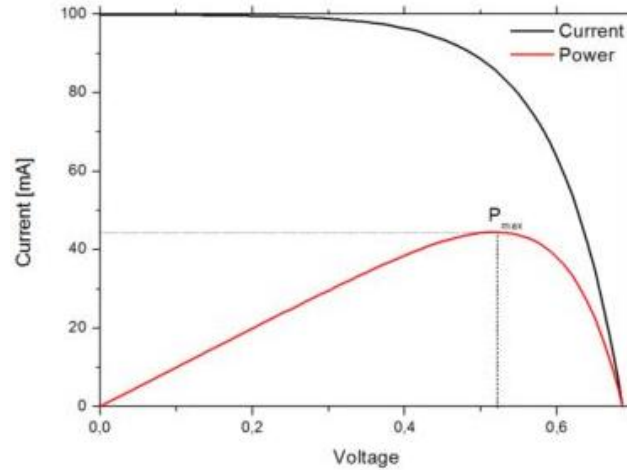


**Figure 2.16** Current versus voltage (I-V) and power curve of PV

**Series resistance:**

$R_s$  is series resistance which arises from ohmic resistance of metallic contact and semiconductor material. It also contains the contact resistance between the metal contact and the semiconductor. Consideration the lower value of series resistance is desirable. Existence of series resistance reduces the fill factor and directly affects the conversion efficiency of solar cells.

Series resistance under illumination condition is defined as the inverse slope of I-V curve around open circuit voltage.

$$R_s = \left. \frac{1}{\frac{dI}{dV}} \right|_{V=V_{oc}} \quad 2.13.6$$

**Shunt resistance:**

$R_{sh}$  is shunt resistance which arises from the leaking current across the junctions near the edge of the cell. That is usually happen because of the manufacturing defects that can affect the interruption of p-n junction. A low shunt resistance leads to increase the leak current and also decrease the fill factor. It affects the lower conversion efficiency. As a result we need to high shunt series for better cell performance [39]. The shunt resistance under illumination condition is represented the inverse slope of I-V curve near short circuit current:

$$R_{sh} = \left. \frac{1}{\frac{dI}{dV}} \right|_{V=0} \quad 2.13.7$$

As a result, series resistance and shunt resistance are the parasitic resistances. For the better operation of the cell performance, these parameters should be determined as correct ratio. Thereby, series resistance should be determined as low as possible while shunt resistance should be as high as possible which result in increase of the fill factor. Therefore, better performance of cell efficiency of solar cells occurs.

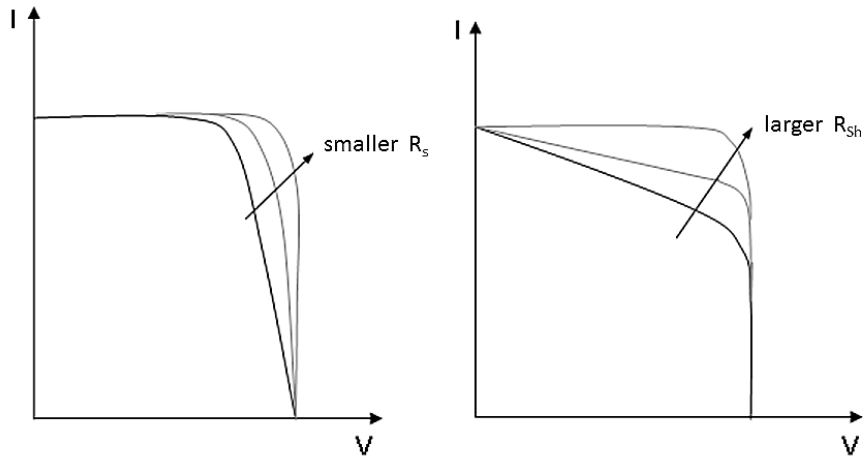


**Figure 2.17** I-V characteristics of a solar cell. A drop in the series resistance and an excess in shunt resistance give rise to an increase in the total output of the cell [40].

### Quantum Efficiency:

External Quantum Efficiency (EQE) is the measure of the number of electrons the device generates per number of photons incident on the device surface, for each wavelength on the solar cell device. If the energy of incident photon is much larger than the band gap of semiconductor, the photons are absorbed and generate electron-hole pairs and resulting carriers are collected. Thereby the Quantum Efficiency (QE) can be measured. However when the energy of incident photon is lower than the band gap, QE is zero.

Recombination effect causes reduction of QE of solar cell, when electron goes to conduction band because of losing energy it comes back to valence band, so the electron cannot move through the external circuit. To get higher efficiency, more electrons should be collected by external circuit; as a result it makes to generate more power.

QE can be measured as either EQE or internal quantum efficiency (IQE). They are different from each other. EQE arises from optical losses which include the transmission and reflection of incident light. That affects on the QE of the solar cell. IQE include electrons which are absorbed by incident light and these electrons can be collected without optical losses, which result in no transmission and no reflection out of the cell.

Reflection and transmission parameters measurements help to get internal quantum efficiency curve by means of the correction of external quantum efficiency.

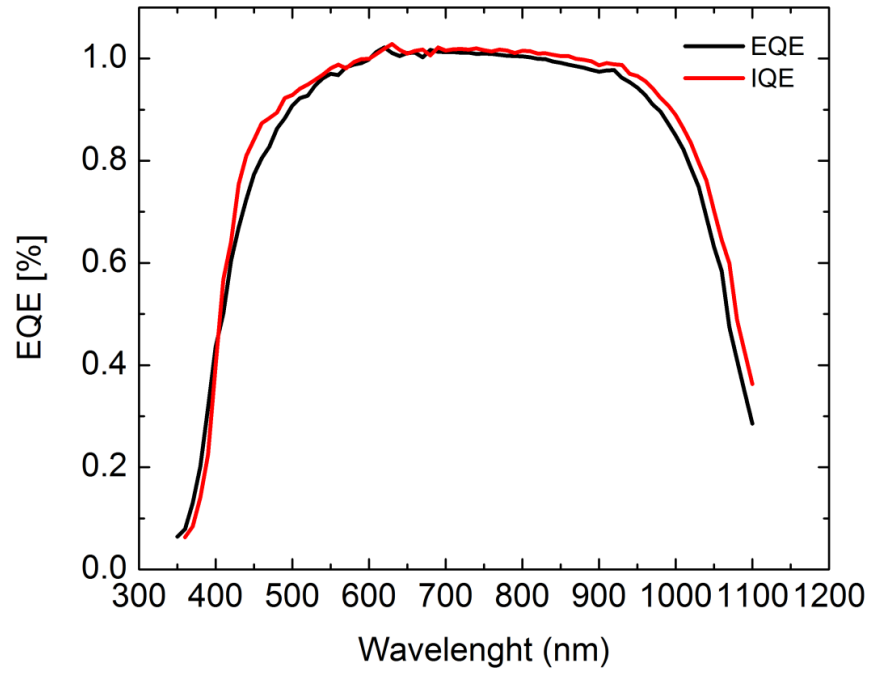


**Figure 2.18** The external and internal quantum efficiencies as a function of wavelength measuring at GÜNAM center for this study.

Total QE can be written as following equation:

$$QE = \frac{100\% * h * c * I_{cell}(\lambda)}{e * \lambda * I_{ref} * R(\lambda)} \quad 2.13.8$$



## CHAPTER 3

### EXPRIMENTAL METHODS

#### 3.1. Fabrication Methods

Throughout this thesis study, the effect of plasmonic NPs on the solar cell device performance is investigated. Step-by-step description of solar cell device fabrication and MNP formation is imperative. In this chapter, I summarize the solar cell fabrication and describe the production methods such as texturing, silicon nitride deposition, metallization, and edge isolation. The self-organized fabrication method of plasmonic NP decoration, named surface dewetting, will also be described in this chapter. First, the details of each step of mono crystalline solar cell production are provided in the following sections.

##### 3.1. 1. Fabrication of Mono Crystalline Silicon Solar Cell

The process steps of mono crystalline silicon solar cell production are summarized in figure 3.1:

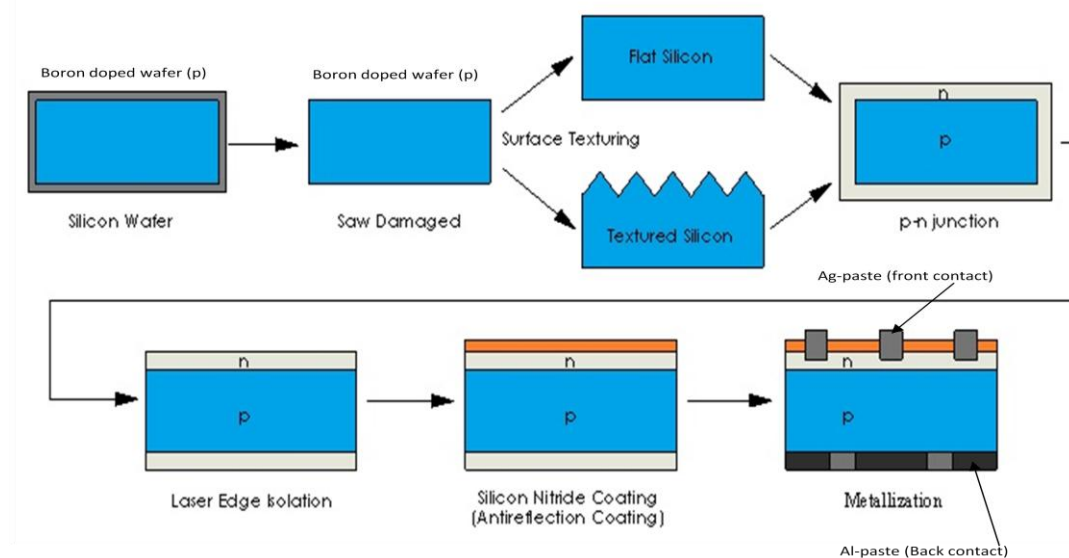


**Figure 3.1** The production steps of a mono crystalline solar cell

The process starts with saw damage removal of a p-type raw Si wafer. Depending on the desired surface profile, the production continues with an etching step that results in either flat or textured Si wafer surface. After the desired surface structure is achieved, the process continues with n-type diffusion doping for achieving a p-n junction close to the surface. Since the doping takes place all over the surface including the sides and the back of the

wafer, there is a need for edge isolation in order to prevent short circuit of the back and front sides of the solar cell. Next, the front surface of the cell is coated with an anti-reflection coating (ARC) such as thin film  $\text{Si}_3\text{N}_4$ . Finally the front electrodes and bus lines together with the back contact electrode is screen printed and co-fired which establishes a  $\text{p}^+$  type of region next to the back contact. The final structure yields a  $\text{p}^+\text{-p-n}$  type of semiconductor junction which is in ohmic contact with the front and back electrodes and therefore possesses a diode structure.

In this work surface texturing step was not applied for all samples. The samples characterizations and performances are investigated for both of flat and textured silicon solar cells. Description of each steps are discussed in this section.

### 3.1.2. Saw Damage Etching (Removal)

The saw damage etching is the first step which is performed before production of the mono crystalline silicon solar cells. The crystalline silicon is grown as ingots commonly produce by Czochralski technique. After the growth of these ingots, they are cut into thin wafers. During the cutting process, the surface of the silicon ingot is damaged from the sawing of wafers. Different chemical etchant solutions such as NaOH or KOH are used to remove shallow cracks and surface defects cutting into the surface of the thin Si wafers. In this thesis, a concentration of 20% KOH at 80 °C is used.

### 3.1.3. Surface Texturing

In solar cell technology good light trapping and light management are important to achieve high efficiency. The silicon substrate surface structure has to be professionally textured to be less reflective which is important for increasing the portion of absorbed light. The enhancement of absorption is mainly due to secondary and tertiary incidences of the initially reflected photons. Multiple incidences are responsible for an induced light trapping effect as illustrated in figure 3.2:

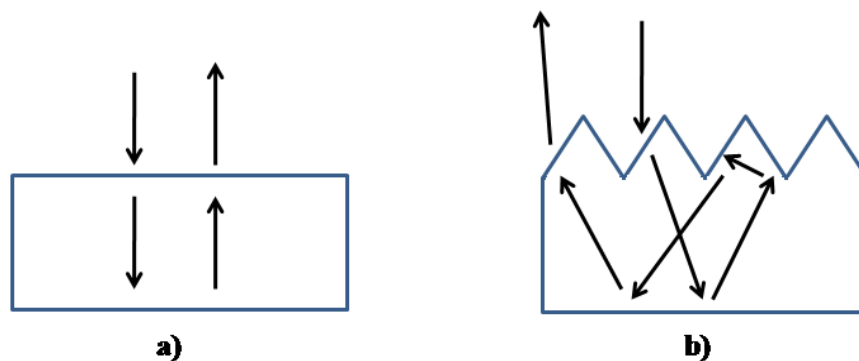


**Figure 3.2** Reflection of incident light: (a) Flat silicon and (b) Textured silicon

In Fig. 3.1.2, panel (a) shows that on a perfectly planar surface the incident photons make a single specular reflection, whereas panel (b) shows that the incident photons, upon the first specular reflection, are still directed into the Si material which gives rise to secondary,

tertiary, etc. reflections. The result is almost nullification of the strong specular reflection and development of a weak haze (diffuse reflection) instead.

In this study, light-absorption behavior of plasmonic mono crystalline silicon solar cells has been extensively investigated on flat silicon substrates and to a limited extent on textured

ones as well. Surface texturing is used to reduce the reflection of light away from the substrate and to improve the light absorption which leads to enhance the amount of light converted into photocurrent in silicon solar cells. N-type mono crystalline silicon surfaces were textured by wet anisotropic KOH chemical etching technique. The pyramid structures and surface roughened create on the surface of the solar cells leads to multi reflection of incident light from the surface. Density of these pyramids is optimized with KOH concentration, etching temperature and etching time. In this work, a concentration of 3% KOH, 10% ISO at 75 °C for 50 minute is used. This recipe is optimized in previous studies at GÜNAM labs.

The obtained random pyramid scatters the light into the substrate leading to a dramatic increase in the efficiency of solar cell as compared smooth silicon surface. Figure 3.3 shows the structure of pyramid on the surface texturing.

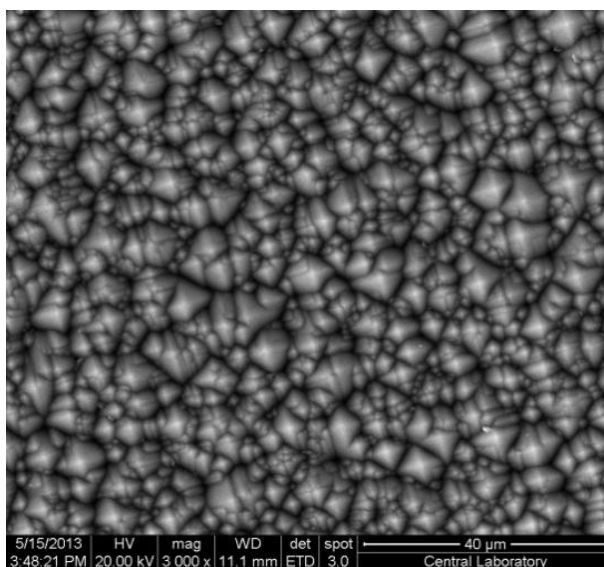


**Figure 3.3** Effect of KOH etching on the formation of pyramid structure

#### **3.1.4. Pre Diffusion Cleaning**

In this step, the silicon wafers should be passed through a cleaning procedure before doping process is performed. Cleaning process is done not only to eliminate organic or inorganic contaminations but also to remove the oxidation during the process. Then wafers dried in a centrifugal drier at the end of the cleaning process.

#### **3.1.5. P-N junction formation**

For construction of solar cell, the p-n junction is formed inside the semiconductor materials. Since production of the solar cell is based on doping in which by adding impurity to the

intrinsic silicon, the electric properties of the semiconductor silicon is changed. In this work, p-n junction created by diffusion of phosphorus from group V into the p-type silicon wafer which is doped with Boron in group III. During the doping process, n-type silicon wafer is subjected to the new dopant phosphorous atoms which are diffused into the material due to concentration gradient. The process is performed by thermal physical vapor deposition system at high temperature. By the formation of the p-n junction in silicon, the electric field is created which leads to generation of the electron-hole pair under illumination. The separation of charge carriers by electric field leads to produce current. Figure 3.4 illustrates the schematic of the p-n junction solar cell.

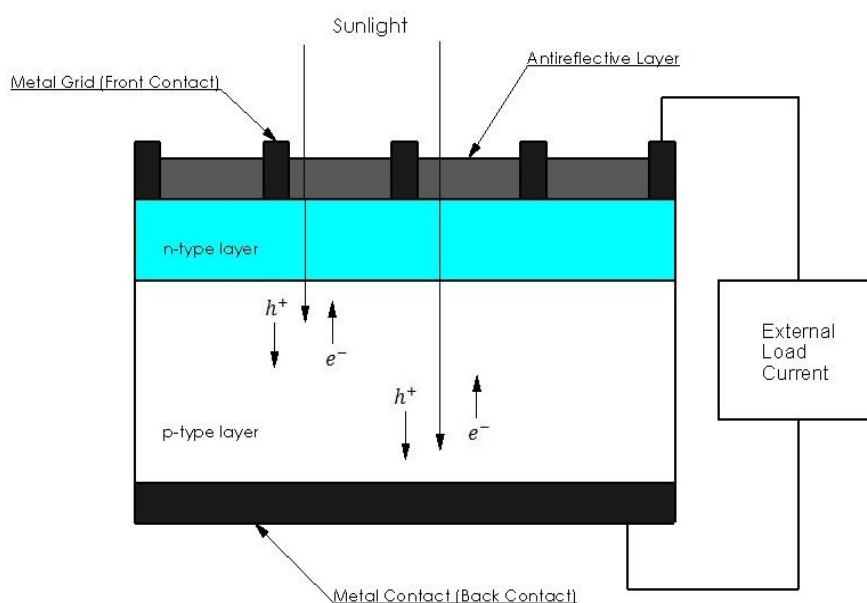
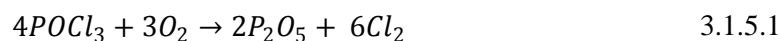


**Figure 3.4** The schematic of p-n junction solar cells

In the solar cell industry, commonly the p-n junction is formed by diffusion of phosphorous dopant atom into the p-type silicon. Liquid  $POCl_3$  is transported to the silicon via  $N_2$  carrier gas to the furnace and  $O_2$  is used to help the creation of n-type silicon layer according to the chemical equation;



Therefore, according to equation 3.1.5.1 and 3.1.5.2, the silicon surface phosphorous-silicate glass is formed. Doping process is carried out at 850 °C for 200 sccm  $POCl_3$  flow. After the doping process is finished, it etched from the surface of silicon.

### 3.1.6. Silicon nitride coating

The cell performance of solar cell decreases by reflection of incident light from the silicon surface which reflects more than 30% for bare silicon due to its high refractive index.

Therefore by applying ARC, the absorption of incident photon increases and leads to reduce the reflection of incident light. The reflected intensity at some specific wavelength is decreased to around the zero which is enhanced the current output and cell efficiency of solar cell. Hence, the reflection of light from the surface is reduced. In theory when the incident wave is reflected from the second layer, it has half phase difference further than the reflected light from top surface. These out-of-phase reflections lead to destructive interference from surface to become zero.

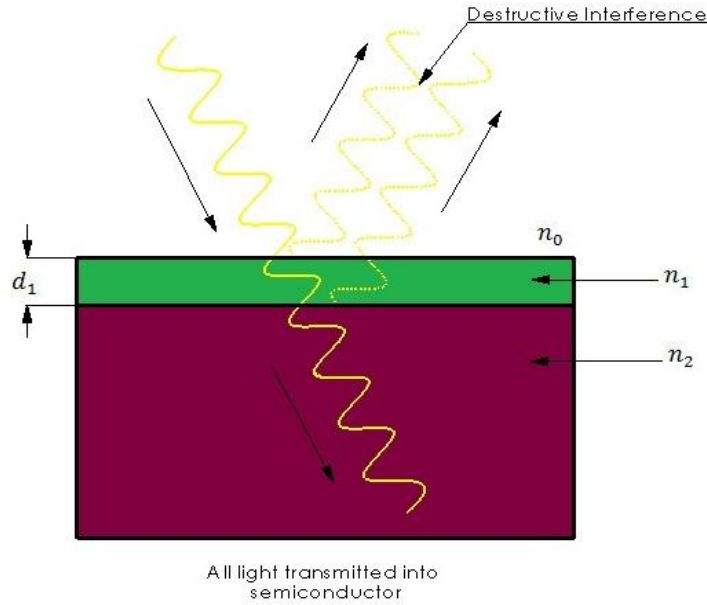


**Figure 3.5** Use of ARC leads to be destructive interference with no reflected light

The formula below is used for calculating the reflectance from a medium that has the refractive index  $n_0$  to another with index of  $n_2$ .

$$R = \left( \frac{n_0 - n_2}{n_0 + n_2} \right)^2 \quad 3.1.6.1$$

When the substrate is coated with dielectric thin films, the reflection spectrum will be calculated as follow:

$$R = \frac{(n_0 - n_2)^2 + \left( \frac{n_0 n_2}{n_1} - n_1 \right)^2 \left( \tan \frac{2\pi n_1 t \cos \theta}{\lambda} \right)^2}{(n_0 + n_2)^2 + \left( \frac{n_0 n_2}{n_1} + n_1 \right)^2 \left( \tan \frac{2\pi n_1 t \cos \theta}{\lambda} \right)^2} \quad 3.1.6.2$$

In this formula, refractive index of the medium from that light is incident, is shown by  $n_0$ , The refractive index of the film is shown by  $n_1$ , substrate refractive index is  $n_2$ . The wavelength at which reflectance is evaluated is  $\lambda$  and  $\theta$  is the angle of incidence. When  $\theta = 0$ , which means the normal incidence, the minimum of reflectance will be as follow:

$$n_1 = \sqrt{n_0 n_2} \quad \Rightarrow \quad d_1 = \frac{\lambda_0}{4n_1} \quad 3.1.6.3$$

Where,  $d_1$  is the thickness of antireflection coating and  $\lambda_0$  is the wavelength at which reflectance is calculated. ARC as a dielectric material should be chosen with appropriate thickness to get the much lower reflection from the surface. To get the optimal ARC thickness, wavelength in the dielectric layer should be one quarter the wavelength of the incident light.

So, the optimum anti-reflective coating refractive index can be calculated as follow by considering the silicon with refractive index of  $n_2 = 3.5$  with light incident from air with  $n_0 = 1$ .

$$n_1 = \sqrt{n_0 n_2} = \sqrt{1 \times 3.5} = 1.87 \quad 3.1.6.4$$

In order to find the thickness of the film with index of 1.87, the wavelength of 600 nm is chosen due to the fact that solar spectrum maximum value at this wavelength. The thickness then will be calculated:

$$d_1 = \frac{600}{4 \times 1.87} = 80.2 \quad 3.1.6.5$$

In this work, silicon nitride ( $Si_3N_4$ ) at different thicknesses was deposited by Plasma Enhanced Chemical Vapor Deposition system (PECVD) at GÜNAM center. In this system, formation of silicon nitride is performed by decomposition of both  $SiH_4$  and  $NH_3$  inlet gasses at low temperature around 380 °C. The plasma is obtained by radio frequency signal with 50 KHZ frequency. The figure 3.1.6 illustrates the schematic of the PECVD:

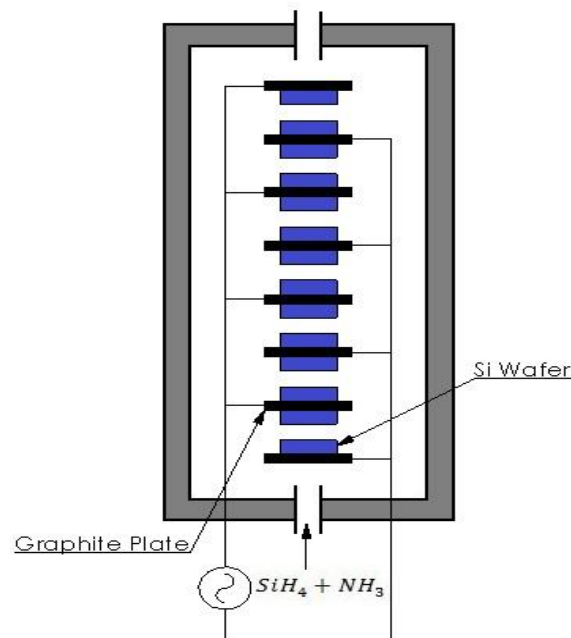
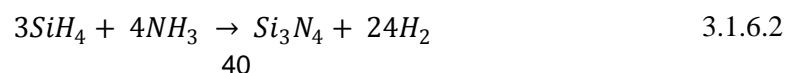


**Figure 3.6** The schematic representation of silicon nitride deposition by PECVD system

The chemical process during the deposition of silicon nitride is given by following equation:



The reflection properties of silicon nitride at the different thicknesses are represented in the next chapter.

### 3.1.7. Metallization

In this process, the metal contacts are created in front and back side of the solar cell to transport the charge carrier's separation to an external load. There are different metallization methods which are used for the construction of the crystalline silicon solar cells. However in the solar cell industry the most commonly method is used by screen-printing which is deposited the Ag/Al paste.

In this work, silver paste was used for front grid metallization contact and aluminum paste is coated fully at the back metallization contact. The pastes are deposited by screen-printing on the device. After deposition of Ag/Al pastes as metal contact, all devices should be passed by firing step under high temperature due to induce the metal diffusion into the device. The high temperature in this process can also result in getting rid of solvent inside the paste, solidification and organic components from the device. The facility for this process is illustrated in figure 3.7.

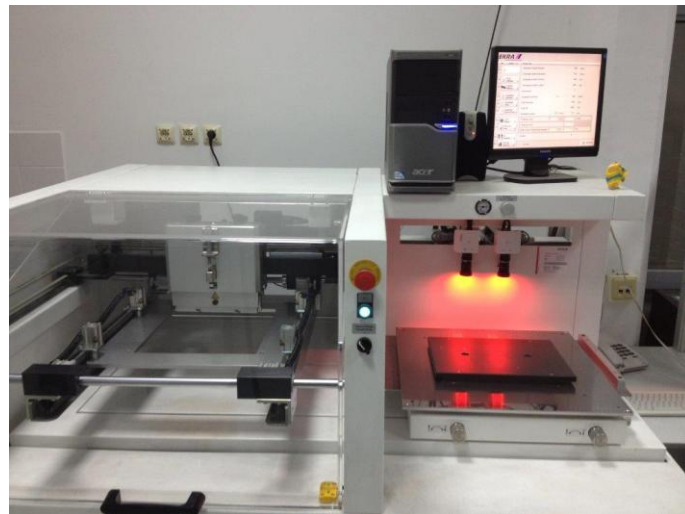


**Figure 3.7** The image of metallization device at GÜNAM

### 3.1.8. Laser Edge isolation:

In the solar cell operation, the separated electron and hole across the junction is important for generating current which produces electrical power. During the doping process n-type layer is deposited on the p-type silicon wafer, the deposited n-layer covers all of the substrate which includes both of the edges, and back side of the wafer. There is aluminum contact at the rear side of the wafer which prevents it to be deposited by n-layer completely. The front and back contacts that are connected by deposition of n-layer around the edge, lead to create shunt current and recombination of separated electron-hole which reduced solar cell operation [41]. Therefore at the end of the process for removing shunt current, the

edges of the wafer are isolated by laser scribing. Figure 3.8 is represented the cell before and after edge isolation:

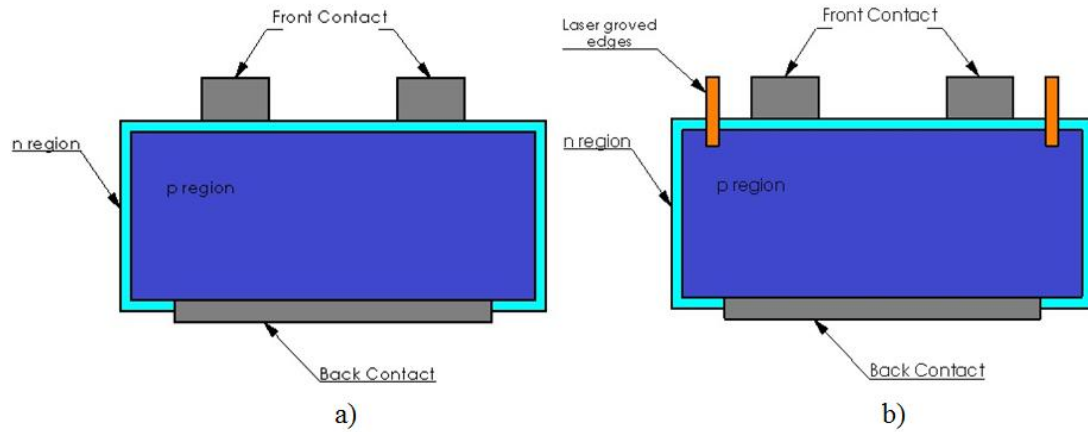


**Figure 3.8** Schematic of the solar cell fabrication (a) before and (b) after edge isolation

This Table 1. proves that edge isolation is a crucial step in solar cell fabrication.

Table 1. Comparison of the Cell efficiency for flat silicon before and after edge isolation

Cell efficiency [%] Thickness [nm]	Before edge isolation	After edge isolation
10 nm $\text{Si}_3\text{N}_4$	8.8	11
20nm $\text{Si}_3\text{N}_4$	9.2	12.3
75nm $\text{Si}_3\text{N}_4$	11.6	13.4

### 3.1.9. Sputtering systems:

In this section, after last step of the fabrication steps, the thin film silver is deposited by sputtering system on the silicon wafer. To reach binding energy levels of atoms, heating is a very suitable way for liquids or solids. This creates a way that atoms can get enough energy to break their atomic bonding. Therefore, each individual atom can easily acquire enough energy to escape from the surface by impacts of thermal stimulation. The circumstance which is ejection of the atoms from the surface is called evaporation. The basic working principle of sputtering is based on this process. In this work, to cover the silicon wafer surface with the silver, our main concern is sputtering because it is a convenient way for covering large areas. During the process, 12 nm thin film silver are deposited on the flat and textured silicon full scale devices with the six small samples for the reflection measurement and the other six ones for the SEM images analysis silver are coated.

The first observation of sputtering is found by using the electrical conductivity of gases in 1952. In that year, W. R Grove found that energetic ions in the gas bombarded the cathode surface of discharge tube. This causes sputtering at the surface. Then, he noticed that there exist the cathode materials on the inner surface of the discharge tube.

In those years, sputtering cannot be considered as a suitable because it is not easy to take bombarded atoms under control. Therefore, the cathode and grid of discharge gas tube are get harmed. Nevertheless, in these days, it is convenient with the increasing improvements. And it is widely used in such processes like surface cleaning, etching, surface deposition, surface and surface ion analysis, and sputter ion resources [42].

In this research, the sputtering process is used for the surface silver deposition because it has such advantages. The first one is better step coverage. The second one is that less radiation damage occurs when comparing with E-beam evaporation. And finally, the deposition of alloys, compounds and elements are done easily.

However, in our deposition process, we focused on bombarding the source with high speed particles instead of ejecting material from the source by rising the temperature. In other words, momentum transfer process takes place an important step for our concern. These high speed particles are mostly be ions. The reason underlying using ions is that it is a great opportunity to accelerate them by electric potential. If the kinetic energy of the ions that contact with the surface is less than about 5 eV, they are reflected or absorbed the surface. In other word, 5 eV can be defined as threshold.

$$E_{threshold} = \frac{\text{Heat of vaporization}}{\gamma(1 - \gamma)} \text{ where } \gamma = \frac{4M_1M_2}{(M_1 + M_2)^2}$$

When the kinetic energy of the ions is more than the binding energy of the surface atoms, they lead to damage on surface because ions have enough energy to pick source atoms from the source. This energy values can be about 10 eV or 30 eV.

For the deposition process, the removable rate of the surface atoms by bombarding ions is important for different process. This rate is called as the sputter yield, S. And it is defined as the mean number of atoms removed from the surface of a solid per incident ion [43].

$$S = \frac{\text{Ejected atoms or molecules}}{\text{incident ion}}$$

The figure 3.9 below illustrates the sputtering system:

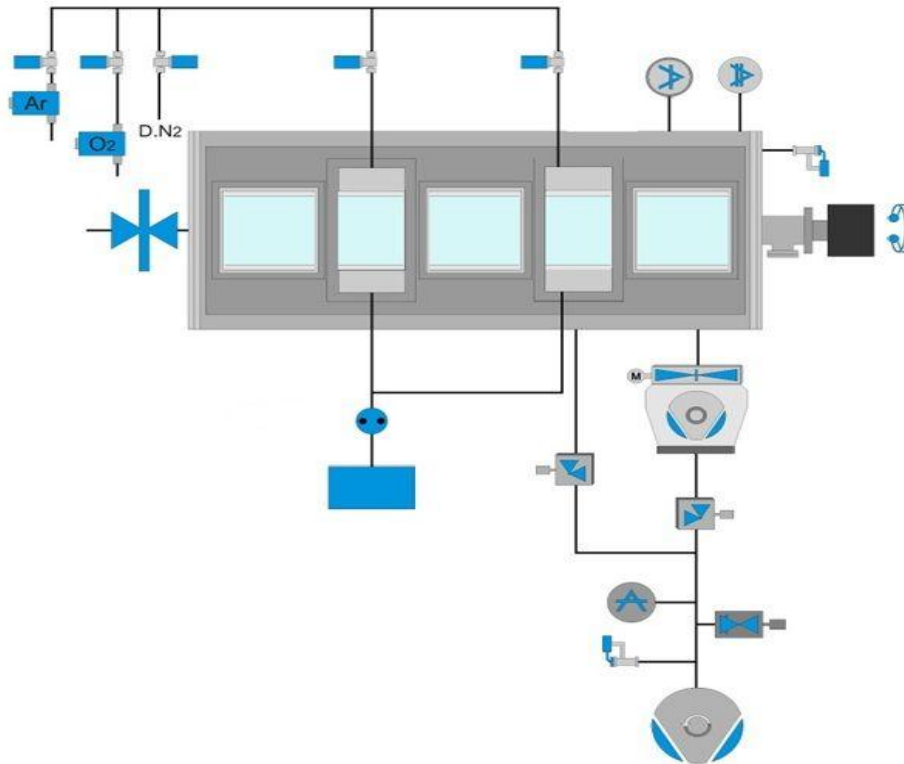


**Figure 3.9** Schematic diagram of the sputtering system

As it is mentioned above, the sputtering occur when the incident particles interact with the surface atoms. However, there are several factors that affect the sputtering yield parameters. These factors can be listed as:

1. Energy of incident particle
2. Type of target materials
3. Incident angle of incident particles
4. Crystal structure of the target surface

For our samples silver is sputtered at 100W power under 5 mTorr pressures, for 176 sccm Ar flow at room temperature.

This figure 3.10 represents below 12 nm thin film silver is deposited by sputtering system on the the full scale solar cell and smaller samples are deposited for the reflection measurements and SEM image analysis.

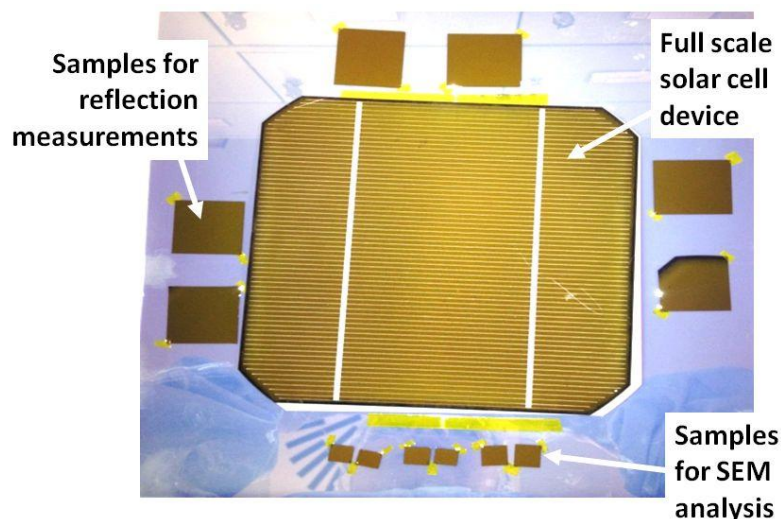


**Figure 3.10** The samples after silver deposition by sputtering

### 3.1.10. The Dewetting Technique

The strategy to choose self-organized NP fabrication is that in Top-Down approaches, such as lithography, the particle size, shape and inter particle distance can be very well adjusted but the capability of technique to very large areas surfaces is limited. Therefore we would like to use of Bottom-Up approach we let particles to form by self-organization on surfaces. The methods that we choose, is called surface dewetting.

Formation of MNPs by dewetting is a quite easy and low cost fabrication technique which makes it a very suitable method of plasmonic interface integration to large area full scale solar cell devices. Formation of the MNPs was performed by using silver metal film which is deposited by sputtering is a process that ejected the silver atoms by means of ion bombarded method at room temperature in a vacuum chamber. The thickness of the silver metal film is considered 12 nm which is desire dimensions for produce the MNP. After the samples were deposited with silver film, they were dewetted by hot plate which is isolated by oven at GUNAM. Figure 3.11 is illustrated the schematic diagram of annealing chamber. During the dewetting, the nitrogen gas is flowing through the oven to avoid the oxidation of AgNPs from the samples. The temperature is set at 200 °C. During the measurement, dewetting at the different time is used as mechanisms to control the shape and size distribution of the NPs.

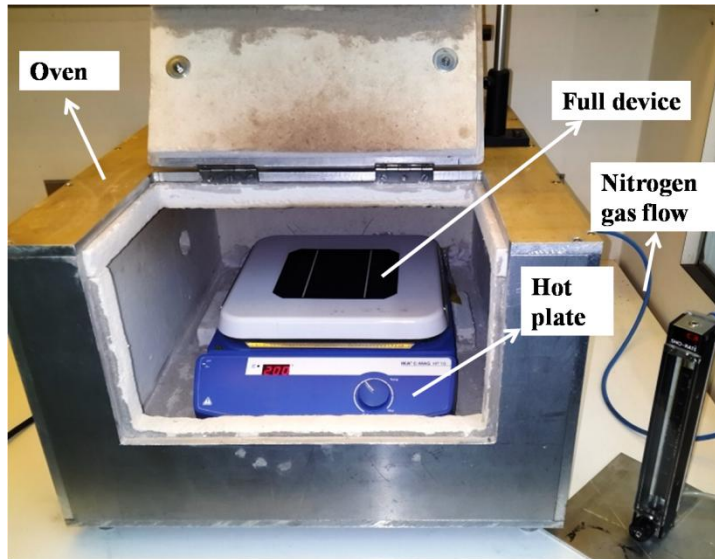


**Figure 3.11** Specially Design Annealing Chamber for Solar Cells devices

There are many experimental methods for fabrication of NPs such as e-beam lithography (EBL) and dewetting. Although, with e-beam lithography, size, shape and inter particle distance of MNPs can be well adjusted, this method is expensive and limited for large area substrates [44]. The dewetting technique is quite easy and low cost fabrication. Consequently, according to various techniques with different advantageous and disadvantageous, about how the metallic NPs are formed on the substrate; thin film dewetting techniques is most acceptable approach for this study since almost all the real films have non-homogeneity and defects in the film thickness.

The approach of thin film dewetting based on the formation of capillary instability. Capillary instability which is driven by surface energy minimization was first introduced by Rayleigh [45], through usage of theoretical analysis to investigate stability of infinite cylinders of liquids without viscosity. Rayleigh expressed that liquid cannot be stable with small perturbations with wavelengths  $\lambda$  that is greater than  $2\pi R$  ( $\lambda > 2\pi R$ ). Liquids decompose into a set of liquid droplets [45].

The similar theoretical study was used by Nichols and Mullins for the analysis of the solid cylinders without any contact with substrates; they got the same result as Rayleigh [46].

For a solid film without defect, the process starts at the edge of the film by a surface energy gradient which is due to the edge agglomeration that is result of capillary instability. In reality, since the films are not without defects and the film thickness contains some non-homogeneity. The tendency of the minimization of interfacial energy with the contributions of defects leads to formation of grooves in the film. These grooves can reach the substrate and form stable voids. Consequently the film decomposes in to separate parts.

From another point of view, the formation of MNP can also be declared by the difference in the thermal expansion coefficients which is between metals and the substrate. Stress gradient is formed because of the distribution of the stress is not homogeneous through the metal film

and the substrate. Finally, the film moves from the stressed region to relaxed region as a hillock. Holes are formed through this surface diffusion [47-49].

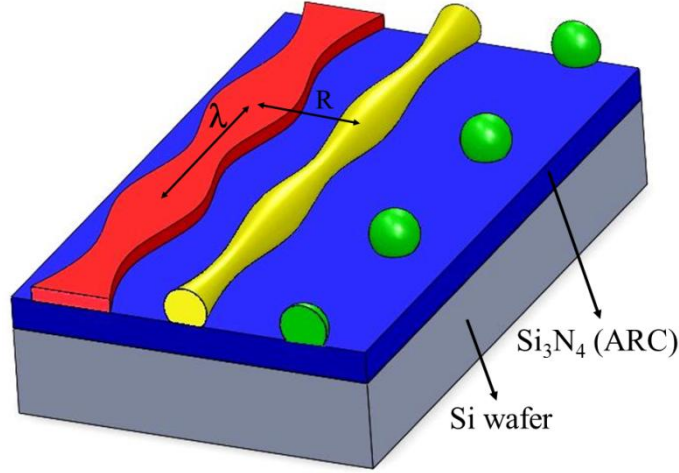


**Figure 3.12** Formation of liquid droplet NP into substrate according to Rayleigh capillary instability

In this work, the plasmonic NPs formation by dewetting techniques during the different time and various silicon nitride thicknesses, Scanning Electron Microscope (SEM) analysis, statistics of the size distribution and shape of the particles will be discussed in next sections.

Properties of MNPs for light-trapping applications are highly efficient. When the MNPs are embedded on the silicon substrate based on metallic material types, the scattering of incident light into the substrate will be changed. In the plasmonic applications the scattering of incoming light is much more important than the absorption of incoming light by particles. Therefore, the material types with respect to the plasmonic behavior and optical properties when interact with electromagnetic wave play an important role in performance of the solar cells. With considering these properties, in this work, silver is chosen as metallic NPs due to the lower absorption and higher free electron density in comparison with the other metals. There are variety of metallic materials such as copper, aluminum and gold with different optical properties. If we consider theory of the MNPs when interact with incident electromagnetic field, the dielectric function of free electron as collective oscillation can be describe by Drude model (see chapter 2) which is represented by following equation :

$$\varepsilon_{Drude}(\omega) = 1 - \frac{\omega_p^2}{\omega^2 + i\gamma\omega} \quad 3.1.10.1$$

Where  $\omega_p$  is plasmon frequency of free electron. By inserting the dielectric function equation into the polarizability of the particle, the polarizability will be:

$$\alpha = 3V \frac{\omega_p^2}{\omega_p^2 - 3\omega - i\gamma\omega} \quad 3.1.10.2$$

The surface plasmon resonance frequency depends on the density of free electrons into the particle which is obtained by this formula:  $\omega_{sp} = \sqrt{3}\omega_p$  .

Therefore selection of the type of metal according to use the Drude model, during the experiment is an easy work. Aluminum and silver in comparison with gold and copper have higher density of free electron which is leded the surface plasmon resonance of the silver and aluminum take place at UV region and for gold and copper occurs in the visible region. As we talked before, the resonance frequency of the particle depends on the shape, size and the surrounding environment and they can be tuned by varying these parameters.

Silver and gold have superior optical properties with the same value of dielectric function for the real part which defines scattering cross-section. However the imaginary part of the dielectric function defines absorption of the particle are quite different. Due to the higher absorption coefficient and higher cost of gold than the silver, in this work the silver was preferred. As a result, choice of the metallic material is important role for both of the plasmonic behavior and the medium environment.

### 3.1.11. Image Analysis

The MNPs formations on the substrate were imaged with QUANTA 400F by Scanning Electron Microscope (SEM) at the Central Laboratory of METU. The images taken from SEM are very important for the both of qualitative and quantitative analysis for each sample. The quantitative analysis, represent the formation of the MNP on the substrate and give an idea about the shape of the particles. For the qualitative part, the images were analyzed by image analysis software program called Gwyddion. The figure 3.13 is illustrated the steps of image analysis.

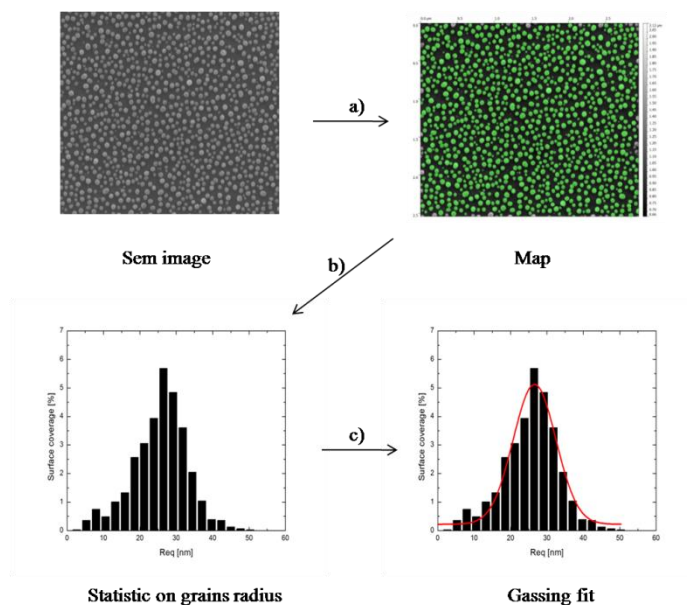


**Figure 3.13** Analysis steps for SEM images: (a) In the SEM image, first grains marking by threshold and reject grains with size less than  $10 \text{ px}^2$  and the grains at edge are removed from the mask (b) The surface coverage of NPs directly are derived from the statistics on grain radius (c) Gaussian fit are applied on statistics.

The figure 3.13 represents the creation of the mask by marking of the particles. The mask is created by the program which includes the integration of the particles with green colors. The image analysis is considered only the region under the mask. For reducing the errors in the images analysis, all of the samples should be considered in the same magnification.

If the image has noise, it can be removed by filtering (denoise) at first. For the separation of the NPs from the underlying substrate, the primary aim is to create the mask by threshold which are marked only the grains. Then the grains by threshold with size less than  $10 \mu\text{m}^2$  are removed; second, the grains which are uncompleted at the edge of the images reject from the mask. Particles based on the need during the analysis can be excluded.

During the image analysis by the program, some important parameters extract from NPs analysis. The statistics of the distribution of various grains (NPs) characteristic give the information about number of the grains (particles), mean particle size and area, their projected area both in absolute values and relative values. The statistics of the equivalent disk radius can be plotted for each sample by means of the size distribution. The overall surface coverage also can be obtained from the statistics of the equivalent disk radius. An example for this kind of the graph in figure 3.13 represents the statistic of the disk radii with their populations.

In this study, the image analysis enables us to investigate the effect of the particle dimensions after dewetting the samples at the different times. Therefore, image analysis gives an idea and information about the particle surface coverage and dimensions of the particles, and how these are influenced by changing dewetting time. All of the measurements from characterization of the solar cell including cell parameter, QE, reflection and image analysis are discussed in the results and discussion parts.

## **3.2. Optical Characterization**

### **3.2.1. Reflectance Measurement Set up**

By dewetting of the thin film silver on silicon, the AgNPs form on the samples. The optical properties of AgNPs respect to the peak position of the plasmonic NPs at resonance condition can be measured by total reflection. The schematic diagram of the system is shown in figure 3.14.

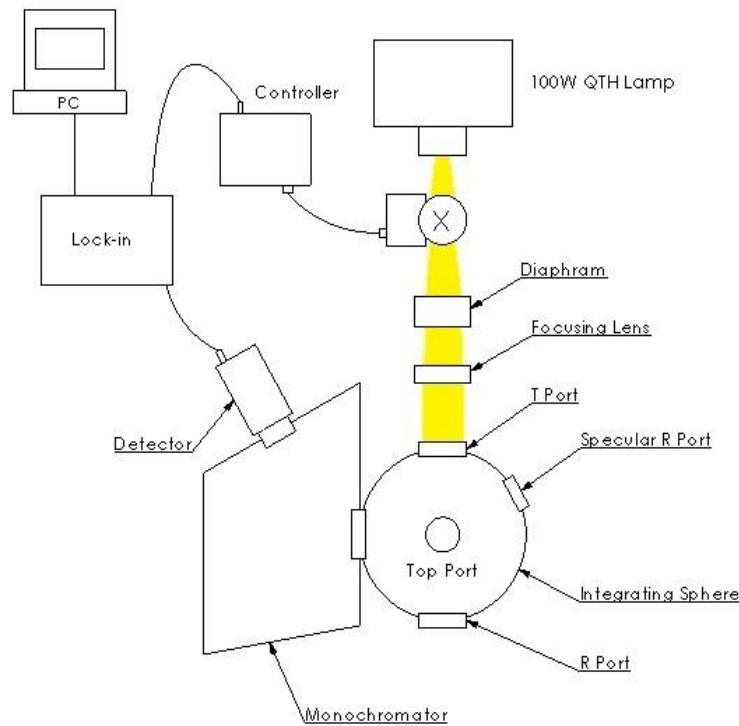


**Figure 3.14** Schematic diagram of the reflectance measurement setup

During the measurement the power of halogen light source is set to 100W. The light from a halogen lamp passes through the chopper result in optical signal modulated at some frequency, which is connected to the controller. The modulated signal at the controller should be the same value when reached at lock-in amplifier. During the measurement it is necessary to well control the sensitivity carefully.

It should not be read an over load signal. The diaphragm subjected behind the lens effects to decreases the spot size. When incoming light passes through the focusing lens, creates an image of the lamp filament on the R port (Reflection port) of the sphere make focus the incoming light.

For reflectance measurement, the collection of both specular and diffuse reflection of incident light from all directions is performed by integrating sphere (8 inch diameter, Oriel 70679NS). The sample is mounted  $8^\circ$  rotation with incoming light. For the reflectance measurement the sample is subjected back side of the integrating sphere port and for transmission, sample is subjected front side of the integrating sphere port. The reflected beam from integrating sphere passes from entrance slit of monochromator (74100). After reaches from output of the UV enhanced Si detector (Newport 70356) the signal is amplified by lock-in amplifier (SRS 830). And finally all these data are collected on a PC by a LabVIEW program. Optical characterization carried out in the range of 300-1100 nm.

The properties of integrating sphere are diffuse the incoming light in all direction and collect all diffuse and specular reflection, result in give accuracy data from whole samples.

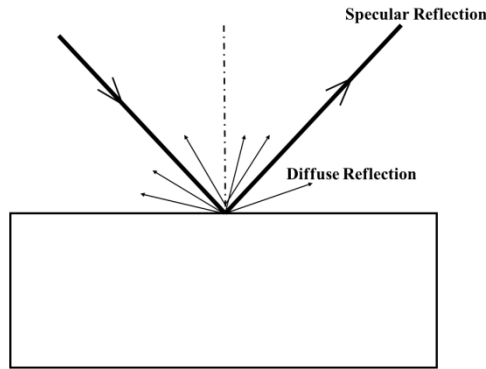


**Figure 3.15** Diffuse and Specular reflection of light from surface

The measured data are calculated from calibration disk and dark measurements. For take a dark background measurement, both of R (reflectance) and T (transmission) port of the integrating sphere is to be empty. For take a reference measurement, the BaSO<sub>4</sub> calibration disk is placed at the sphere R (reflectance) port and is assumed to have 100% reflectivity.

So the total reflection from measured data with considers as calibration disk and dark data, is calculated by:

$$Total\ Reflection = \frac{R - Dark}{Ref - Dark} \quad 3.2.1$$

Where  $R$  is represent as collection of data from light signal which is reflected by samples.  $Ref$  is collection of data from calibration disk and  $Dark$  defined as collection of all data from directly light passes through integrating sphere.

### 3.3. Electrical Characterization

#### 3.3.1. I-V Characterization Set up

The illuminated I-V characteristic is performed by solar cell simulator. It measures I-V analysis and characterizes solar cell parameters including short circuit current ( $I_{sc}$ ), open circuit voltage ( $V_{oc}$ ), maximum power point ( $P_{max}$ ), fill factor (FF), and cell efficiency ( $\eta$ ) as well. Intensity of incident light strikes on solar cell is equal to  $1KW/m^2$  under standard solar cell spectrum at AM1.5. The cell area is 0.0243. Sample is connected by two probes in front and back contact of solar cell to the current-voltage source (Keithley sourcemeater). The controlling between solar simulator and sourcemeater is performed by computer software. The system is illustrated in figure 3.16:

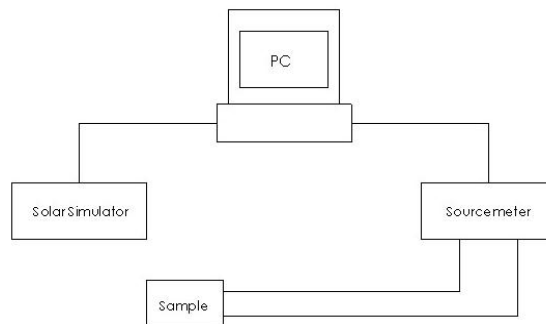


**Figure 3.16** Schematic diagram of I-V characterization

These figures below represent equivalent circuit under dark and illuminated PV cell which comprise as a photodiode.

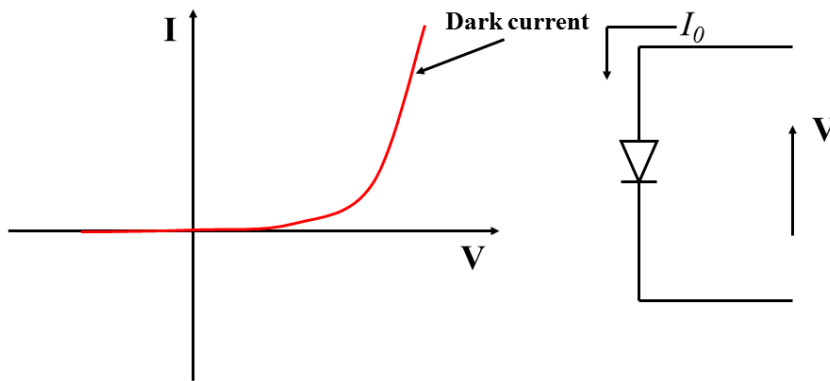


**Figure 3.17** I-V characteristic with equivalent circuit of photovoltaic cell under dark condition

Under dark condition PV cell behave as a diode at which no current flows through the external circuit.

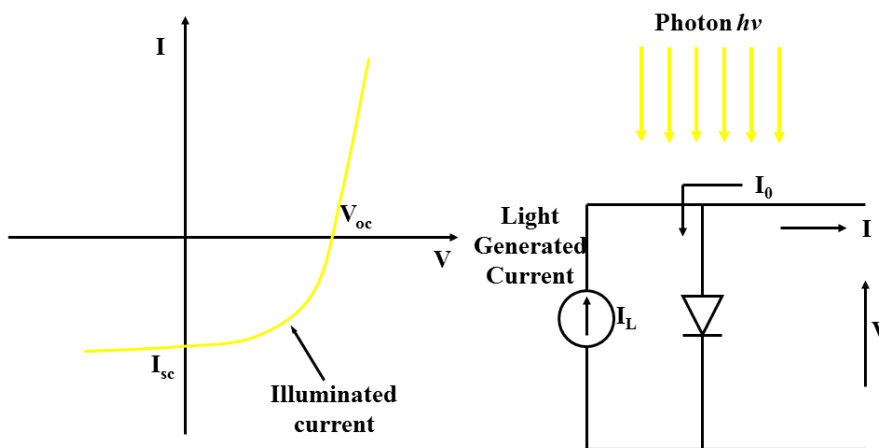


**Figure 3.18** I-V characteristic with equivalent circuit of PV cell under illumination

In an ideal PV cell when the light incident PV cell, the (I-V) characteristic shifts to the fourth quadrant. When the photon energy is greater than the band gap of the material, electron excited to the conduction band if the external load connected to output of the circuit, the photo generated current will flow through the external circuit.

### 3.3.2. Quantum Efficiency Setup

The QE experiment is measured by this set up. The schematic diagram of the system is represented in figure 3.19.

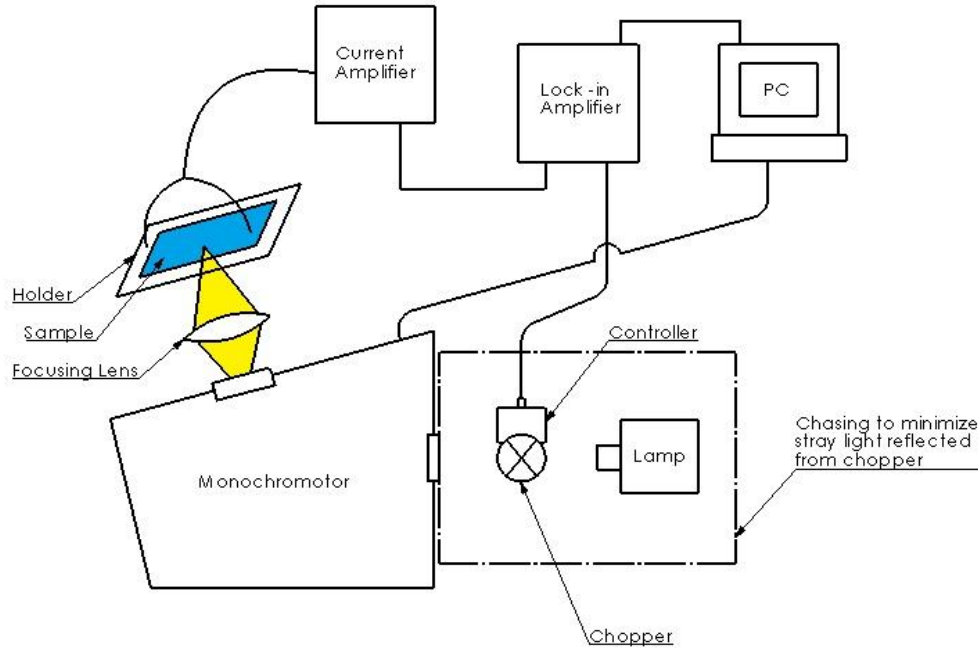


**Figure 3.19** Schematic diagram of the QE measurement setup

QE is the measure of the number of electrons the device generates per number of photons incident on the device surface, for each wavelength.

During the measurement, the light from a halogen lamp (at 100W) passes through a chopper, which modulates it at a reference frequency (set to 135Hz), and then through a monochromator. At the exit of the monochromator, this modulated light is focused on the surface of the tested cell using a converging lens. The light incident on the cell generates a photocurrent, which is amplified and transformed to a proportional voltage using a current amplifier. This voltage is connected to the lock-in amplifier.

The lock-in only measures the electrical signal that matches its reference frequency, which is supplied by the chopper controller. Therefore, noise due to other (un-modulated) light sources is rejected. The measured signal is proportional to the photocurrent due to the modulated light coming from the monochromator; dividing this voltage by the gain (V/A) of the amplifier and the charge of an electron gives the number of electrons the tested cell generates, at each wavelength.

Now, to measure the number of incident photons, the tested cell is replaced with a photodetector with known detectivity (A/W). The same procedure is applied and the same beam of light is focused on the detector surface. This time, the measured signal is divided by the detector's gain (V/A) and detectivity (A/W), resulting in the incident power (W) at that wavelength. This is further divided by the energy carried by each photon at that wavelength ( $h \cdot c / \lambda$ ), giving the number of photons incident at the surface of the detector, at each wavelength.

The ratio of these two gives out the external quantum efficiency. The characterization is carried out in the 350-1100 nm range. All these data are collected on a PC by a LabVIEW program.

The QE defines the attribution of incident light power to electrical power. Before power density was measured from output of monochromator, by multiplying the power density at that wavelength with area of the cell, the power incident of the cell can be calculated. Hence number of photon incident on the surface of the cell is founded at each wavelength, after simple calculation. Number of electrons collected from the cell surface yielded from current output at each wavelength by measurement of sourcemeter. The QE is defined as by following equations:

$$QE = \frac{\textit{number of collected charge carriers by solar cell surface}}{\textit{number of absorbed photons incident}}$$

The total optical and electrical characterizations and image analysis are discussed in the results and discussion part.

## CHAPTER 4

### RESULTS AND DISCUSSIONS

After the description of the experimental methods in the previous section, in this study the effect of the MNP as light-trapping to improve the cell efficiency of solar cell is investigated for both of flat and textured silicon. By measuring optical and electrical properties of full scale device, the plasmonic behavior of AgNPs is determined when placed on full scale device. This chapter is structured into three parts. In the first part, I present and discuss the reflection data obtained from test samples produced under the same conditions as the full PV device. In the second part, I present and analyses the SEM images to obtain the surface coverage and size distribution of AgNPs decorated on samples and compare with the Mie theory. In the third part, the full device electrical characterizations are present. The results of all measurements are discussed in the following section.

#### 4.1. Optical Reflection Results

In the plasmonic application there are two important parameters that effect solar cell performance: near field effect and light scattering from MNPs to enhance the light trapping into the solar cell devices. In this study, scattering of incident light from MNPs into the substrate is important to enhance the travelled optical path length of photon that lead to increase in the energy conversion efficiency. Hence, by measuring the reflection of incoming light from AgNPs in all directions, the effect of scattering light from NP can be characterized. The figures below are represented the total reflection measurement of flat and textured silicon with different time dewetting and various silicon nitride thicknesses.

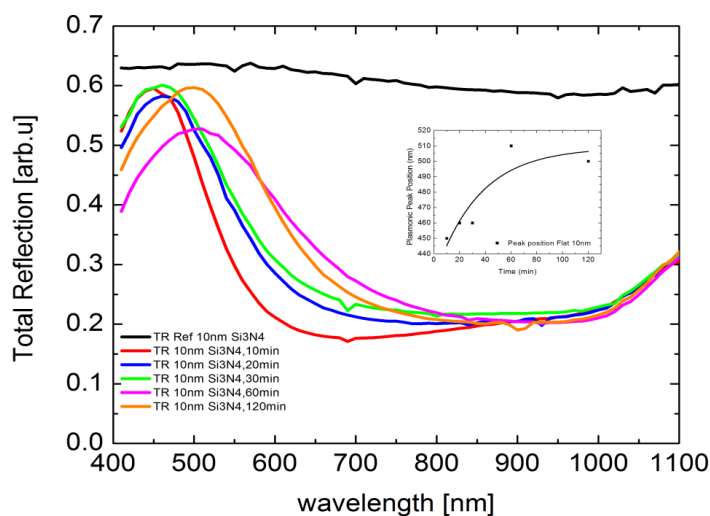


**Figure 4.1** Reflection behaviors from AgNPs at different time dewetting for flat Silicon with 10 nm silicon nitride thicknesses.

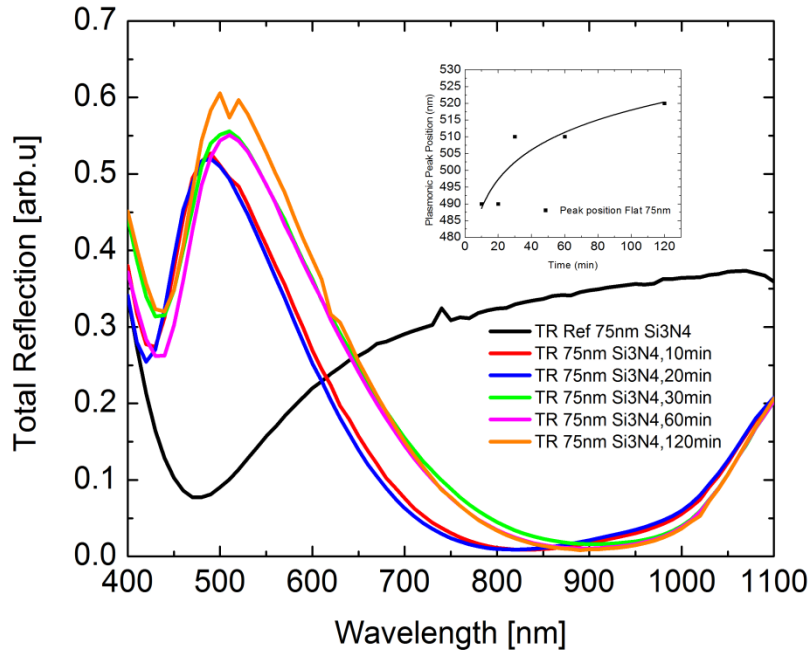


**Figure 4.2** Reflection behaviors from AgNPs at different time dewetting for flat Silicon with 75 nm silicon nitride thicknesses.

In this work, the reflections of incident light from AgNPs are measured by two types of silicon solar cell such as flat and textured silicon. Both of them are deposited with silicon nitride as an ARC with different thicknesses which are: 10 nm and 75 nm by Plasma Enhanced Chemical Vapor Deposition (PECVD). The continuous 12 nm silver film is deposited by sputtering system at room temperature under high vacuum. The samples are annealed at different times in the furnace under nitrogen flow due to avoid from oxidation. After dewetting, the AgNPs are formed on substrate. The size of the formation particle depends on dewetting time. We investigate the size distribution and particle size by Gwyddion program. By reflection measurement, plasmonic resonance peak position can be directly obtained from samples. Therefore, the optical response of AgNPs decorated on silicon is measured when reflect the incoming light. Likewise reflectivity measures reflected photon proportion of incident photon as a function of wavelength.

According to the results in flat silicon, we observe interesting correlation between dewetting time and plasmonic peak position. As increasing the dewetting time, the resonance peak of the electron clouds inside the MNPs shift to higher wavelength. By increase of the thickness of silicon nitride, the reflection peak wavelength respect to the Plasmon resonance increase either.

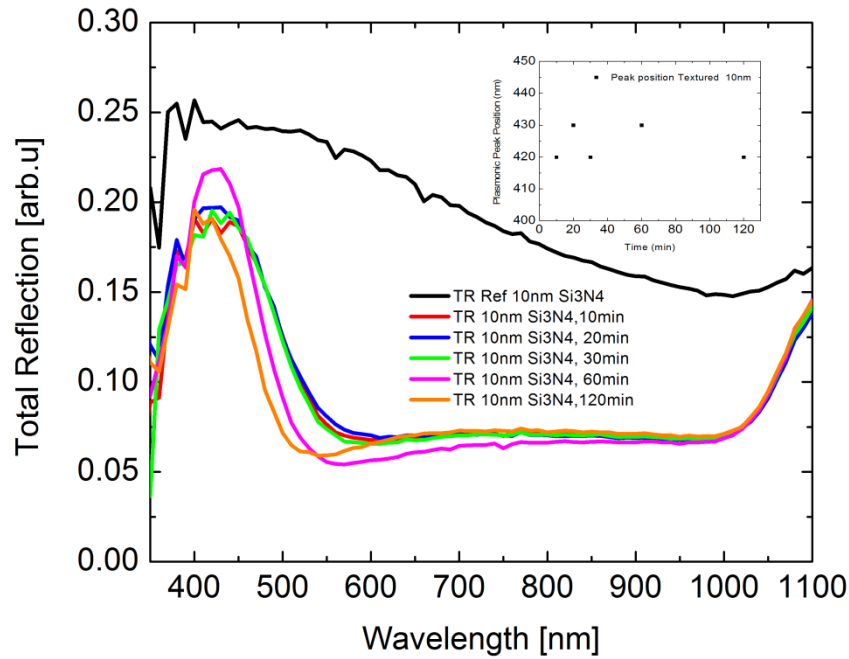


**Figure 4.3** Reflection behaviors from AgNPs at different time dewetting for textured Silicon, with 10 nm silicon nitride thickness

In this case, the previous process is performed; however type of the silicon is changed. We investigated the reflection of textured silicon from incoming light. Here, n-type mono crystalline silicon surfaces were textured by wet anisotropic KOH chemical etching technique. The results below, illustrate the textured silicon with 10 nm and 75 nm silicon nitride thicknesses and the samples are dewetted at different times.

As we observed, the surface texturing by KOH, altered the smoothness of the surface and hindering the homogenous flowing of silver, leading to very random distribution of AgNPs decorated on sample. This random distribution of AgNPs results in uncontrolled plasmonic resonance shifts as the dewetting time is increased.

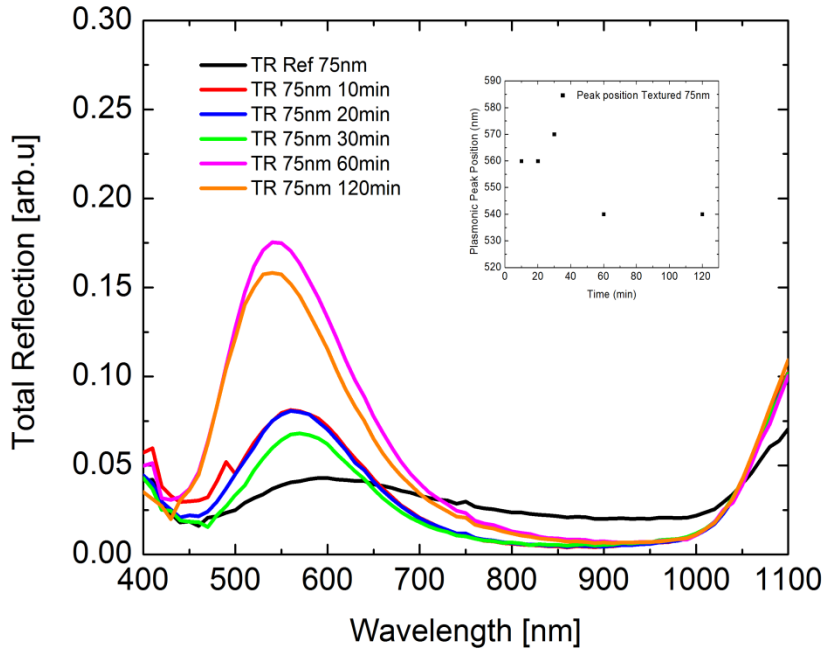


**Figure 4.4** Reflection behaviors from AgNPs at different time dewetting for textured Silicon, with 75 nm silicon nitride thickness

According to figures 4.1, 4.2, 4.3 and 4.4 for both types of flat and textured silicon, we observed there is an interesting correlation between the dewetting time and resonance peak position in flat silicon. With increasing dewetting time the resonance peak position shifts to higher wavelength. For the texturing silicon the optical losses means reflection of incoming light from AgNP is much lower than the flat silicon. It is clear that texturing the substrate is one way to reduce the reflectivity from substrate and increase the light-trapping approach in solar cell applications.

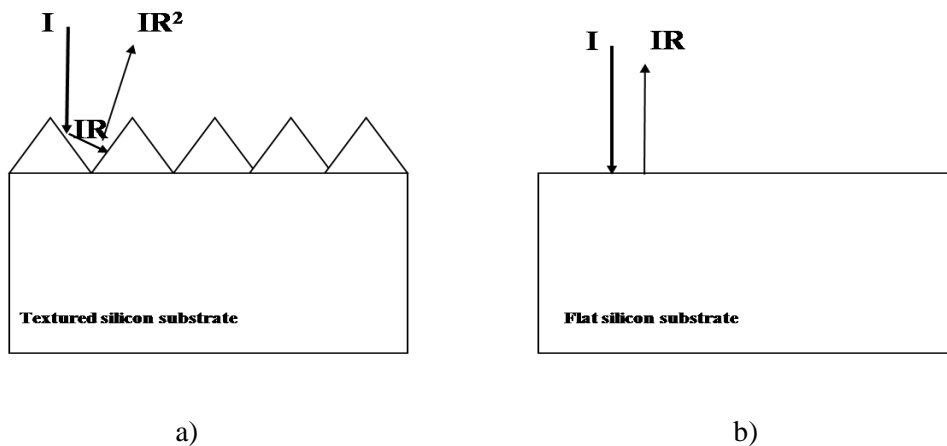
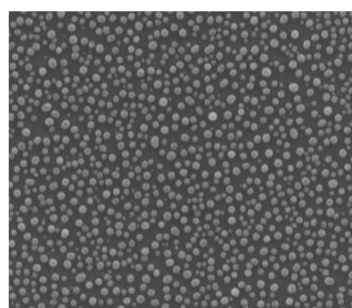


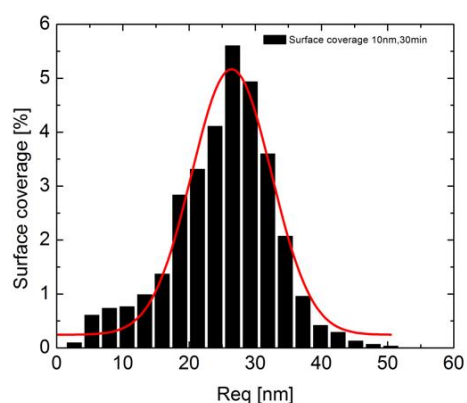
**Figure 4.5** Reflection of incident light from (a) textured substrate, (b) flat substrate

## 4.2. Formation of AgNPs by Dewetting Techniques

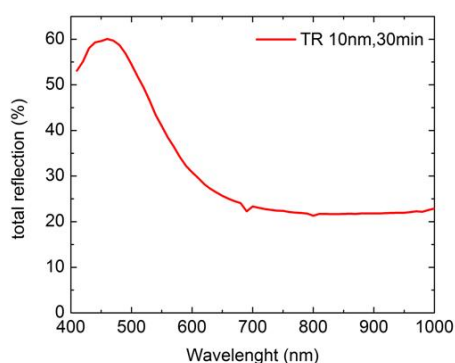
In this section, the small samples are deposited with 12 nm silver by sputtering system. The formation of AgNPs by dewetting technique is done at 200 °C in a furnace under nitrogen gas flow. Two main parameters that altered during this process are different times and various silicon nitride thicknesses. The samples are imaged by Scanning Electron Microscope (SEM). The images are analyzed by software image analysis named as Gwyddion. Some important parameters that are investigated by analyzing AgNPs include the particle surface coverage and dimensions of the particles, and how they are influenced by changing dewetting time. The result of image analysis on formation of AgNPs is investigated on the different silicon nitride thicknesses which are 10 nm and 75 nm. The y-axes of the size distribution graph represented the surface coverage of the AgNPs in percentage and x-axes correspond to the radius of an equivalent circular disk. The affect of dewetting time at 30 minutes as an example is described at the different silicon nitride thicknesses which are 10 nm and 75 nm. The optical response of the NPs by reflection measurement can be seen in the Figures 4.6 (c) and 4.7 (c).



a) SEM image



b) equivalent disc radius distribution

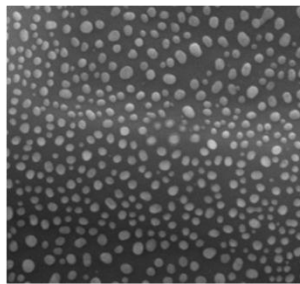


c) Total Reflection

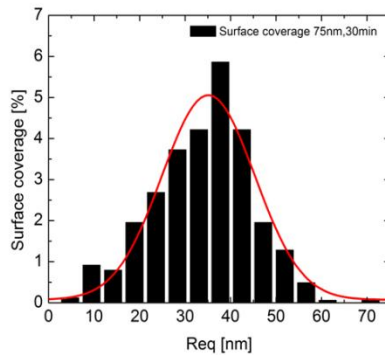
<b>Mean Radius (nm)</b>	<b>26.4</b>
<b>FWHM (nm)</b>	<b>14.2</b>
<b>Total Reflection Peak Position (nm)</b>	<b>460</b>

d) Table of content

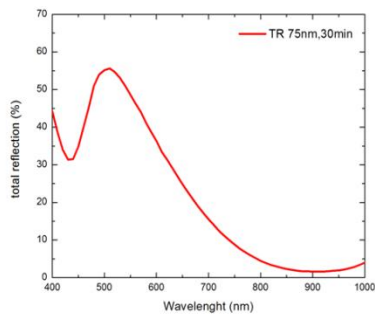
**Figure 4.6** Representation of AgNPs fabricated on 10 nm silicon nitride, with 30 minute dewetting time at 200 °C, (a) SEM image, (b) equivalent disc radius distribution, (c) Total Reflection, (d) Table of content



a) SEM image



b) equivalent disc radius distribution



c) Total Reflection

<b>Mean Radius (nm)</b>	<b>35.1</b>
<b>FWHM (nm)</b>	<b>24</b>
<b>Total Reflection Peak Position (nm)</b>	<b>510</b>

d) Table of content

**Figure 4.7** Representation of AgNPs fabricated on 75 nm silicon nitride, with 30 minute dewetting time at 200 °C, (a) SEM image, (b) equivalent disc radius distribution, (c) Total Reflection, (d) Table of content

According to figures 4.6 and 4.7, size of AgNPs in 75 nm silicon nitride thickness appears to be larger than AgNPs on 10 nm silicon nitride thickness, however smaller particles are disappeared in 75 nm silicon nitride thickness. The affects of the silicon nitride thickness clearly can be seen from the resultant data. Therefore, when thickness of silicon nitride increases, the plasmonic resonance peak shifts to higher wavelength with increasing particle mean size. Likewise, the FWHM increases with increasing the silicon nitride thickness as expected. These results are in agreement and confirmation with pervious published experimental results [50].

These figures below, are represented the same samples, 10 nm and 75 nm silicon nitride thicknesses with different dewetting times. The affects of dewetting time on median particle size and resonance peak position are investigated from corresponding samples.

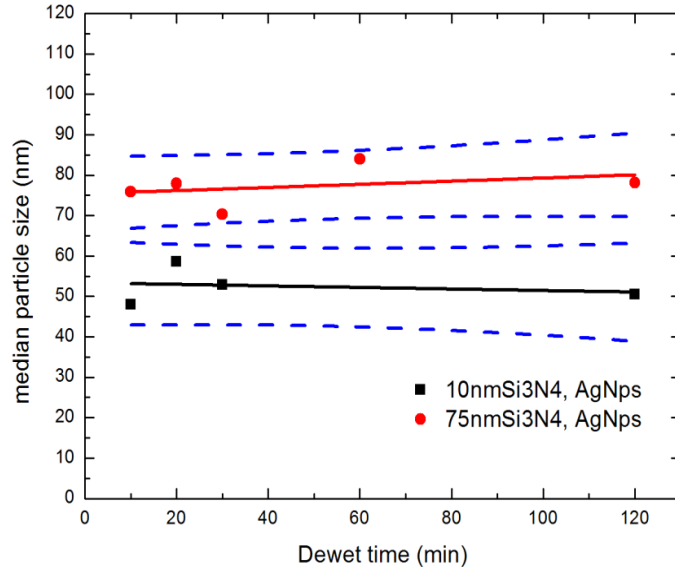


**Figure 4.8** Influence of dewetting time on mean particle size

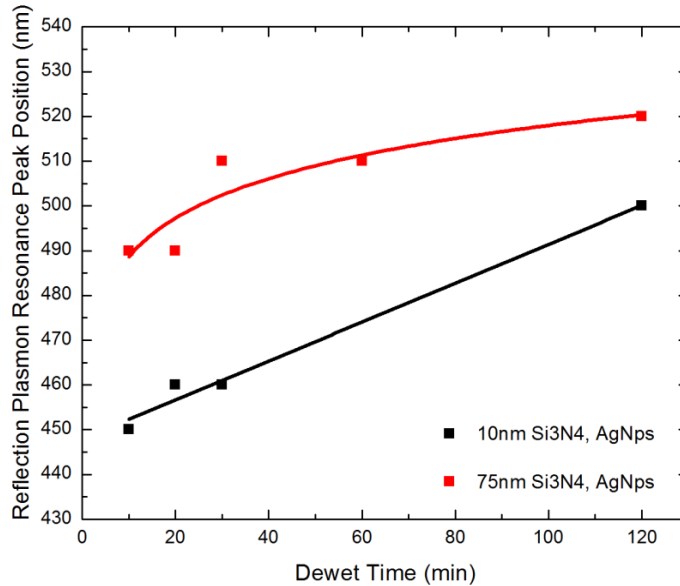


**Figure 4.9** Influence of dewetting time on resonance peak positions

For 200 °C annealing condition, the dewetting dynamics shows a stable configuration for annealing duration for longer than 15 minutes. This fact is observed from both SEM data and reflection peak- position obtained from corresponding samples. We can conclude that for mild annealing temperature of 200 °C, prolonged annealing time longer than 30 minutes are not beneficial in tuning the mean particle size and hence the reflection peak position wavelengths. These results are in agreement and confirmation with pervious published experimental results [50]. For thicker Si<sub>3</sub>N<sub>4</sub> (75 nm) the particle size is larger than for thinner Si<sub>3</sub>N<sub>4</sub> (10 nm) thin film layer. This is in agreement with the findings of Tanyeli et al. [50]. Larger particles are formed on substrates having lower thermal conductivities. Silicon has lower thermal conductivity as compared to Si<sub>3</sub>N<sub>4</sub>. Therefore, when Si<sub>3</sub>N<sub>4</sub> has 10 nm thicknesses, the thermal conductivity of Si governs the silver dewetting and smaller particles

are formed. For 75 nm  $\text{Si}_3\text{N}_4$ , the higher thermal conductivity of  $\text{Si}_3\text{N}_4$  governs the dewetting of silver and larger particles are formed.

The scattering from particles rely on the dielectric properties of the particle and the medium surrounded the particle. In this study, the surrounding medium is not uniform therefore; some parts of the particle contact with underlying surface and some parts are in the air. For making logical evaluation according to theoretical considerations, the overall dielectric structure which is generated the observed reflection spectra, should be represented.

For this representation, an effective dielectric constant which is related to the contact areas of the particle to the surrounding media is offered. In this work, the contribution of media to the effective dielectric constant of the particles is supposed to be equal. Therefore; the geometric average of the dielectric functions of each medium was considered as the dielectric function of the effective homogenous medium. In this thesis, three different hypothetical cases were tested to make up the effective index. These cases are as follows:  $n_1$  represents the effective index which is due to %50 air and 50% silicon nitride contribution;  $n_2$  represents the effective index which is due to %23 air and 77% silicon nitride contribution;  $n_3$  represents the effective index which is due to %10 air and 70% silicon nitride, and 20% silicon contribution. As the SEM image indicate mean inter particle distance is the same order of the magnitude average particle size and there is no accurate particle size; As a result, only one of the samples were examined for comparison between theory and experiments. The calculations are done by using the Mie light scattering theory for single spherical AgNPs with given size and surrounding medium specifications. This scattering cross section curves are weighted averages of scattering curves obtained from single particle of radii equals to ranging 30 nm to 60 nm [51].

In this work, the sample was annealed at 200 °C with mean diameter 70 nm with silicon nitride refractive index of 2.016 and silicon refractive index of 3.5. Resonance peak positions obtained from both theory and experiment for AgNPs with a mean diameter of 70 nm is represented by figure 4.10.

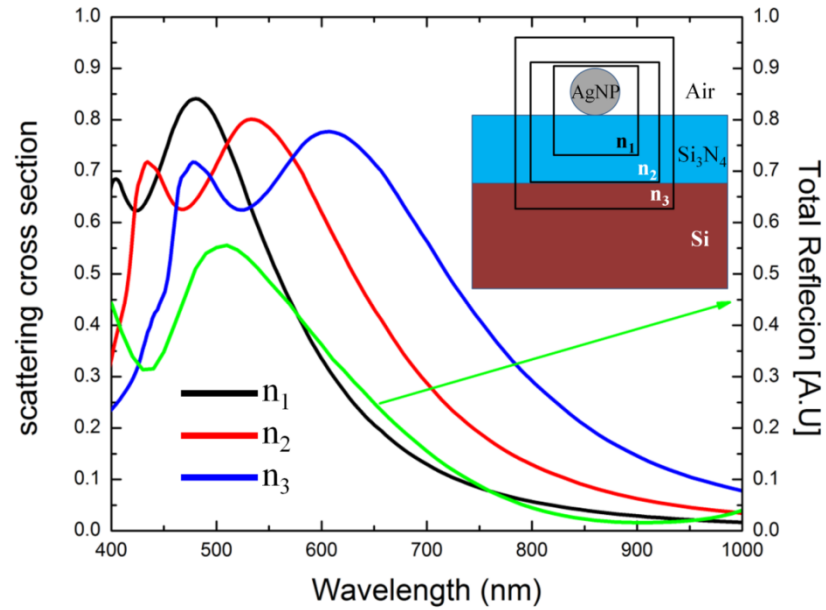


**Figure 4.10** Scattering cross-sections obtained from size weighted average of Mie scattering theory with three different effective index models and experimental reflection data belonging to silicon surface decorated with AgNPs of 70 nm mean diameter

Figure 4.10 shows a comparison between Mie light scattering theory and total reflection spectrum obtained from the same sample as presented in figure 4.7. As it is shown in the figure, the main peak positions from experiment are 510 nm. As it was declared above for theoretical part, three sets with different refractive indexes were considered. For effective refractive indices equal to  $n_1= 1.5$ ,  $n_2= 1.8$ ,  $n_3= 2.2$ , the peak positions are approximately 480 nm, 533 nm, and 608 nm, respectively. As it is shown in figure 4.10 in theoretical diagrams by reducing refractive index, the main resonance peak position will shift to lower wavelengths; this main peak seen in both experimental and theoretical curves is because of the plasmonic resonance of dipole oscillations. From theoretical graph results, the main peak position in graph with refractive index of 1.5 has almost the same position of the experimental peak position.

The change in plasmon resonance due to the location of NPs with respect to the substrate, interactions among them, their shapes, and sizes as well as dielectric properties of substrate are discussed theoretically and implications of these for the experiment are deliberated. For verification of this part of thesis, the study which was done by Gunendi et al. [52] is considered. In this article, for calculation of the scattering efficiencies, The FDTD method was used. As it was shown in figure 4.10 in the graph of experimental result, the main resonance plasmonic peak was in 510 nm wavelength which in comparison with the resonance plasmonic peak theoretical graph result of Gunendi et al. that occurs in 540 nm wavelength , are very close.

### 4.3. Effect of temperature on cell efficiency of full scale device without silver deposition

In this study, the resistance of the sample against temperature is investigated. The silicon wafer with 20 nm silicon nitride thickness as a test sample is annealed at different temperature for one hour. Figure 4.11 illustrates the result of the temperature study:

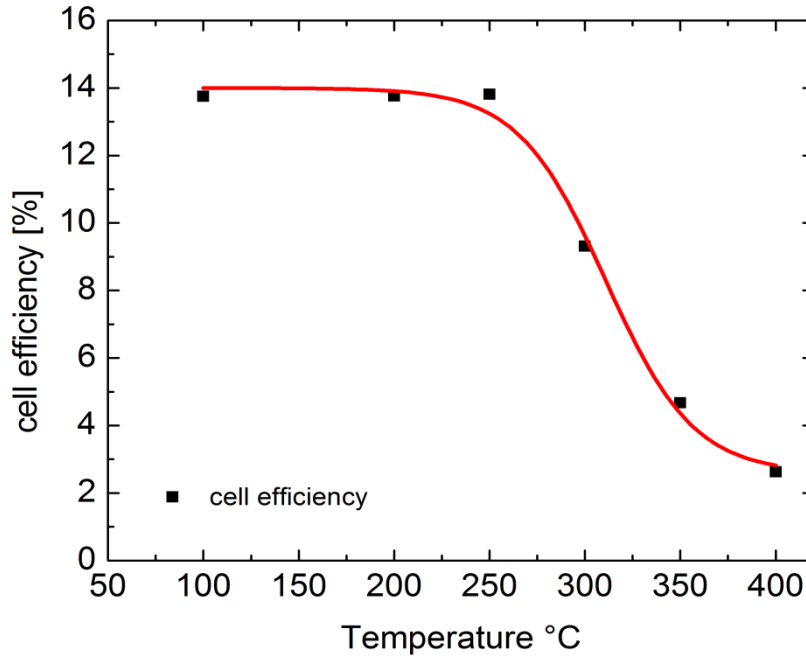
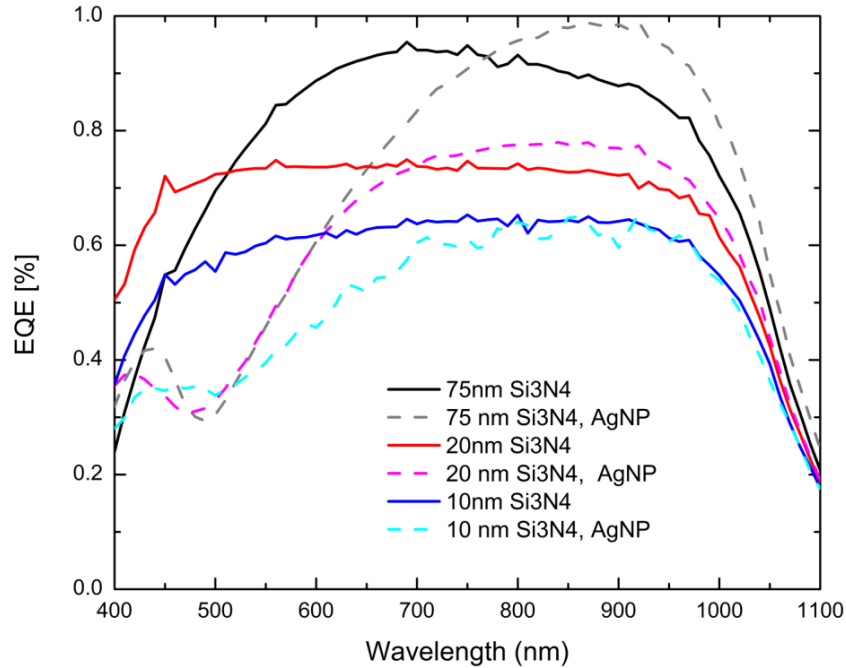


Figure 4.11 Temperature study on solar cell device

The annealing dynamic shows significant unstable configuration for annealing temperature larger than 250 °C. This fact is observed from graph. We can conclude that optimum temperature for annealing the device is between 200 °C and 250 °C. With increasing the temperature above 250 °C the cell efficiency is decreased dramatically. For 400 °C annealing the cell efficiency is reached to 2.63% while at 250 °C is 13.81%. It is important to notice that cell efficiency is not influenced by time duration for annealing.

### 4.4. Quantum Efficiency

After brief description of EQE in pervious section, is the measure of the number of electrons the device generates per number of photons incident on the device surface, for each wavelength. EQE is carried out for both of the flat and textured silicon solar cells for different silicon nitride thicknesses film which are 10 nm, 20 nm and 75 nm. The results are shown in Fig. 4.12 below:



**Figure 4.12** EQE curves for flat silicon with different silicon nitride thicknesses before and after dewetting 2 hours @ 200 °C

Figure 4.12 shows the QE of silicon full scale solar cell with different thicknesses of silicon nitride including 10 nm, 20 nm and 75 nm standard solar cell products in GÜNAM. First of all, samples are measured without AgNPs. The curves include 10 nm, 20 nm and 75 nm with colors blue, red and black respectively. The curves in dashed ones include the EQE after coating 12 nm silver and dewetting the cells in furnace under nitrogen flow at 200 °C for 2 hours. By comparing these two curves it is clear that before silver coating, EQE increases with the increases the thickness of silicon nitride as ARC. We attribute to improve anti reflection properties of the surface of solar cells due to reduce the reflection of external photon. However EQE after dewetting and formation of plasmonic AgNPs, in 20 nm and 75 nm became larger in longer wavelength in compare with before dewetting result in enhancement the photocurrent efficiency.

EQE and IQE in flat silicon solar cell after 2 hour dewetting are investigated. IQE is larger than EQE because of IQE is include of the absorbed photons that is not reflected or transmitted out of the cell, in other word is total solar cell device absorption. While EQE contains optical losses from out of the cell such as reflection and transmission leads to decrease EQE in compare with IQE. This result is shown in Figure 4.13:

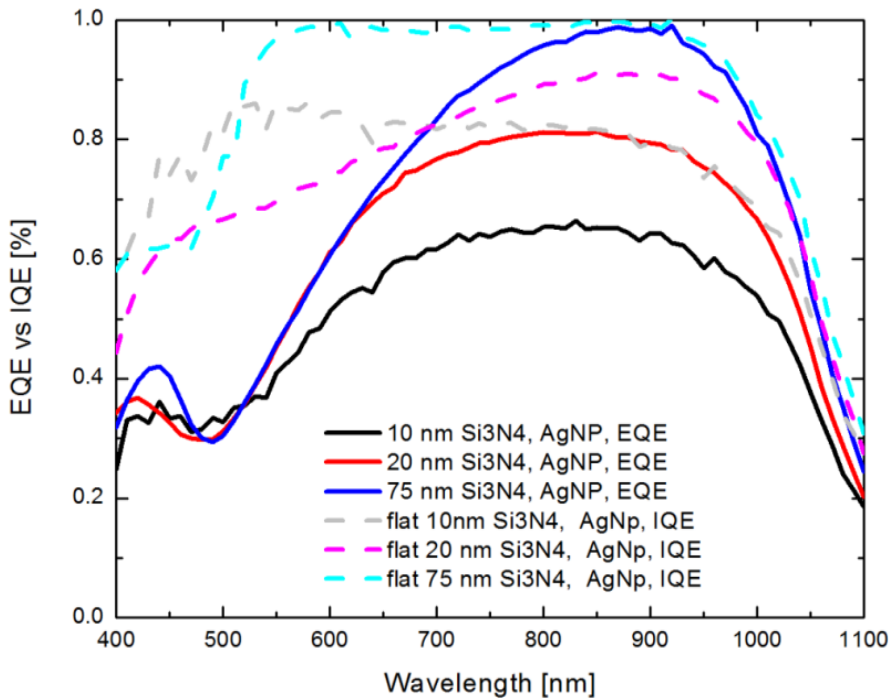


**Figure 4.13** EQE vs IQE curves for flat silicon with different silicon nitride thicknesses after dewetting 2 hours @ 200 °C

According to results, in the EQE, a loss is observed at shorter wavelengths of light compared to IQE, which is due to light absorption by particles. However, the plasmonic effect after dewetting and formation of AgNPs in longer wavelengths leads to an increase in light absorption by AgNPs. The AgNPs reduce the reflection of light out of the cell, leading to an increase in QE.

Figure 4.14 below illustrates the EQE of textured silicon solar cells with different silicon nitride film thicknesses: 10 nm, 20 nm, and 75 nm. The results represent the EQE of bare and AgNPs-decorated textured silicon solar cells.

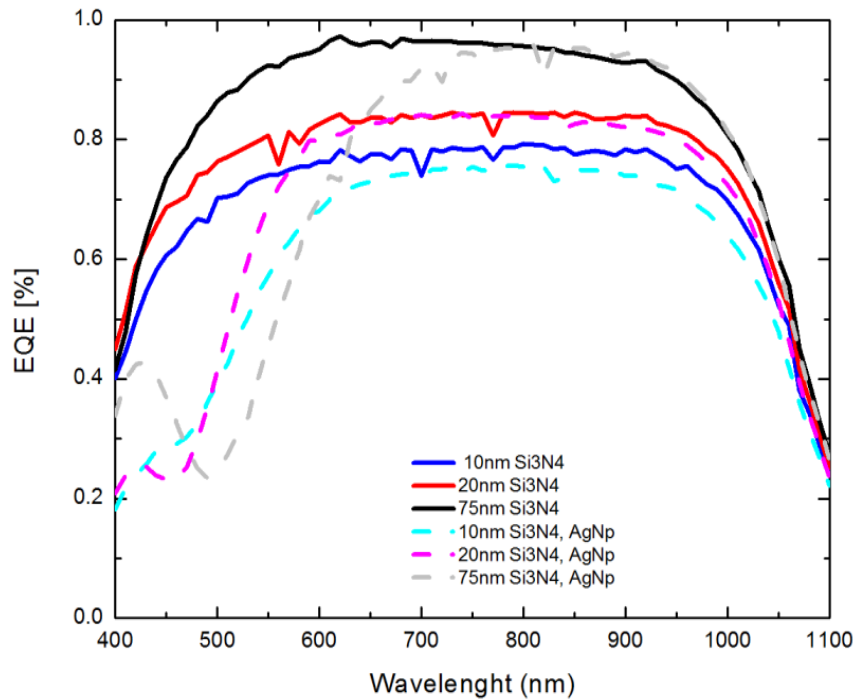


**Figure 4.14** EQE curves for textured silicon with different silicon nitride thicknesses without AgNPs and with AgNPs produced by dewetting for 2 hours @ 200 °C

These results show before AgNPs, the EQE increases with increasing thickness of the silicon nitride act as an absorber layer leading incident photon energy absorb by ARC layer and reduce the reflection of light. Therefore increases the QE of cells. After dewetting the cells EQE less than 600 nm wavelength, became smaller. The AgNPs at the resonance condition between 450 nm to 550 nm wavelengths have maximum reflection. This reduction can be due to the NP reflectivity at lower wave length and also because of the absorption of the incident photon by particle result in QE became lower and loss is obtained. While EQE is increased in longer wavelength with increases the silicon nitride thicknesses.

In this section, EQE and IQE are compared in textured silicon solar cell after 2 hour dewetting. IQE is larger than EQE as we discuss before. This result is shown in figure 4.15:

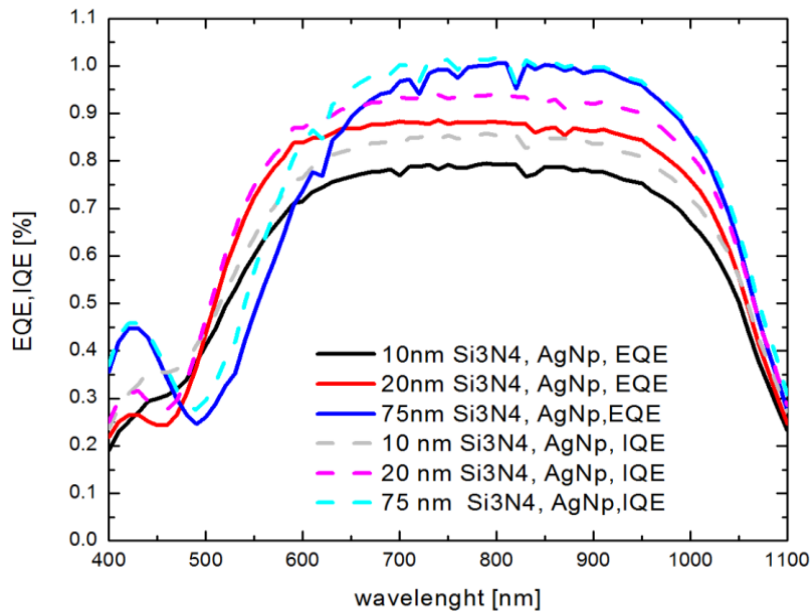


**Figure 4.15** EQE and IQE curves for textured silicon with different silicon nitride thicknesses after dewetting for 2 hours @ 200 °C

It is clear that EQE for 10 nm, 20 nm and 75 nm silicon nitride thicknesses is lower than IQE. Because of EQE includes the optical losses such as reflection out of the cell, it affects the quantum efficiency became lower. As a result with increasing the silicon nitride thicknesses, quantum efficiency increases. It depends on the ARC thicknesses leads to reduce the reflection of light and increase absorption of incident photon in the active layer solar cell.

This result represents the relation between the EQE and reflection respect to the wavelength.

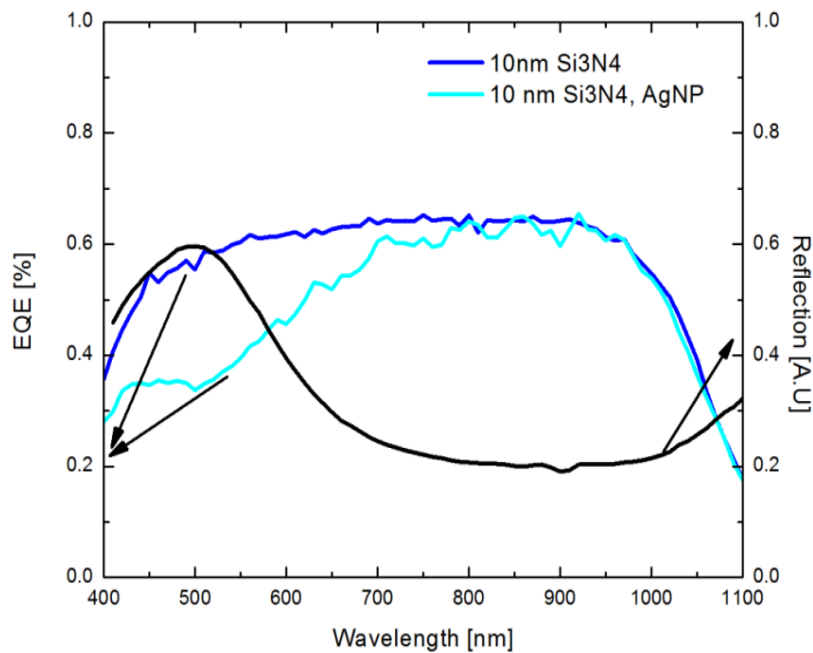


**Figure 4.16** EQE and reflection for flat silicon with 10 nm silicon nitride thickness

This graph includes two parts. The left side indicates EQE with respect to the wave length and the right side indicates the reflection with respect to the wavelength. There is a relation between EQE and reflection curves. As can be seen from the figure, the reflection is the maximum in UV region because of the silver coating. In infrared region the silver coating behaves like ARC. In the same manner for the EQE analysis, in UV region EQE is lower since the number of photons collected from solar cell decreases. However in infrared region since silver coating behave like ARC, the number of photon collected from cell increases because of the ARC absorbs more photon. As a result in infrared region the silver dewetted behave as ARC and absorb much more photon therefore the amount of EQE is maximum.

#### 4.5. FWHM and resonance peak position for both flat and textured silicon without silicon nitride

In this work, for both flat and textured without silicon nitride, the full width at half maximum (FWHM) and resonance peak position and are investigated for different dewetting time. The results are shown below:

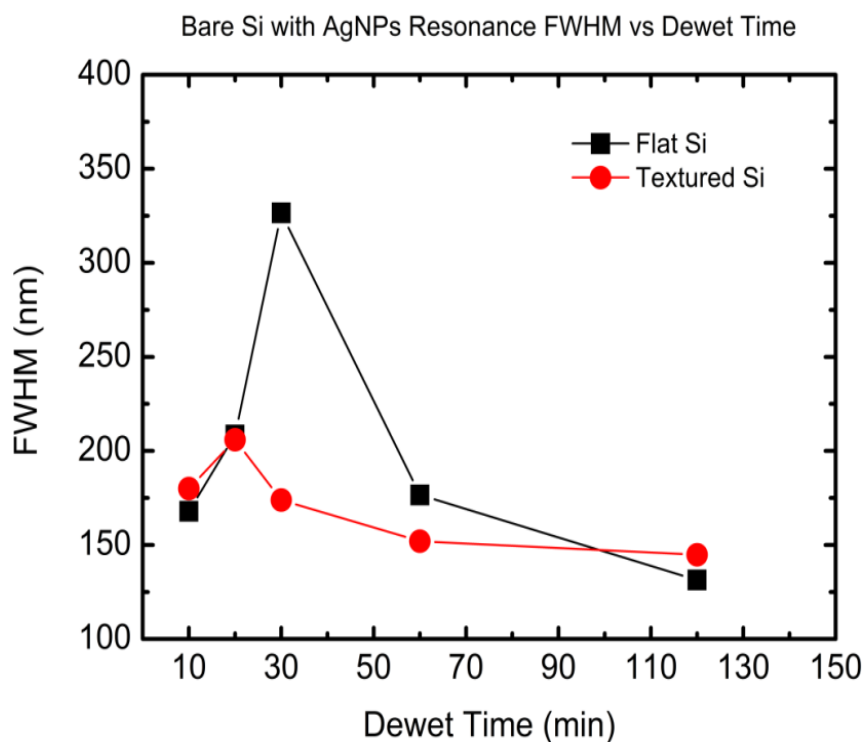


**Figure 4.17** FWHM for both flat and textured silicon

This curve shows by increasing the dewetting time, the full width at half maximum (FWHM) of particle size distribution decreases indicating that the particles tend to have a common range of diameter for both of flat and textured silicon. For textured silicon 30 minute can be the optimum dewetting time to obtain a homogenous particle size. However for flat silicon 60 minute can be the optimum time.

2 hours for both cases dewetting time gives the lowest full width at half maximum (FWHM), but it is too long dewet time which may affect the silicon wafer.

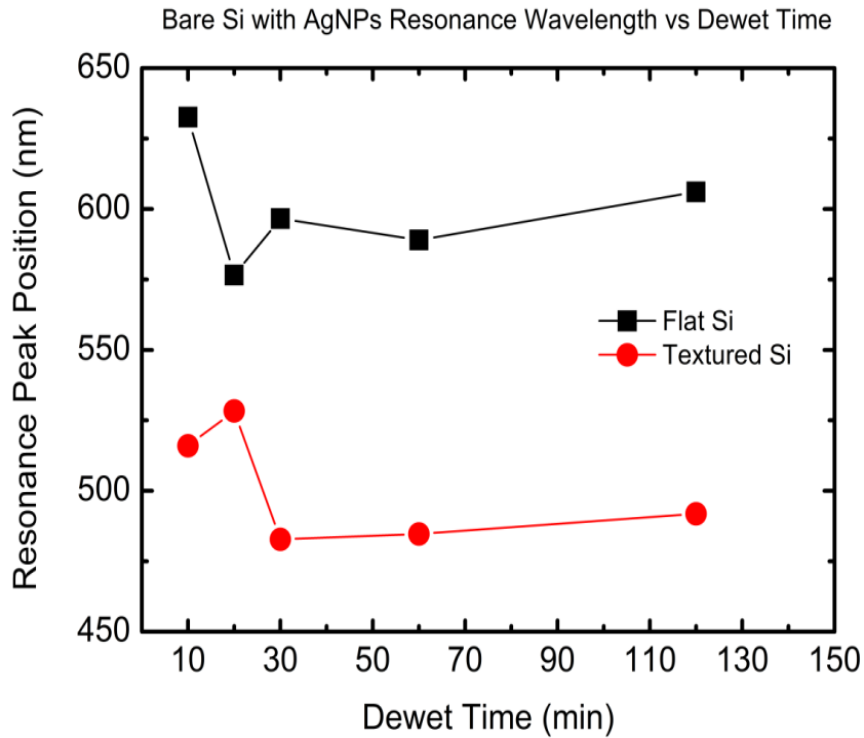


**Figure 4.18** Resonance peak position for both flat and textured silicon

We observe from these curves, although the dielectric medium are the same for both of flat and textured silicon, in flat silicon much longer resonance positions is observed with respect to the textured silicon. For instance, for 60 minute dewet time in flat silicon the peak position is 589 nm and in textured is 484.70 nm. Therefore, the resonance positions shift is approximately 100 nm or more. These results are true for other dewet time.

#### 4.6. Results of cell performance measurements by I-V characterization

In this section, we measured the current versus voltage (I-V) characteristics under  $1000 \text{ W/cm}^2$  and AM1.5 standard solar spectrum for flat and textured silicon with different silicon nitride thicknesses which are 10 nm, 20 nm and 75 nm. These measurements are done in two steps. In the first step bare silicon is deposited with different silicon nitride thicknesses. In the second step, the same samples are dewetted in furnace under nitrogen flow at  $200 \text{ }^\circ\text{C}$  for 2 hours dewet time which results in formation of AgNPs on samples. The figure 4.6.1 and 4.6.2 represents the experimental results before and after dewetting the samples.

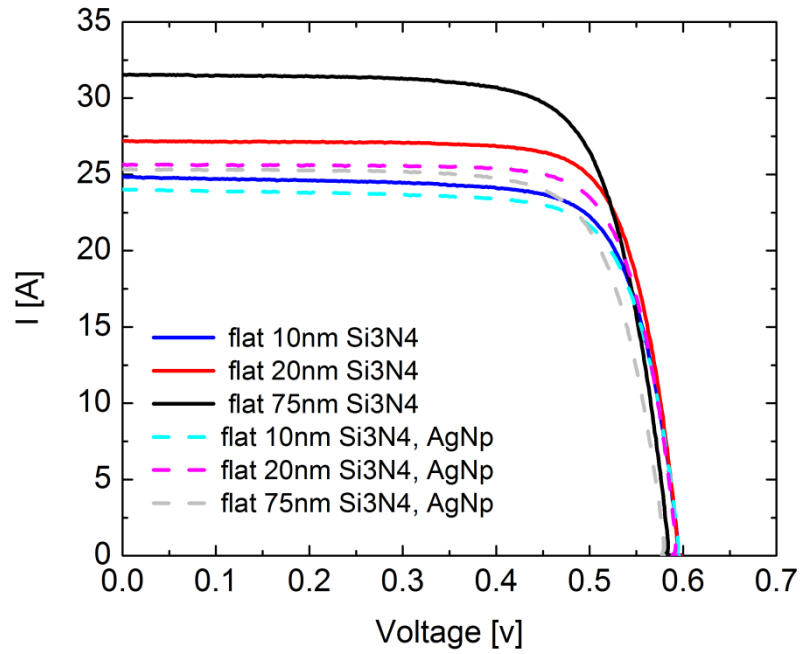


**Figure 4.19** I-V curves for flat silicon with different silicon nitride thicknesses with and without AgNPs

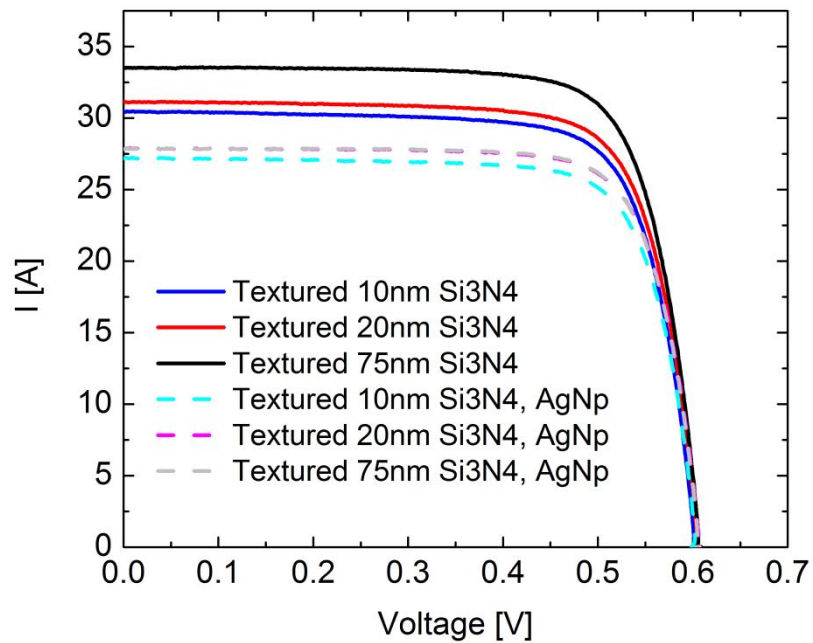


**Figure 4.20** I-V curves for textured silicon with different silicon nitride thicknesses with and without AgNPs

For investigation of plasmonic affect on full scale silicon solar cell, the current versus voltage characteristic (I-V) is plotted. As can be seen in figure 4.19 When the thickness of the silicon nitride before dewetting increase the current ( $I$ ) increase from 24.68 A ( $5.9 \text{ mA/cm}^2$ ) to 31.38 A ( $7.5 \text{ mA/cm}^2$ ), and the open circuit voltage  $V_{oc}$  decrease from 0.602 V to 0.593 V. Meanwhile, after dewetting and forming of AgNPs with respect to the influence of plasmonic interface, the current ( $I$ ) increase from 24.26 A ( $5.8 \text{ mA/cm}^2$ ) to 25.52 A ( $6.1$

$\text{mA}/\text{cm}^2$ ), and the open circuit voltage  $V_{oc}$  decrease from 0.603 V to 0.587 V. According to table 2, in flat silicon at 10 nm and 20 nm silicon nitride thicknesses, the amount of the current before and after dewetting is much close to each other. In conclusion, if the thickness of silicon nitride decreases, the plasmonic affect improves the cell performance and it can enhance the cell efficiency.

Figure 4.20 represents I-V curves for textured silicon with different silicon nitride thicknesses with and without AgNPs. If we compare the current of flat silicon solar cell with textured ones in the same thicknesses of silicon nitride (10 nm, 20 nm, and 75 nm), the current in textured silicon is larger than flat silicon. In textured silicon the pyramid and rough surfaces have affect on minimizing reflection and increasing light trapping by helping light stay longer in active solar cell layers, these properties can lead to higher efficiencies through increasing absorption and generating more current in the solar cell devices. When the thickness of the silicon nitride before dewetting increase, the current ( $I$ ) increase from 30.46 A ( $7.28 \text{ mA}/\text{cm}^2$ ) to 33.47 A ( $8 \text{ mA}/\text{cm}^2$ ), and the open circuit voltage  $V_{oc}$  slightly increases from 0.606 V to 0.610 V. After dewetting and formation of AgNPs with respect to the influence of plasmonic, the current ( $I$ ) slightly increased from 6.5 A to 6.6 A, and the open circuit voltage  $V_{oc}$  increased from 0.606 V to 0.609 V.

The figure 4.21 represents the overall comparison of flat and textured silicon after dewetting for 2 hours at 200 °C temprature. The affect of plasmonic AgNPs are investigated to improve the light-trapping of solar cell.

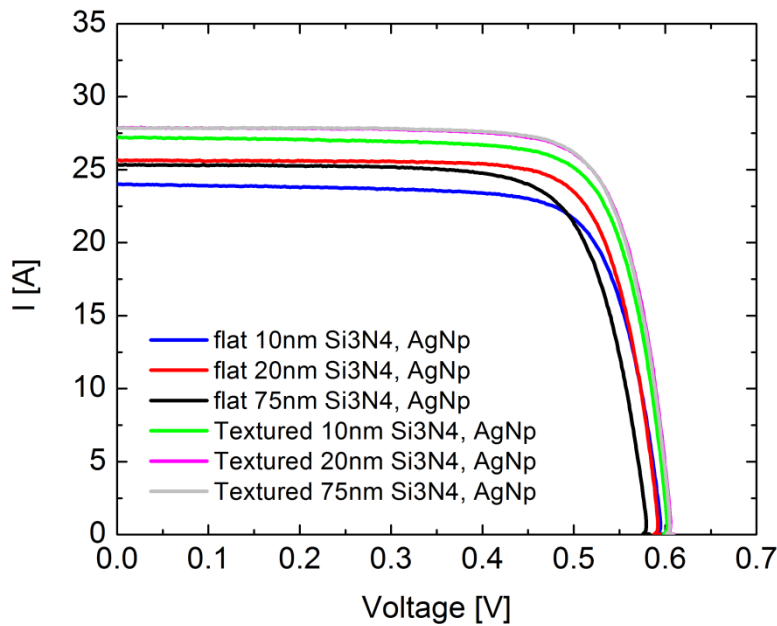


**Figure 4.21** I-V curves for textured and flat silicon with different silicon nitride thicknesses before and after dewetting

In this study, light-trapping behavior of mono crystalline silicon solar cells has been extensively investigated on both flat silicon and textured substrates. Surface texturing which increase the light absorption leads to increase the short circuit current in solar cells. In this work, we observed that plasmonic affects in optical response of AgNPs, in flat silicon have

better performance and result than textured silicon. In textured silicon solar cell, the high roughness surface of substrates increases the multiple reflections. Light trapping is a factor for improving the current and cell efficiency. However, the addition of plasmonic NPs on textured silicon can be parasitic and result in large optical loss during multiple reflections. The presence of the AgNPs cause both scattering and absorption of incoming light. The effect of absorption cannot be denied as compared to the scattering. This absorption blocks the second order reflections from the surface of textured silicon. Therefore, this situation causes the decrease in the efficiency of solar cell, while in flat silicon with low roughness and smooth substrate, plasmonic NPs themselves can introduce excellent light trapping these results in enhancement of the current and increase the cell efficiency [17]. According to table 2, in flat silicon, the difference between cell efficiency of samples of bare silicon and samples that contain AgNPs, is negligible when the thickness of silicon nitride is 10 nm and 20 nm.

As investigated, from current versus voltage (I-V) under illumination, one can extract several important parameters such as: Short circuit current ( $I_{sc}$ ), open circuit voltage ( $V_{oc}$ ), Fill Factor (FF) and Cell efficiency ( $\eta$ ). The cell parameters are investigated for both flat and textured silicon solar cells with and without AgNPs. Different silicon nitride coating represented before and after dewetting in furnace under nitrogen flow for 2 hours at 200 °C. Bare flat and bare textured means the samples are deposited with different silicon nitride thicknesses before dewetting. AgNPs flat and textured, represent the AgNP decorated on samples after dewetting.

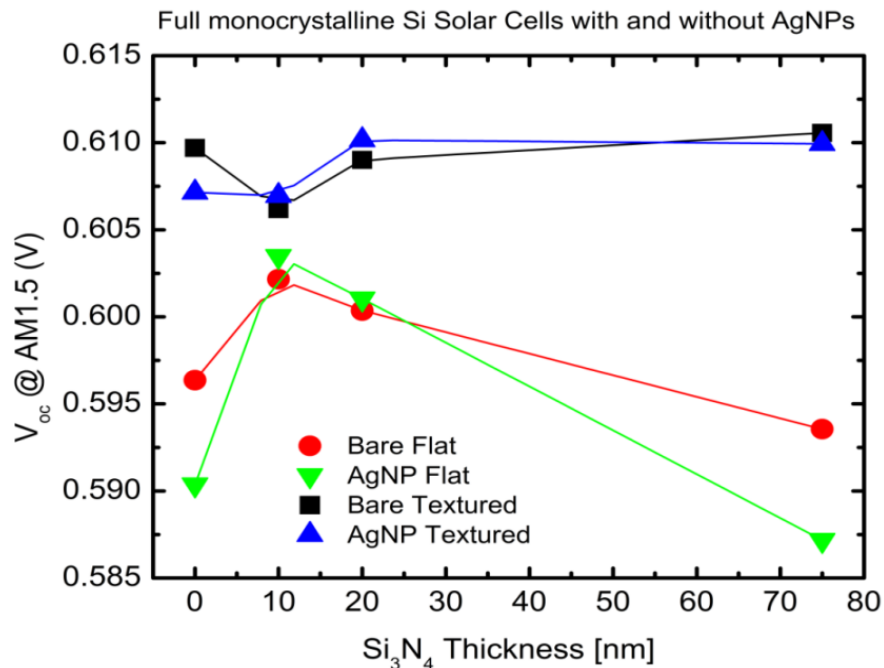


**Figure 4.22** The open circuit voltage for both flat and textured silicon @ AM1.5G.

Figure 4.22 demonstrates the open voltage circuit versus silicon nitride thicknesses. The results show for very thin silicon nitride thicknesses between 10 nm and 20 nm, the open circuit voltage are increased for both textured and flat with AgNPs. Thus AgNPs enhances the electric field and the junction when they are placed at 10 nm to 20 nm away from the absorber layer.

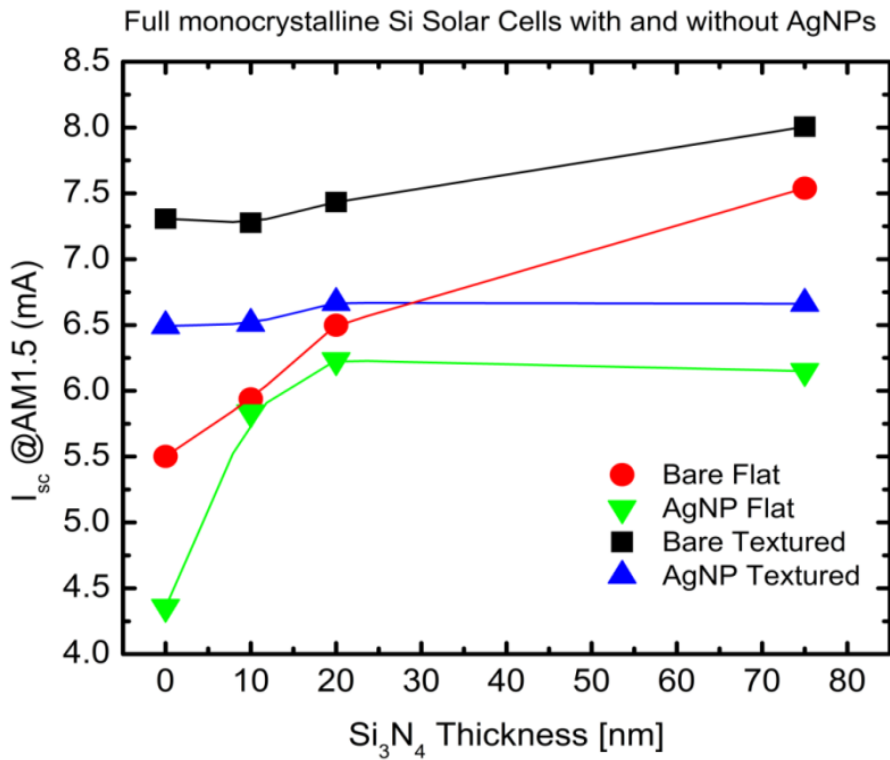


**Figure 4.23** The short circuit current for both flat and textured silicon @ AM1.5G.

Figure 4.23 displays short circuit current versus silicon nitride thicknesses. For the both AgNPs flat and textured, It seems that the silver diffuses into the silicon without silicon nitride thicknesses, Therefore creating recombination centers and defects. When silicon nitride thicknesses increases, short circuit current increases due to surface passivation. Yet the bare textured without NPs shows the best circuit current for all silicon nitride thicknesses. For silicon nitride until 20 nm, AgNPs on textured silicon demonstrates the better short circuit current than the bare flat. However short circuit current decreases only in 10 nm and 20 nm.

the fill factor for both of flat and textured silicon solar cells is illustrated in figure 4.6.6:

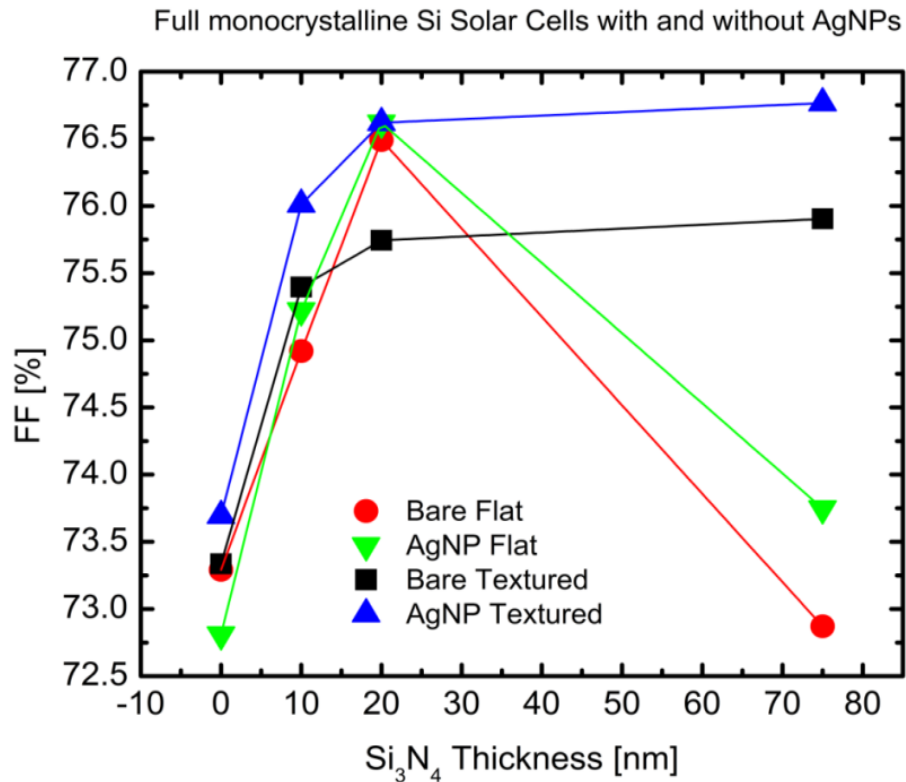


**Figure 4.24** The fill factor for both flat and textured silicon @ AM1.5G.

According to results in figure 4.24, AgNPs on textured silicon shows the best fill factor as compared to the fill factor of all the cells for all silicon nitride thicknesses, which is due to the enhancement in open circuit voltage and the overall cell performance. By comparing AgNPs flat and bare flat, in flat silicon it can be shown that for all cells with silicon nitride greater than 10 nm, plasmonic AgNPs increases the fill factor. Nowadays standard crystal silicon solar cells is produced 75 nm silicon nitride; by placing NPs, we exceed the fill factor of the standard solar cells includes (textured silicon with 75 nm silicon nitride) which are shown in both flat and textured silicon those have AgNPs.

The overall cell efficiency in bare textured silicon represents better efficiency than the AgNPs. Bare flat shows better efficiency than the AgNPs based flat for all silicon nitride thicknesses, which is due to lower short circuit current, even though open circuit voltage and fill factor are higher with AgNPs as we discussed already. The current is important parameter for cell efficiency. Increase in short circuit current leads to increase the cell efficiency.

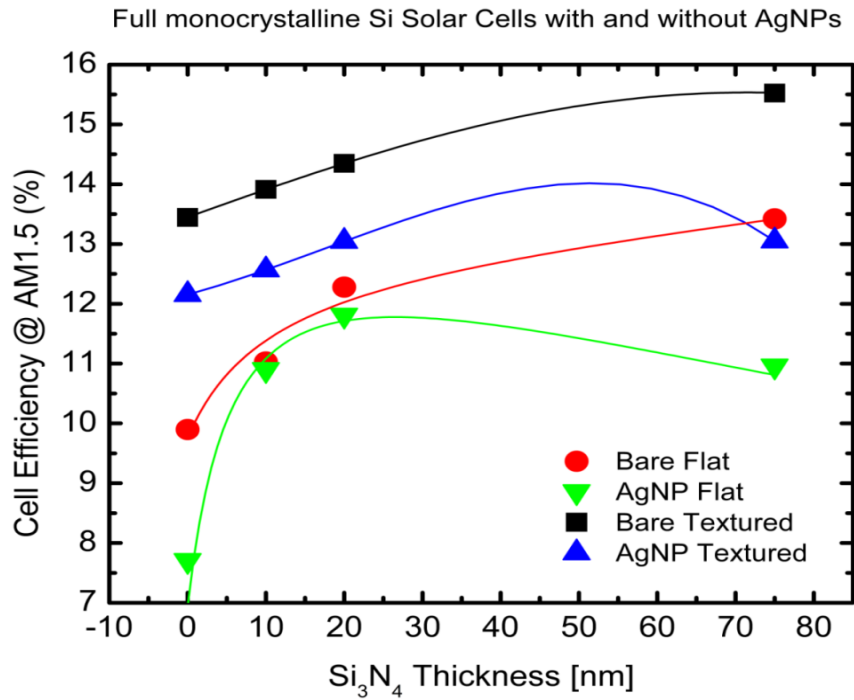


**Figure 4.25** The cell efficiency for both flat and textured silicon @ AM1.5G.

As it is shown in figure 4.25, for thin silicon nitride thicknesses in 10 nm and 20 nm for both flat and textured silicon, we could get cell efficiency in the plasmonic AgNPs to the point of bare one with the least difference.

For performance of AgNPs decorated on solar cells leads to have bad impact in the cell efficiency and reduces both of bare flat and textured cells. As we observed in bulk crystal silicon solar cells, decoration of cells with plasmonic AgNPs needs further optimization for better enhancement. The total surface coverage of ~30% needs to be pushed down to ~10% for avoiding unnecessary losses due to metal absorption. Better coupling of light through optimally attained surface coverage is expected to return higher cell efficiencies in near future. It is evident that a 10 nm silicon nitride film on flat silicon is an optimum parameter for a more detailed work in that direction.

Table2. Characteristics of flat and textured silicon solar cells having various silicon nitride film thickness with and without AgNPs.

<b>Cell p.m Device</b>	<b>Voc(V)</b>	<b>Isc(A)</b>	<b>FF (%)</b>	<b>Cell Efficiency(<math>\eta\%</math>)</b>
<b>bare textured</b>	<b>0.6097</b>	<b>7.3066</b>	<b>73.335</b>	<b>13.444</b>
<b>Ag NP textured</b>	<b>0.60714</b>	<b>6.4923</b>	<b>73.695</b>	<b>12.154</b>
<b>bare flat</b>	<b>0.59636</b>	<b>5.5022</b>	<b>73.291</b>	<b>9.896</b>
<b>Ag Np flat</b>	<b>0.59037</b>	<b>4.3572</b>	<b>72.809</b>	<b>7.707</b>
<b>10 nm bare textured</b>	<b>0.60618</b>	<b>7.2757</b>	<b>75.396</b>	<b>13.913</b>
<b>10 nm Ag NP textured</b>	<b>0.60696</b>	<b>6.5104</b>	<b>76.010</b>	<b>12.567</b>
<b>10 nm bare flat</b>	<b>0.60216</b>	<b>5.9383</b>	<b>74.919</b>	<b>11.024</b>
<b>10 nm Ag Np flat</b>	<b>0.60348</b>	<b>5.8347</b>	<b>75.222</b>	<b>10.90</b>
<b>20 nm bare textured</b>	<b>0.60901</b>	<b>7.4337</b>	<b>75.743</b>	<b>14.347</b>
<b>20 nm Ag NP textured</b>	<b>0.61015</b>	<b>6.6683</b>	<b>76.619</b>	<b>13.043</b>
<b>20 nm bare flat</b>	<b>0.60036</b>	<b>6.4980</b>	<b>76.490</b>	<b>12.28</b>
<b>20 nm Ag Np flat</b>	<b>0.60104</b>	<b>6.2320</b>	<b>76.618</b>	<b>11.81</b>
<b>75 nm bare textured</b>	<b>0.61056</b>	<b>8.0057</b>	<b>75.903</b>	<b>15.523</b>
<b>75 nm Ag NP textured</b>	<b>0.60994</b>	<b>6.6612</b>	<b>76.765</b>	<b>13.050</b>
<b>75 nm bare flat</b>	<b>0.59355</b>	<b>7.5394</b>	<b>72.870</b>	<b>13.419</b>
<b>75 nm Ag Np flat</b>	<b>0.58718</b>	<b>6.1495</b>	<b>73.747</b>	<b>10.958</b>



## CHAPTER 5

### CONCLUSION

In this thesis, the plasmonic properties of MNPs on both of flat and textured crystalline silicon solar cell have been examined for the improvement of solar cell efficiency. The MNPs were fabricated by self-organization on substrates. The method that was chosen is called surface dewetting which is a suitable method for plasmonic interface integration to large area full-scale solar cell devices. Different metals can be used in plasmonic applications such as copper, aluminum, silver and gold each with different optical properties. In this study, silver is preferred as MNPs due to the high scattering cross-section of particles into the substrate which is expected to lead to increased optical path length and absorption of incoming photon. AgNPs also possess plasmonic resonances that span the solar spectrum from UV to NIR. For the formation of AgNPs, a 12 nm continuous silver layers were deposited under high vacuum on both of flat and textured full scale silicon cells and also simultaneously on test samples with smaller areas for the reflection measurements and SEM image analysis. In this thesis, three external control mechanisms on the self-organized production of plasmonic interfaces were investigated. One of these is the tuning of the top ARC layer thickness, which is a control mechanism on the optical and device properties of solar cells. The tuning was achieved by changing the ARC thickness of silicon nitride from 0 nm to 10 nm, 20 nm and 75 nm. Another one of these mechanisms was the dewetting duration, in which 10,20,30,60 and 120 minutes of dewetting times have been investigated. A third mechanism was the pre-patterning of the cell surface. We observed the effects of plasmonic NPs on both of flat and textured silicon and how these are influenced by changing the dewetting time and various thickness of silicon nitride on the improvement performance of solar cell. The effect of dewetting temperature is studied as well, and the critical process temperature for this kind of technology is determined to be a maximum of 250 °C. This is a surprising but unambiguous finding since the solar cell production process involves much higher treatment temperatures for the diffusion based doping of Si and the co-firing of the metal contacts. The finished solar cell device is found to be vulnerable to even one third of the co-firing temperature of 800 °C when exposed for prolonged durations.

A comparison of the optical properties of plasmonic AgNPs decorated flat silicon with the AgNP decorated textured silicon was made by reflection measurements. In flat silicon, there is a clear correlation between dewetting time and plasmonic peak position. By increasing the dewetting time and/or the thickness of silicon nitride, the reflection peak wavelength due to the plasmon resonance by AgNPs increases and shifts to red. On textured silicon, however, reflection data displays uncontrolled plasmonic resonance shifts by increasing dewetting time because of the random distribution of AgNPs achieved on the surface. Interestingly, the reflection of incident light is expected to be lower than that of the flat cell, not only because of multiple scattering from the structured cell surface, but also from the elevated optical losses introduced by multiple scattering of light from AgNPs. It is clear that texturing the substrate is one way for reducing the reflectivity of the substrate. The particle size versus

changing dewetting time was studied on samples that were treated at a mild annealing temperature of 200 °C (50 °C below the critical process temperature of 250 °C determined in this study). It is found that prolonged annealing durations longer than 30 minutes are not beneficial in tuning the mean particle size and hence the reflection peak position wavelengths. In these samples, the median particle size became larger when the thickness of silicon nitride was increased.

The experimental and Mie theory results were compared. In fact, because of the uncertainties in the system that was used for this study, it is not a straight forward task to compare the results. The dielectric layers were not completely homogenous, and this supposedly affects the formation of particles and surface diffusion of ad-atoms. The size distributions of AgNPs are broad and the particles are not perfectly of spherical shape. Due to these limitations, comparison of the theoretical and experimental results is not easy task. For these reasons, Mie scattering theory was applied with three different effective medium model and some approximations for geometry and size of spherical particles.

The electrical characterizations were done before and after decoration of full scale solar cell devices with AgNPs. The samples were annealed in a hot-plate furnace under nitrogen flow at 200 °C for 2 hours. It was observed that the plasmonic effects on flat silicon solar cells are beneficial under certain conditions and an improvement of cell performance is feasible. However, the plasmonic interface proved to be not beneficial when incorporated with a textured and ARC coated already optimally photon managed solar cell. It is found that the cell efficiency of a flat silicon cell with 10 nm silicon nitride ARC is the same as the efficiency of the same cell without NPs. This fact is direct evidence that the self-organized plasmonic interface produced on a flat solar cell surface embodies sufficient benefits which equilibrate, if not overcome, its lossy side effects. It can be argued that the short come of using self-assembly to produce AgNPs is that the surface coverage cannot be selected freely and is an innate property of the production technique. It can be seen from Fig. 4.2.2 that the integrated surface coverage yields about 30%, which is undoubtedly higher than the estimated optimum value of 10% in the literature. The extra 20% does not contribute to enhancement of the scattering into the substrate yet does contribute significantly to absorption losses. In the light of this view, my finding that the cell efficiency of a flat silicon cell with 10 nm silicon nitride ARC is the same as the efficiency of the same cell without NPs, is actually a great promise. I expect the plasmonic interfaces made of AgNPs to be of more evident success in thin-film solar cells. This is because, unlike in bulk solar cells, in thin film solar cell devices they can be incorporated with all three of the back reflectors, the active regions and the ARCs, and can exhibit a multitude of performance boosting effects such as near field enhancement and excitation of long range surface plasmon polaritons. It shall not be conferred from this last argument that there is nothing to do for the bulk solar cells. The bulk solar cell efficiency can be improved, for example, by an additional brief Ag etch step after the dewetting step in an attempt to decrease the surface coverage from 30 to 10%.

## REFERENCES

- [1] Ostwald W., Lehrbuch der Allgemeinen Chemie, 2-1 (1896); Ostwald, W., "Studienüber die Bildung und Umwandlung fester Körper" (Studies on the formation and transformation of solid bodies), *ZeitschriftfürphysikalischeChemie*, 22, 289-330 (1897).
- [2] Alvarez, M. M., J. T. Khoury, T. G. Schaaff, M. Shafigullin, I. Vezmar, and R. L. Whetten. "Critical sizes in the growth of Au clusters." *Chemical physics letters* 266, no. 1 (1997): 91-98.
- [3] Garnett, JC Maxwell. "Colours in metal glasses, in metallic films, and in metallic solutions. II." *Philosophical Transactions of the Royal Society of London. Series A, Containing Papers of a Mathematical or Physical Character* (1906): 237-288.
- [4] Turkevich, J., G. Garton, and P. C. Stevenson. "The color of colloidal gold." *Journal of colloid Science* 9 (1954): 26-35.
- [5] Bouhelier, Alexandre, and Lukas Novotny. "Near-field optical excitation and detection of surface plasmons." In *Surface Plasmon Nanophotonics*, pp. 139-153. Springer Netherlands, 2007.
- [6] Kneipp, Katrin, HaraldKneipp, and Janina Kneipp. "Surface-enhanced Raman scattering in local optical fields of silver and gold nanoaggregates from single-molecule Raman spectroscopy to ultrasensitive probing in live cells." *Accounts of chemical research* 39, no. 7 (2006): 443-450.
- [7] Stuart, Howard R., and Dennis G. Hall. "Island size effects in nanoparticle-enhanced photodetectors." *Applied Physics Letters* 73, no. 26 (1998): 3815-3817.
- [8] Schaadt, D. M., B. Feng, and E. T. Yu. "Enhanced semiconductor optical absorption via surface plasmon excitation in metal nanoparticles." *Applied Physics Letters* 86 (2005): 063106.
- [9] Derkacs, D., S. H. Lim, P. Matheu, W. Mar, and E. T. Yu. "Improved performance of amorphous silicon solar cells via scattering from surface plasmonpolaritons in nearby metallic nanoparticles." *Applied Physics Letters* 89 (2006): 093103.
- [10] Pillai, S., K. R. Catchpole, T. Trupke, and M. A. Green. "Surface plasmon enhanced silicon solar cells." *Journal of applied physics* 101 (2007): 093105.
- [11] Ferry, Vivian E., Marc A. Verschuuren, Hongbo BT Li, Ruud EI Schropp, Harry A. Atwater, and Albert Polman. "Improved red-response in thin film a-Si: H solar cells with soft-imprinted plasmonic back reflectors." *Applied Physics Letters* 95, no. 18 (2009): 183503-183503.
- [12] Bohren, Craig F., and Donald R. Huffman. *Absorption and scattering of light by small particles*. Wiley. Com, 2008.

- [13] Kim, Jeehwan, Ahmed Abou-Kandil, Keith Fogel, Harold Hovel, and Devendra K. Sadana. "The role of high work-function metallic nanodots on the performance of a-Si: H solar cells: offering ohmic contact to light trapping." *ACS nano* 4, no. 12 (2010): 7331-7336.
- [14] Westphalen, Michael, Uwe Kreibig, Jörn Rostalski, Hans Lüth, and Dieter Meissner. "Metal cluster enhanced organic solar cells." *Solar Energy Materials and Solar Cells* 61, no. 1 (2000): 97-105.
- [15] Rand, Barry P., Peter Peumans, and Stephen R. Forrest. "Long-range absorption enhancement in organic tandem thin-film solar cells containing silver nanoclusters." *Journal of Applied Physics* 96, no. 12 (2004): 7519-7526.
- [16] Hägglund, Carl, S. Peter Apell, and Bengt Kasemo. "Maximized optical absorption in ultrathin films and its application to plasmon-based two-dimensional photovoltaics." *Nano letters* 10, no. 8 (2010): 3135-3141.
- [17] Tan, Hairen, Rudi Santbergen, Arno HM Smets, and Miro Zeman. "Plasmonic light trapping in thin-film silicon solar cells with improved self-assembled silver nanoparticles." *Nano letters* 12, no. 8 (2012): 4070-4076.
- [18] Python, M., D. Dominé, T. Söderström, F. Meillaud, and C. Ballif. "Microcrystalline silicon solar cells: effect of substrate temperature on cracks and their role in post-oxidation." *Progress in Photovoltaics: Research and Applications* 18, no. 7 (2010): 491-499.
- [19] Boccard, Mathieu, Corsin Battaglia, Simon Hänni, Karin Söderström, Jordi Escarré, Sylvain Nicolay, Fanny Meillaud, Matthieu Despeisse, and Christophe Ballif. "Multiscale transparent electrode architecture for efficient light management and carrier collection in solar cells." *Nano letters* 12, no. 3 (2012): 1344-1348.
- [20] Söderström, T., F.-J. Haug, X. Niquille, and C. Ballif. "TCOs for nip thin film silicon solar cells." *Progress in Photovoltaics: Research and applications* 17, no. 3 (2009): 165-176.
- [21] Springer, J., A. Poruba, L. Mullerova, M. Vanecek, O. Kluth, and B. Rech. "Absorption loss at nanorough silver back reflector of thin-film silicon solar cells." *Journal of Applied Physics* 95, no. 3 (2004): 1427-1429.
- [22] Yablonovitch, Eli. "Statistical ray optics." *JOSA* 72, no. 7 (1982): 899-907.
- [23] Sai, Hitoshi, Yoshiaki Kanamori, and Michio Kondo. "Flattened light-scattering substrate in thin film silicon solar cells for improved infrared response." *Applied Physics Letters* 98, no. 11 (2011): 113502-113502.
- [24] Winneker, Craig. "World's Solar Photovoltaic Capacity Passes 100-Gigawatt Landmark After Strong Year." *European Photovoltaic Industry Association* (2013).

[25] European Photovoltaic Industry Association. "Global market outlook for photovoltaics until 2014.

"[http://www.epia.org/fileadmin/EPIA\\_docs/public/Global\\_Market\\_Outlook\\_for\\_Photovoltaics\\_until\\_2014.pdf](http://www.epia.org/fileadmin/EPIA_docs/public/Global_Market_Outlook_for_Photovoltaics_until_2014.pdf) (2010). (last accessed on 07.2013)

[26] Grätzel, Michael. "Dye-sensitized solar cells." *Journal of Photochemistry and Photobiology C: Photochemistry Reviews* 4, no. 2 (2003): 145-153.

[27] Atwater, Harry A., and Albert Polman. "Plasmonics for improved photovoltaic devices." *Nature materials* 9, no. 3 (2010): 205-213.

[28] Catchpole, K. R., and Albert Polman. "Plasmonic solar cells." *Opt. Express* 16, no. 26 (2008): 21793-21800.

[29] Catchpole, K. R., and A. Polman. "Design principles for particle plasmon enhanced solar cells." *Applied Physics Letters* 93 (2008): 191113.

[30] Stuart, Howard R., and Dennis G. Hall. "Island size effects in nanoparticle-enhanced photodetectors." *Applied Physics Letters* 73, no. 26 (1998): 3815-3817.

[31] Pillai, S., and M. A. Green. "Plasmonics for photovoltaic applications." *Solar Energy Materials and Solar Cells* 94, no. 9 (2010): 1481-1486.

[32] Hulst, Hendrik Christoffel, and Hendrik C. van de Hulst. *Light scattering: by small particles*. Courier Dover Publications, 1957.

[33] Bohren, Craig F., and Donald R. Huffman. *Absorption and scattering of light by small particles*. Wiley. com, 2008.

[34] Griffiths, David J. *Introduction to electrodynamics*. Pearson, 2013.

[35] Pohl, Dieter W. "Near-field optics and the surface plasmonpolariton." In *Near-Field Optics and Surface Plasmon Polaritons*, pp. 1-13. Springer Berlin Heidelberg, 2001.

[36] Novotny, Lukas, and Bert Hecht. *Principles of nano-optics*. Cambridge university press, 2012.

[37] "AM 1.5 Spectrum" TU Delft, <http://theopenacademy.com/content/lecture-3-solar-radiation> (last accessed on 08.2013).

[38] Luque, Antonio, and Steven Hegedus, eds. *Handbook of photovoltaic science and engineering*. Wiley. com, 2011.

[39] Goetzberger, Adolf, Joachim Knobloch, and Bernhard Voss. *Crystalline silicon solar cells*. Chichester: Wiley, 1998.

[40] Pagliaro, Mario, Rosaria Ciriminna, and Giovanni Palmisano. "Flexible solar cells." *ChemSusChem* 1, no. 11 (2008): 880-891.

- [41] Kyeong, Dohyeon, MuniappanGunasekaran, Kyunghae Kim, Heejae Kim, Taeyoung Kwon, Inyong Moon, Youngkuk Kim, Kyumin Han, and Junsin Yi. "Laser edge isolation for high-efficiency crystalline silicon solar cells." *Journal of Korean Physical Society* 55 (2009): 124.
- [42] Stuart, Robley V. *Vacuum technology, thin films, and sputtering: An introduction*. Access Online via Elsevier, 1983.
- [43] Wasa, Kiyotaka, Makoto Kitabatake, and Hideaki Adachi. *Thin film materials technology: sputtering of control compound materials*. Springer, 2004.
- [44] Haynes, Christy L., Adam D. McFarland, LinLin Zhao, Richard P. Van Duyne, George C. Schatz, Linda Gunnarsson, Juris Prikulis, BengtKasemo, and Mikael Käll. "Nanoparticle optics: the importance of radiative dipole coupling in two-dimensional nanoparticle arrays." *The Journal of Physical Chemistry B* 107, no. 30 (2003): 7337-7342.
- [45] Frantzeskakis, Emmanouil. "Analysis of potential applications for the templateddewetting of metal thin films." PhD diss., Massachusetts Institute of Technology, 2005.
- [46] Responsive Database Services (Business & Industry Database), Website: <http://rdsweb2.rdsinc.com>
- [47] Thornton, John A., and D. W. Hoffman. "Stress-related effects in thin films." *Thin solid films* 171, no. 1 (1989): 5-31.
- [48] Chang, Chih-Yeuan, and R. W. Vook. "Thermally induced hillock formation in Al-Cu films." *Journal of Materials Research* 4, no. 05 (1989): 1172-1181.
- [49] Iwamura, Eiji, Takashi Ohnishi, and Kazuo Yoshikawa. "A study of hillock formation on Al Ta alloy films for interconnections of TFT-LCDs." *Thin Solid Films* 270, no. 1 (1995): 450-455.
- [50] Tanyeli Irem, Nasser Hisham, Es Firat, Bek Alpan, and Turan Raşit. "Effect of surface type on structural and optical properties of Ag nanoparticles formed by dewetting." *Optics Express* 21, no. 105 (2013): A798-A807.
- [51] Mie ScatteringTheory, <http://nanophotonics.csic.es> (last accessed on 08.2013).
- [52] Günendi, M., Tanyeli İrem, Gürsoy B. Akgüç, Bek Alpan, Turan Raşit, and Oğuz Gülseren. "Understanding the plasmonic properties of dewetting formed Ag nanoparticles for large area solar cell applications." *Optics express* 21, no. 15 (2013): 18344-18353.